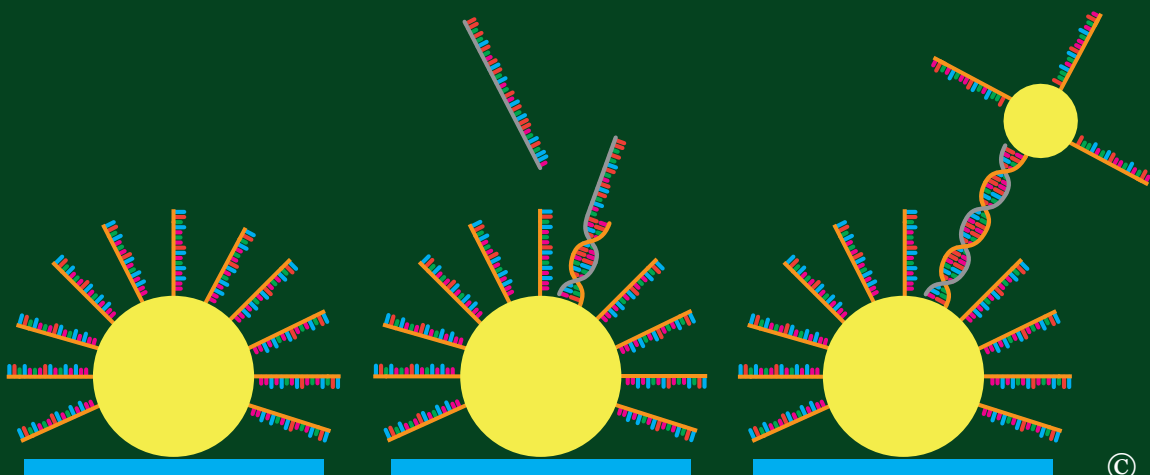


SCATTERING GOLD NANOPARTICLES



REMCO VERDOOLD



©

STRATEGIES FOR ULTRA SENSITIVE DNA DETECTION

SCATTERING GOLD NANOPARTICLES:

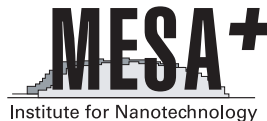
STRATEGIES FOR ULTRA SENSITIVE DNA DETECTION

By Remco Verdoold

Members of the dissertation committee:

Prof. dr. G. van der Steenhoven	University of Twente (Chairman)
Prof. dr. V. Subramaniam	University of Twente (Supervisor)
dr. R. P. H. Kooyman	University of Twente (Ass. Supervisor)
Prof. dr. ir. A. van den Berg	University of Twente
Prof. dr. J. J. L. M. Cornelissen	University of Twente
Prof. dr. G. T. Robillard	University of Groningen
Prof. dr. A. H. Velders	Wageningen University

The research described in this thesis was carried out at the Nanobiophysics Group, MESA+ Institute for Nanotechnology and Faculty of Science and Technology, University of Twente, P. O. Box 217, 7500 AE Enschede, The Netherlands.



This research has been financially supported by Microned SMACT 2F workpackage

Cover Design: Remco Verdoold

Typeset with Adobe Indesign.

Printed by: Wöhrmann Print Service, Zutphen, the Netherlands.

ISBN: 978-90-365-3408-6

DOI: 10.3990/1.9789036534086

URL: <http://dx.doi.org/10.3990/1.9789036534086>

E-mail: rverdoold@gmail.com

Copyright © Remco Verdoold, Deventer, the Netherlands 2012

All rights reserved. No part of the material protected by this copyright notice may be reproduced or utilized in any form or by any means, electronic or mechanical, including photo copying, recording or by any future information storage and retrieval system, without prior permission from the author.

This thesis is printed on FSC certified paper for a sustainable future!

SCATTERING GOLD NANOPARTICLES:

STRATEGIES FOR ULTRA SENSITIVE DNA DETECTION

PROEFSCHRIFT

ter verkrijging van
de graad van doctor aan de Universiteit Twente,
op gezag van de rector magnificus,
prof. dr. H. Brinksma,
volgens besluit van het College voor Promoties,
in het openbaar te verdedigen
op woensdag, 5 september 2012 om 12.45

door

Remco Verdoold

geboren op 18 november 1982
te Rotterdam

Dit proefschrift is goedgekeurd door:

Prof. dr.	V. Subramaniam	(Promotor)
dr.	R. P. H. Kooyman	(Assistent Promotor)

*Aan mijn ouders,
mijn broer en
Ilzei*

Table of contents

Chapter 1	Aim and thesis outline	9
Chapter 2	Introduction to optical detection of DNA	13
Chapter 3	Chemistry in DNA sensing	37
Chapter 4	Physics of surface plasmon based sensing	69
Chapter 5	Gold nanoparticle amplified surface plasmon resonance: the effect of size	87
	<i>Appendix A, Model for GNP amplified SPR</i>	102
Chapter 6	Femtomolar DNA detection by parallel colorimetric darkfield microscopy of functionalized gold nanoparticles	105
Chapter 7	Alternative gold nanoparticle detection strategies	123
Chapter 8	Concluding remarks and recommendations for future work	149
	Summary	163
	Samenvatting	167
	Acknowledgements	171
	About the author	172
	List of publications	173

Chapter 1

Aim and thesis outline



This chapter provides the reader with a brief introduction to the thesis ‘Scattering gold nanoparticles: Strategies for ultra sensitive DNA detection’. This chapter starts with the description of the MicroNed project ‘Fluorescence on a chip’ and its aims. Then the aim of the thesis is introduced. The chapter concludes with a brief outline of the thesis.



1.1 Scope of the project

The MicroNed program started in the beginning of 2004 and was aimed at “*establishing a market oriented, dynamic and sustainable public-private knowledge infrastructure on microelectromechanical systems*”. The program consisted of 33 partners with different scientific backgrounds and was divided into four research clusters. The clusters ‘micro satellite’ and ‘smart microchannel technology (smact)’ were application driven, while the other two clusters ‘microfactory’ and ‘fundamentals, modelling and design of microsystems’ were focused on fundamental knowledge. The project described in this thesis is a part of the ‘smart microchannel technology’ cluster. Originally the project was named ‘Fluorescence on a chip’; however, the increasing interest in non-fluorescent and non-bleaching light scattering nanoparticles such as gold nanoparticles inspired us to change our focus to non-fluorescent probes. The goal of this project is to develop a new type of highly sensitive biosensor, preferably using simple and inexpensive components.

1.2 Aim of the thesis

More specifically the aims are:

- 1) The functionalisation of gold nanoparticles with receptor molecules in such a way that the receptor molecules remain biologically active and are stable over time;
- 2) The development of a gold nanoparticle sensor interface for detection of nanoparticle scattering;
- 3) The development of gold nanoparticle based assays to sensitively detect specific DNA target strands using a simple optical system.

1.3 Outline

A brief summary of the chapters is provided below.

Chapter 2: “*Introduction to optical detection of DNA*”. This chapter contains a short history of DNA, its structure and physicochemical properties, and further concentrates on the importance of detecting DNA. It is followed by a review of various DNA detection strategies with emphasis on optical detection methods and the use of gold nanoparticles as reporters.

Chapter 3: “*Chemistry in DNA sensing*”. In this chapter the various aspects of methodology involved in the preparation of biosensors are described. The chapter starts with a description of surface preparation, such as optimal surface coatings for covalent or non-covalent biomolecule modifications. It continues with a description of the functionalisation of gold nanoparticles with DNA strands and approaches to testing the activity and functionality of the conjugated particles. The chapter concludes with a description of how analyte solutions are brought to the sensor surface.¹



Chapter 4: “*Physics of surface plasmon based sensing*”. This chapter explains the basics of surface plasmon resonance of a planar layer and local surface plasmon resonance (LSPR) of gold nanoparticles. Furthermore, the use of gold nanoparticles as individual biosensors and the basics of sensing using LSPR are explained, followed by methods for interpretation of the data and estimating concentrations and affinity constants of the binding molecules.¹⁻³

Chapter 5: “*Gold nanoparticle amplified surface plasmon resonance: the effect of size*”. In this chapter experiments are described where gold nanoparticles of various sizes are used to investigate the mass amplification effect in a conventional surface plasmon resonance approach.

Chapter 6: “*Femtomolar DNA detection by parallel colorimetric darkfield microscopy of functionalized gold nanoparticles*”. This chapter describes the use of gold nanoparticles as a sensor for a specific DNA strand. The particles are functionalised with DNA strands, followed by a real-time measurement monitoring the binding interactions. The results are compared with the expected effect acquired from simulations.⁴

Chapter 7: “*Alternative gold nanoparticle detection strategies*”. This chapter outlines two alternative detection strategies that we studied. Both are based on the detection of scattering of individual gold nanoparticles.

Chapter 8: “*Concluding remarks and recommendations for future work*”. The experiments conducted to achieve the project aim of this thesis are summarised and the major conclusions are drawn. This chapter also describes recommendations to improve the sensitivity of the gold nanoparticle detection system.

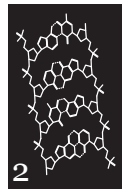
1.4 Bibliography

- (1) Verdoold R., Ungureanu F., Wasserberg D., Kooyman R.P.H. Gold nanoparticle assays: towards single molecule unamplified DNA detection. *Proceedings of SPIE* **2009**; 7312: 73120N.
- (2) Ungureanu F., Halamek J., Verdoold R., Kooyman R.P.H. The use of a colour camera for quantitative detection of protein-binding nanoparticles. *Proceedings of SPIE* **2009**; 7192: 71920O.
- (3) Ungureanu F., Wasserberg D., Yang N., Verdoold R., Kooyman R.P.H. Immunosensing by colorimetric darkfield microscopy of individual gold nanoparticle-conjugates. *Sensors & Actuators: B Chemical* **2010**; 150: 529-36.
- (4) Verdoold R., Gill R., Ungureanu F., Molenaar R., Kooyman R.P.H. Femtomolar DNA detection by parallel colorimetric darkfield microscopy of functionalized gold nanoparticles. *Biosensors & Bioelectronics* **2011**; 27: 77-81.



Chapter 2

Introduction to optical detection of DNA



This chapter gives an introduction to the technology of gold nanoparticle based optical sensing of deoxyribose nucleic acids (DNA). First, it covers a general introduction of DNA and the importance of DNA detection. Then, it reviews several concepts of specific DNA detection with an emphasis on gold nanoparticle based methods. Subsequently, we discuss possible future methods for specific and sensitive detection of DNA.

2.1 Introduction

When the structure of DNA was revealed by Watson and Crick¹ in 1953, we could not have foreseen the immense impact of this discovery. DNA is basically constructed from two polymers each made from four base nucleotides, namely, adenine (A), thymine (T), guanine (G) and cytosine (C). In ribose nucleic acid (RNA) the thymine is replaced by uracil (U). These two polymers have a backbone made from sugar and phosphate groups which hold the nucleotides in place as illustrated in Figure 2-1. The genetic code of an organism is based on the sequence in which the bases A, T, C and G are ordered. Translation of this sequence forms the basis for protein production. Currently we have learned that parts of the DNA sequence are highly specific for individual species and even individual organisms.² This sequence specificity enables the possibility of accurate detection of individual species.^{3,4}

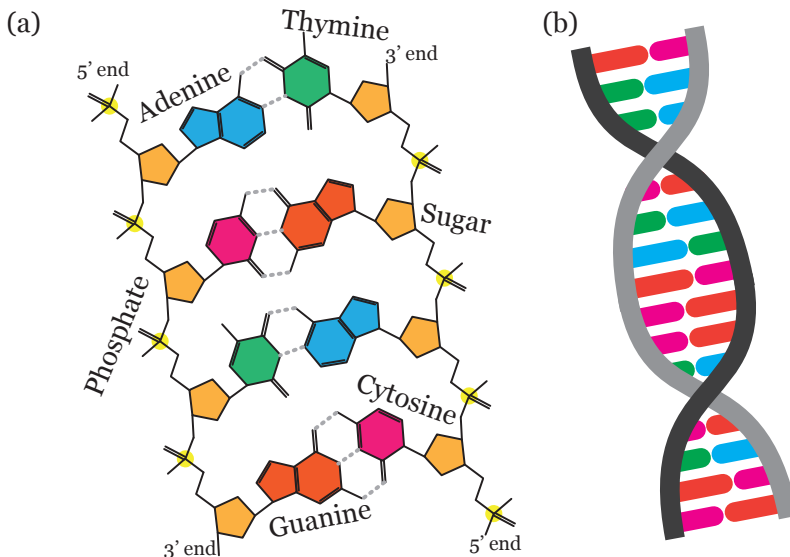


Figure 2-1: Structure of double stranded DNA (a) shows the layout of the nucleotides with sugar/phosphate backbone. The two strands are bound via hydrogen bonds, two between A and T and three between C and G. (b) DNA double helix, length 0.34 nm per base, radius ~2.3 nm.³

It took until the early 70s of the previous century before recombinant DNA technology enabled the isolation of sequence specific DNA from an organism.⁴⁻⁶ A few years later Sanger and co-workers⁷ developed a method to amplify an unknown strand of DNA using radioactively labelled DNA chain terminators. Owing to this sequencing method it was possible to obtain very reliable sequence information. Subsequently, this research led to the development of the polymerase chain reaction (PCR), which helps to copy a sequence of DNA. Before PCR, DNA amplification methods used *E.*

coli derived DNA polymerase, an enzyme that copies a single strand of DNA, but could only be used for one cycle.⁸ The amount of DNA copied was low, because only one duplicate was made. With PCR this changed. A thermally stable DNA polymerase from *Thermus aquaticus* was used, which was able to copy a specific DNA strand again and again.^{9,10} Latest developments have enabled quantitative and real-time monitoring of analyte specific amplifications.^{11,12} Because of this progression a Quantitative-PCR (q-PCR) apparatus can now be found in nearly any diagnostic lab around the world.

Rapid detection of biological threats is essential.^{13,14} This was emphasized by the 2009 H1N1 influenza-A pandemic, caused by a rapidly spreading virus.¹⁵ However, soon after the outbreak the H1N1 sequence was decoded¹¹ and the World Health Organisation published a world wide applicable q-PCR protocol which allowed rapid determination of infected organisms.¹² The principle of q-PCR is illustrated in Figure 2-2.

2-2.

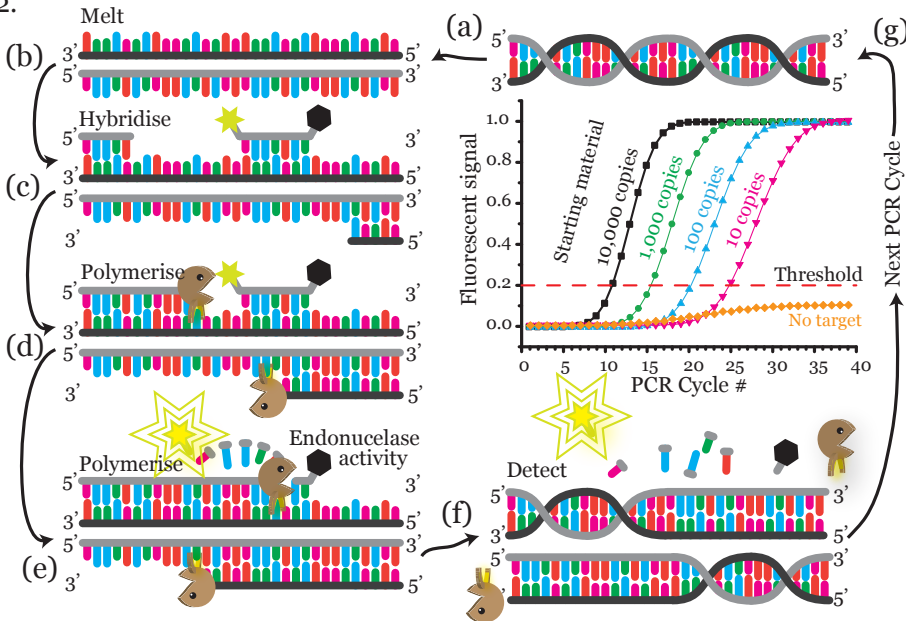


Figure 2-2: Amplification by q-PCR using reporter probes with internal quenchers (Taq-man method). (a) The dsDNA is separated into two single strands by elevating the temperature to 96 °C, (b) followed by lowering the temperature for optimal hybridisation of the primers and probe. (c) This is followed by an increase of temperature for the polymerisation of Taq polymerase. (d) The *Taq* polymerase endonuclease activity breaks the probe and the fluorescent label is freed from the quencher. After elongation (e) is finished, the amount of fluorescence is measured (f). This is followed by a repeat of the cycle with a continuous duplication of the analyte DNA (g). The threshold indicates the autofluorescence due to release of fluorophores from their quenchers. When a large number of copies are already present in the sample at the beginning, more probes are released after fewer amplification cycles.



A fast and specific detection of messenger RNA (mRNA), RNA or DNA is important. New methods are developed continuously, each with their own advantages and disadvantages. Every new method must compete with currently accepted methods, therefore it should combine several aspects, namely (i) a very high specificity for the analyte among other molecules, (ii) the ability to obtain a response from very low numbers of analyte molecules or even a single molecule in (iii) a very small sample volume, (iv) the ability of high throughput analysis and (v) low cost. Another factor to keep in mind is pre-sample processing which is very important and often time consuming. Implementing isolation and purification steps or, preferably, making it possible to use a raw sample is a direct advantage. Reducing the time per measurement generally also decreases the cost per measurement. Multiplexing capabilities are favoured, but in many cases not necessary. To a lesser extent, a method should be highly automated, thus reducing the chances of an operator error. On the other hand, a simply constructed device from low cost components is an advantage in the upcoming markets such as out of the lab testing in diagnostics at home or in resource-poor settings.

Most DNA biosensors consist of three components: (i) a receptor molecule with a high affinity for the (ii) analyte and often, (iii) a reporter molecule, as illustrated in Figure 2-3. Methods without a reporter molecule are called label-free and have the advantage of reducing one step, and therefore reducing time and cost. The receptor is usually a single stranded molecule made of DNA or peptide nucleic acid (PNA) and is either immobilised onto or in a support matrix, or is free in solution. An advantage of having receptor molecules free in solution is the increased probability of hybridisation with the analyte. Receptors are covalently immobilised on the support matrix in such a way that the direct surrounding is free and does not hinder the binding of the analyte. The analyte is usually a product of PCR amplification since the amount of DNA molecules is initially too low to detect. However, being able to detect single molecule hybridisation events could eliminate this time consuming and expensive step. Unamplified analyte detection will be one of the main key points by which a new method could distinguish itself.

The reporter is a molecule that also specifically binds the analyte and is able to make it detectable. Usually this is achieved with a fluorescent label; however, radioactive isotopes are widely used as well. The main disadvantages of fluorescent labels are photobleaching, quenching and difficulties to detect single molecule hybridisation events. For this reason non-photobleachable quantum dots¹³ and noble metal nanoparticles are gaining popularity.^{14,16} Currently fluorescent detection is still one of the most favoured methods, although it requires a complex and expensive apparatus for detection.

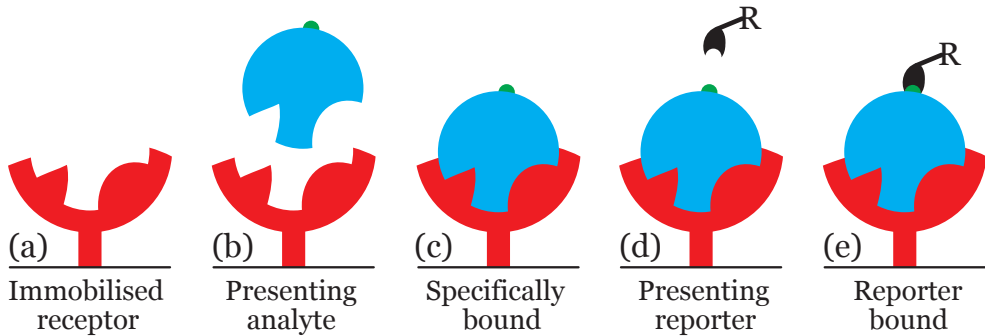


Figure 2-3: Basics of specific analyte detection. (a) The receptor is immobilised on the surface with the active site available for binding. (b) Analyte is presented and at the right circumstances (e.g., concentration and temperature) it will (c) bind specifically to the receptor. Most label-free detection methods can follow the process of analyte binding. For label based detection methods, (d) an analyte specific reporter is presented and (e) bound to the receptor. Unbound reporters are removed and an endpoint measurement gives the total response of the reporters. Reporters can be fluorescent probes, radioactive probes, enzymes, light scattering nanoparticles, etc.

2.2 Current technologies

q-PCR is the current benchmark for rapid, highly specific and quantitative DNA detection. However, pre-processing is necessary before PCR can be performed. Viable organisms can be screened on organism specific gene expression by detecting ribosomal RNA (rRNA)¹⁷ or messenger RNA (mRNA).¹⁸ An advantage is that the copy numbers per organism of RNA strands are usually higher than of DNA. The direct detection of rRNAs and mRNAs is mostly performed on microarrays and has a rather good detection limit.^{19,20} mRNA first has to be transcribed to complementary-DNA (cDNA) on which the quantitative analysis (e.g., q-PCR) can be performed, since cDNA is more stable than mRNA. q-PCR can give the amount of starting mRNA that was available at the beginning; however this available mRNA is isolated from an unknown number of organisms. q-PCR is well developed, wide spread and able to simultaneously analyse up to 384 samples.²¹ However, the apparatus is costly and so are the fluorescent labels and amplification enzymes.²²

An emerging analysis format is the microarray of which the sensing method can vary. The microarray, as by Southern, was developed in early 1970s for gene expression level detection by blotting.²³ However, gene expression level detection is less suitable for diagnostic purposes. Generally, a microarray is a convenient format to analyze large numbers of samples simultaneously in the same manner, which is very suitable for diagnostic purposes. A microarray essentially consists of sample areas

that are organised in an array shape. The type of assay determines how each spot is constructed. For instance, to analyse multiple analytes from a single patient, each spot contains receptors for individual diseases. The analytes from various possible diseases present in the patient will bind to the receptor and only those present will show a signal. Detection of analyte binding on the microarray can be both with labels or label-free. Depending on the detection approach (e.g., optical, electrochemical or gravimetric detection), labelled methods generally utilise fluorescent probes,^{24,25} enzyme-linked probes^{26,27} or functionalised nanoparticles.^{16,28-31} In label-free methods hybridisation causes a change in the local refractive index^{32,33} or absorption, usually at wavelengths of 260–280 nm.³⁴ Using a microarray can therefore give a quick diagnosis of the disease or even the specific variant of infection. Microarrays can consist of any layout and spot number.

2.2.1 Optical ensemble DNA detection methods based upon absorption

Absorbance measurements of bulk DNA in a 1 cm cuvette have a limited sensitivity of approximately 2 ng μl^{-1} which corresponds to $\sim 1.0 \times 10^{-7}$ M for a 60 nucleotide analyte or $\sim 6.5 \times 10^{10}$ strands measured in 1 μl sample volume. These numbers are rather exciting for a measurement performed in a few seconds. However the analyte cannot be distinguished from other light absorbing molecules in the solution, e.g., other DNA or proteins, thus making this method unsuitable for specific detection of analytes. In 1997 this changed when Elghanian and co-workers¹⁶ developed a method utilizing gold nanoparticles (GNPs). The very high extinction coefficient of GNPs ranging from $\sim 5.0 \times 10^5$ (\varnothing 2 nm) to $\sim 4.0 \times 10^{12}$ (\varnothing 250 nm) $\text{M}^{-1} \text{cm}^{-1}$ depending on shape and size makes them ideal as a non-bleaching label for optical detection. The high extinction coefficient is the result of collective resonance of surface plasmons of individual particles.³⁵⁻³⁷ GNPs were functionalised with various strands of oligonucleotides (ODNs) and upon specific analyte hybridisation the particles in solution aggregated, as illustrated in Figure 2-4. The aggregation of GNPs was measured in time in a UV-VIS spectrophotometer. Further exploration of this approach led to the possibility to detect specific analytes³⁸ and single nucleotide polymorphisms (SNPs);³⁹⁻⁴² however, the sensitivity is limited to the picomolar range (~ 100 pM,^{16,43} 200 pM⁴⁴). The method is fast and utilises only a standard spectrophotometer which can be constructed from simple components. Another disadvantage of bulk methods is the need for a relatively large sample volume, usually above 100 μl . Reynolds *et al.* used a different approach for analyte DNA detection; instead of using small ~ 13 nm GNPs they used 50 and 100 nm GNPs to improve sensitivity leading to a 50 pM detection limit.⁴⁵

As an alternative to the spectrophotometric analysis of aggregating GNPs, it is possible to analyse aggregation in a lateral flow assay or with dipstick-type biosensors. This type of assay became the first home-use test for the hormone human chorionic gonadotrophin (hCG), a biomarker for pregnancy. In this immunoassay mouse anti-hCG functionalised GNPs bind the hCG from urine or serum and in a capillary flow they move to the test strip. Here two lanes of antibodies are attached to the surface, the first is the same mouse anti-hCG and the second is an anti-mouse antibody as control. GNPs that captured hCG will bind to the anti-hCG strip showing a red line, and the remaining GNPs will bind on the anti-mouse strip showing the red control line.

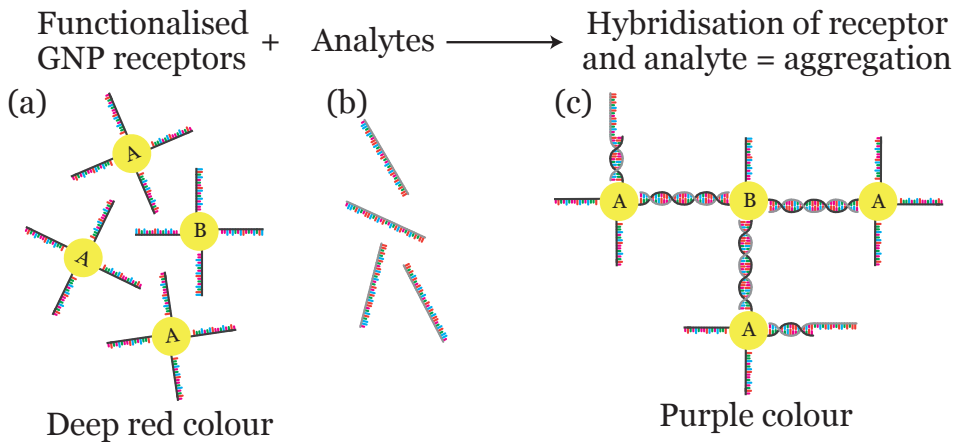


Figure 2-4: Illustration of a gold nanoparticle based bulk assay. (a) Functionalised GNPs are mixed in solution and (b) upon mixing with analytes (c) specific DNA strand hybridisation occurs. The specific aggregation of the GNP solution is visible as a colour change from deep red to purple. Eventually, the solution will become colourless due to precipitation of the GNP-analyte aggregates.

This type of assay has been adapted for DNA analytes instead of proteins. The group of Christopoulos used anti-biotin functionalised GNPs.^{46,47} In a PCR step the analyte DNA was amplified and during the amplification a biotin group was added. For analysis lanes, microspheres were functionalised with a receptor ODN and spotted on the strip, as illustrated in Figure 2-5.^{46,47} Using this method they were able to achieve a sensitivity of 1.6 fmol in 10 μ l which corresponds to 160 pM.¹⁷ This is in the same range as in the bulk aggregation assays, only without the use of a spectrophotometer. In the group of Van Amerongen a similar type of assay was performed using carbon nanoparticles which resulted in black lines compared to red lines from GNPs.^{48,49} The sensitivity obtained for various *E. coli* virulence factors was expressed in colony forming units (cfu) and was between 10^4 to 10^5 cfu/ml. A single colony forming unit

is a viable cell, which is able to grow on agar plates with optimal growth medium. Depending on the species, the copy number of the DNA analysed varies, making it hard to convert to molar concentrations. However, both strip assays still rely on the amplification of the analyte DNA before they can be measured on the strip. An advantage of this strip assay is the elimination of fluorescent probes thus halving the cost of the assay compared to q-PCR.

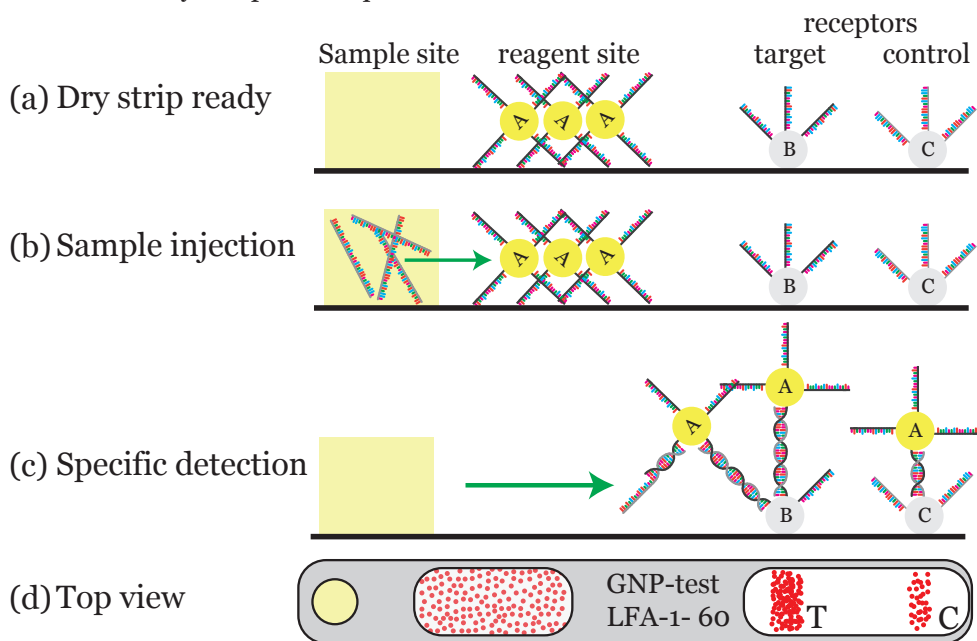


Figure 2-5: Lateral flow assay, (a) in the cassette all reagents and functionalised GNPs and beads are ready for use. (b) The analyte is injected and transported to the functionalised GNPs by capillary flow. (c) The hybridised GNPs bind to the beads B, the remaining free GNPs bind to the control area C. In the Top view (d) the functionalised GNPs are shown in a window; when the assay is finished these will have all moved to the read-out zone. The T in the read-out zone shows the line for target binding and C - the line for control. If the specific analyte was not present in the sample, only the control band appears. If the control band does not appear then the strip was faulty. It is also possible that assays have multiple target recognition sites in the read-out zone to perform multiplexing assays.

An alternative surface based method was pioneered by the group of Mirkin.^{34,50,51} This so-called biobarcoding scanometric method, as illustrated in Figure 2-6, is based on (a) in bulk capture of the analytes by functionalised paramagnetic nanoparticles, followed by (b) magnetic separation from unbound molecules and (c) analyte hybridisation with a functionalised 'barcode-DNA' GNP, which is again (d) magnetically separated. Eventually DTT is used to remove the 'barcode-DNA' (e) which then (f) hybridises on a DNA microarray surface (g). A second functionalised

GNP complementary to the 'barcode-DNA' is (h) hybridised with the 'barcode-DNA' resulting in green spots on the microarray surface when viewed with a darkfield microscope. (i) Subsequently, silver enhancement can be used to increase the signal allowing the (j) use of a normal office flatbed scanner to acquire the intensity levels. By using this method it was possible to obtain sensitivity down to 7 aM using 30 nm GNPs.⁵² An advantage of this method is the elimination of PCR amplification of the analyte. The amplification is incorporated in the 'barcode-DNA' GNP. A 30 nm GNP can host up to 300 'barcode-DNA' strands, thus a single analyte capture results in a 300-fold amplification (equivalent of nine PCR cycles). Using an even larger 'barcode-DNA' GNP this method could become even more sensitive.

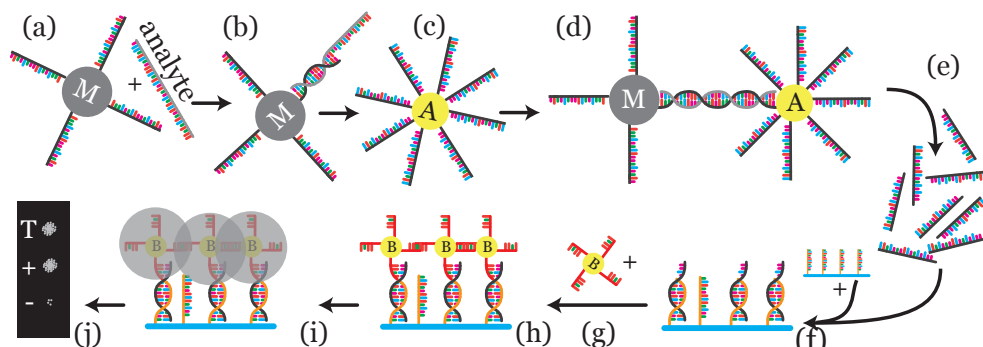


Figure 2-6: (a) In bulk capture of the analytes by functionalised paramagnetic nanoparticles. (b) Magnetic separation from unbound molecules. (c) Analyte hybridisation with 'barcode-DNA' GNP. (d) Magnetic separation of bound complexes. (e) DTT treatment to liberate 'barcode-DNA' from GNPs. (f) 'Barcode-DNA' hybridisation on a DNA microarray surface. (g) Barcode-DNA binder GNP, (h) hybridises with the 'barcode-DNA'. (i) Silver enhancement to increase signal for (j) office flatbed scanner image acquisition. Adapted from Hill *et al.*⁵¹

Bao and co-workers studied the use of 80 nm GNPs for gene expression microarrays. Compared to the commonly used Cy3 dye it was found that at high concentrations of the analyte the differences were very low. However, at low concentrations the scattering of the GNPs was visible but not the Cy3 dye fluorescence.⁵³ This shows that for surface detections fluorescent dyes can be replaced by non-photobleachable GNPs which can easily be detected with a camera in a darkfield set-up.

2.2.2 Surface plasmon resonance sensing

Surface plasmon resonance (SPR) is a very popular method for real-time and quantitative analysis of immunological samples. SPR can occur when p-polarised light hits a thin metal film (~ 50 nm thickness) under total internal reflection (TIR). Under TIR conditions, the photons interact with the free electrons of the

metal film resulting in a coherent oscillation of conduction electrons (denoted as a surface plasmon) on both sides of the film. Usually measurements are performed by changing the angle of incidence of the light beam. At the angle (the 'resonance' angle) where a minimum in the reflectance occurs, surface plasmons are excited. Binding of biomolecules on the surface causes a change in the refractive index at the sensor surface. Hence the SPR conditions change resulting in a shift of the resonance angle. The shift is proportional to the amount of material bound on the sensor surface and is illustrated in Figure 2-7.⁵⁴ Since the signal response is based on refractive index changes, SPR is well-suited to monitor surface binding reactions where high refractive index molecules with a high molecular weight are involved. Proteins and DNA have a refractive index around 1.5,⁵⁵ which is higher than the refractive index of commonly used aqueous buffers ($n = 1.34$). However, measuring molecules smaller than 20 kDa requires a high sensitivity of the apparatus.⁵⁶ Several groups made efforts to detect short DNA sequences using a conventional⁵⁷ or imaging SPR set-up.⁵⁸⁻⁶¹ The group of Corn was able to reach a 10 nM limit of detection for a 5.5 kDa ssDNA analyte.⁵⁸

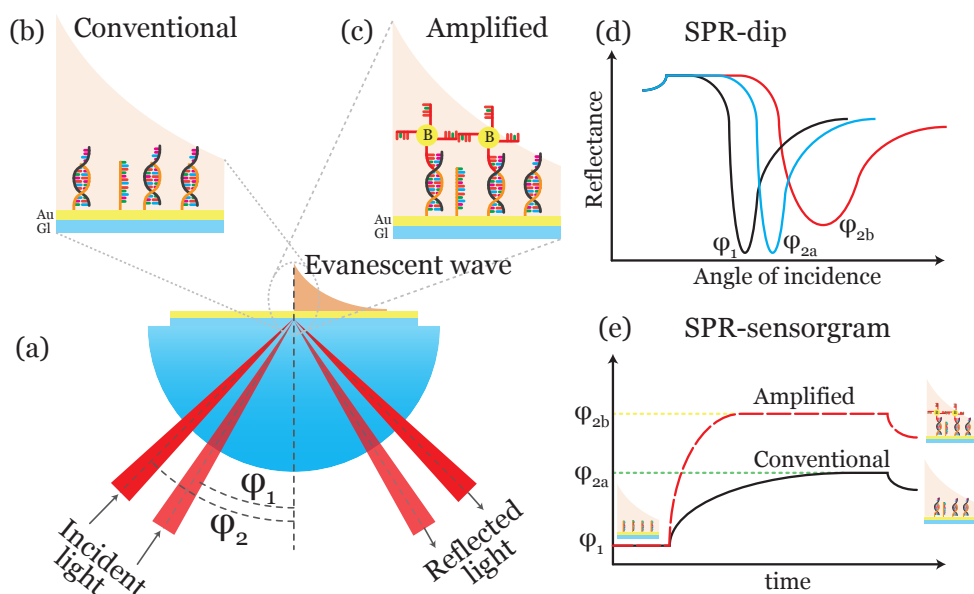


Figure 2-7: (a) Schematic representation of SPR (Kretschmann configuration). Incident light enters the hemispherical prism and at total internal reflection the photons interact with the free electrons resulting in a plasmon field on both sides of the metal layer. The change of refractive index in this plasmon field results in a change of the angle of minimum reflectance. (b) Conventional SPR of DNA in the plasmon field, (c) amplified SPR using GNPs for amplification. (d) Reflectance curve for the SPR-dip determination, when molecules bind the dip shifts, in the amplified assay the GNPs also change the shape of the dip. (e) SPR-sensorgram shows the change of the incident angle as a function of time.⁵⁴

In order to increase the sensitivity of DNA detection high molecular weight or high refractive index labels can be used,⁶² such as DNA enzymes,⁶³ DNA binding protein⁶⁴ or GNPs.⁶⁵⁻⁷⁰ The limit of detection with GNPs was improved to 10 pM for 24-mer ssDNA analytes⁷⁰ and even >1 fM for short strands when combined with high affinity PNA receptors.^{66,69} Furthermore, the GNP enhancement of the SPR shift enables the possibility to detect single nucleotide polymorphisms of analyte DNA.^{71,72} This very sensitive method allows the detection of unamplified DNA but remains essentially a bulk detection.

2.2.3 Noble metal nanoparticle based sensor

As discussed before, gold nanoparticles are widely used to amplify well accepted detection methods. However, it is also possible to use individual GNPs as a sensor. Spherical GNPs with a diameter below 150 nm are relatively easy to fabricate as a monodisperse colloidal solution by the Turkevich citrate reduction method.^{65,66} For functionalisation purposes smaller particles tend to be more favourable due to their higher stability in buffered solutions.⁴⁵

The main reason of the GNPs popularity is the excitation of localised surface plasmons. This physical phenomenon occurs when GNPs are situated in an electromagnetic field containing the wavelength (λ_{\max}) that excites these plasmons.⁷³ For GNPs $\lambda_{\max} \sim 540$ nm.⁶⁷ At λ_{\max} , the scattering cross section of an individual GNP with a diameter of 60 nm is 10^5 fold larger than that of a fluorescein molecule in the same conditions.³⁵ Individual GNPs can easily be visualised with a conventional darkfield (DF) or total internal reflection illuminating microscope, in combination with simple detection equipment such as a CCD-camera.

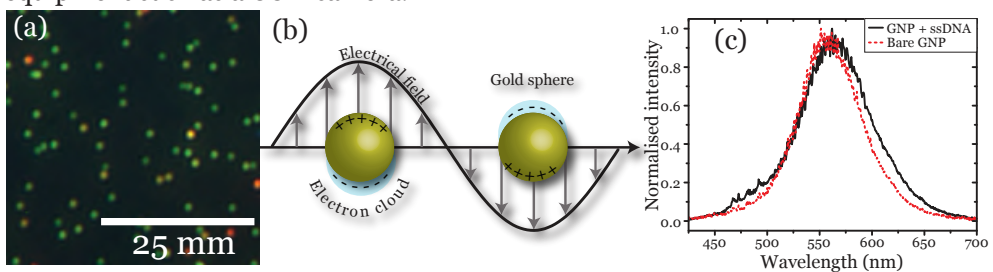


Figure 2-8: (a) Typical darkfield image of 80 nm gold nanospheres, (b) excitation of local surface plasmons directly at the surface of the GNP. Changes of the refractive index in the direct vicinity of the GNPs causes their plasmon resonance to change, this change can be observed (c) as a red shift of the scattering plasmon peak, e.g., due to the binding of DNA strands on the GNP surface.

The wavelength at which surface plasmons are excited around a nanoparticle depends on its composition, size and shape as well as the local refractive index. Local



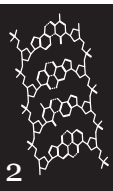
refractive index changes result in a direct change of the extinction maximum. This phenomenon enables the use of noble metal nanoparticles for local refractive index sensing.⁷⁴ The local refractive index changes when molecules with a higher refractive index enter the induced plasmon field. Contrary to planar SPR where the sensing field extends to approximately half the wavelength of the used light, this field decays up to a distance of approximately half the particle diameter in the case of spherical particles.⁷⁵

As illustrated in Figure 2-8, individual GNPs can easily be visualized under darkfield conditions. When receptor molecules are immobilised on a transparent surface a functionalised GNP can be used to sandwich a captured analyte. Each individual GNP that is visible on the surface is the result of a single analyte binding event. Provided the density of receptor strands on the surface is known, the analyte concentration can be determined. Schultz and co-workers demonstrated that a highly sensitive detection can be obtained by counting individual scattering nanoparticles as compared to an average colour change in the biobarcode assays.^{28,76,77} An 8.3 pM sensitivity was obtained which was approximately 60-fold more sensitive than the fluorescence-based method. Additionally, the possibility of observing SNP hybridisation was demonstrated. However, it is still orders of magnitude lower than the more complex bio-bar-code assay that demonstrated attomolar sensitivity.

An alternative method is to capture a single GNP by a long receptor strand. Brinkers *et al.* showed that the tethered particle motion (TPM) depends on the single- or double-stranded state of the receptor strand due to the large difference in persistence length of ss- or dsDNA.⁷³ However, presently TPM seems more suited for hybridisation studies than for sample concentration analysis.

The local surface plasmon resonance of GNPs can also be exploited to analyse analyte concentrations. As in planar SPR, it is possible to follow the kinetics of molecule binding to the surface of individual GNPs.⁷⁸ The sensitivity depends on the shape and size of the GNP. Simulations show that for a 60 nm sphere the binding of approximately 100 ssDNA strands on the surface of an individual GNP can be detected.⁷⁹ The binding of ssDNA strands to GNPs can be monitored as a plasmon peak shift in a spectrophotometer. However, spectrophotometers can usually take spectra only of individual particles or a line of the image. Alternatively, the use of a calibrated colour camera enables monitoring the colour change of hundreds to thousands of GNPs simultaneously.⁷⁵

The use of a single GNP as an individual sensor is not sufficiently sensitive for single binding event detection. The addition of a second GNP dramatically improves the sensitivity due to the effect of plasmon coupling. Sönnichsen and co-workers showed that when a single GNP was coupled to another immobilised single GNP



the plasmon peak showed an appreciable shift.⁸⁰ This was the basis for a whole new type of biosensor shown in Figure 2-9; the plasmon peak shift caused by the close proximity of the two particles allows the detection of a single binding event.^{81,82} The amount of plasmon peak shift depends on the proximity between particles as well as the size of both particles.⁸³

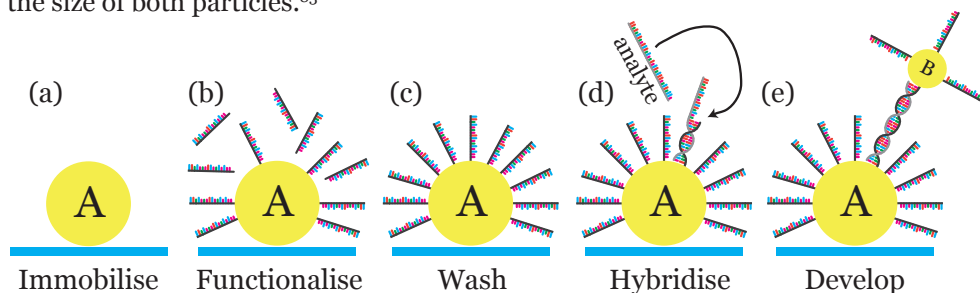


Figure 2-9: A two particle close proximity assay. (a) Large GNP A is immobilised on a glass surface and (b) functionalised with thiolated receptor strands. (c) After washing an active receptor is present on the surface. From the shift of the plasmon peak maximum the number of receptors on each GNP can be estimated. (d) Specific analyte hybridisation followed by amplification by (e) a hybridisation with a smaller functionalised GNP B. The close proximity of both GNPs allows single hybridisation event detection. Under darkfield conditions this can be monitored as a change from green to red of the GNP scattering colour.

Ideally, a surface is covered with thousands of functionalised GNPs, each with a known amount of receptor molecules. Subsequently, the total amount of receptors in the sensing area can be determined. In principle, a single event can be detected from a very large *known* number of receptors, thus a concentration of the analyte solution can be calculated.

2.3 Future technology, label-free sensing

The close proximity assay uses the 2nd GNP for amplification. However, this implies that the 2nd particle is used as a label. The trend in biosensing is towards multiplex label-free sensing of molecules. Conventional SPR imaging indeed allows label-free sensing of large molecules; however, the detection of low concentrations of smaller molecules still remains a challenge.

Ginger and co-workers showed an alternative approach based on the close proximity of two GNPs.⁸⁴ Two GNPs were bound together via DNA receptor strands with a hairpin-loop, thereby bringing the particles close to each other. The binding of the analyte around the hairpin-loop results in a stretched DNA receptor strand, causing an increase in the distance between the two particles. This could be seen as a blue shift of the plasmon peak of the individual particles. An advantage of this approach is that the number of receptors is known; moreover there is no additional label



since the second particle is incorporated, as depicted in Figure 2-10. Every GNP hybridisation pair consists of a single receptor strand, therefore on a darkfield image every GNP visible can only bind one target strand. The disadvantage is a low amount of total receptors in the sensing area. Compared to the close proximity assay where the receptor particle is able to host > 1,000 receptor strands depending on the GNP size, in this assay only one receptor strand per GNP can be active. This lowers the total number of receptors and therefore reduces the sensitivity.

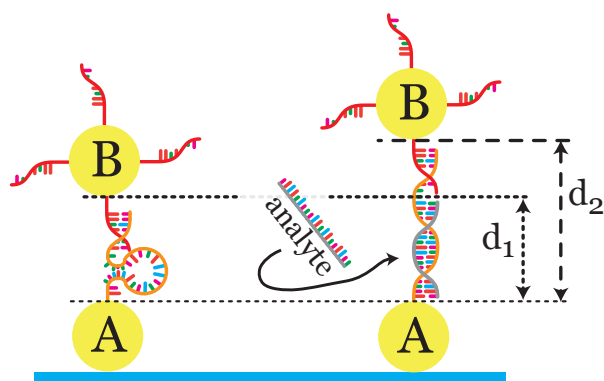


Figure 2-10: The label-free assay as published by Ginger *et al.* The GNPs are held together by a strand of DNA which has a hairpin-loop and therefore reduces the distance between the GNPs. Upon binding of the target strand the hairpin-loop opens and becomes a double helix strand which is longer. This increases the distance between the particles, resulting in less plasmon coupling between particles, and thus a blue shift of the plasmon peak. Under darkfield conditions this can be seen as a change from red to green of the GNP scattering colour.

An alternative label-free approach for single hybridisation event level detection can be based on the physical principles of a GNP close to a planar gold surface, as described by Mock and co-workers.⁸⁵ The basic principle is similar to the close proximity approach of two GNPs described previously. They describe that a GNP under darkfield conditions close to a planar gold surface exhibits plasmon coupling because of the GNP mirror image as shown in Figure 2-11.⁸⁶ This means that when the distance is reduced the plasmon peak shifts to the red. This can be translated to a sensor by having receptor strands fixed on the surface with a GNP attached on top. The receptor strand has an incorporated hairpin-loop which opens upon binding of the analyte. This results in an increased distance from the gold surface, and thus a blue shift of the plasmon peak. Unfortunately, also in this method the limiting factor is the amount of receptor strands which can be spaced on the planar gold surface in such a way that individual GNPs still can be monitored.

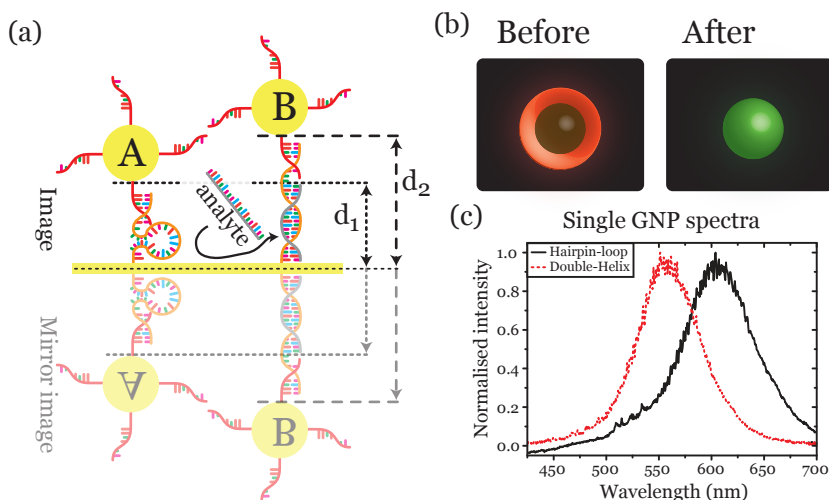


Figure 2-11: (a) Basic principle of the proximity assay. A GNP is tethered to the surface via ssDNA strands. Upon binding of the analyte the strand conformation changes to dsDNA which is shorter in length. Due to the gold layer the plasmon field of the particle sees itself in the mirror image, therefore this approach is similar to the close proximity approach of two GNPs. (b) Under darkfield conditions the scattering of the tethered particle is green and changes to a doughnut shape red upon binding of the analyte (simulated picture). The change in spectra (c) of the particle can be seen as a large shift in the red. In the assay it is a simple comparison between the image before and after analyte incubation. Adapted from Mock *et al.*⁸⁵

2.4 Conclusion

Each of the techniques described in this chapter has its advantages and disadvantages. The most important of these are summarised in Table 2-1.

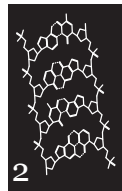
In summary, the use of gold nanoparticles has enhanced the detection of DNA in many ways by various approaches. In the future a label-free detection of DNA is certainly possible using GNPs. It will be sensitive as well, but many surface-related problems should be solved first. For labelled methods the close proximity of two particles seems most promising. An important improvement of GNP immobilisation will be the implementation of nano-imprint lithography methods where hundreds of thousands of GNP ‘patches’ in a regular pattern on a field of view of around $200 \times 200 \mu\text{m}^2$ can be fabricated,^{87,88} as opposed to the current method of random deposition of few hundreds of GNPs on the same sensing area. This will dramatically improve the sensitivity of the assay. An additional improvement could be the use of silver instead of gold, in view of the increased inherent silver plasmon sensitivity to a changing environment.⁸⁹

Table 2-1: A comparison of methods described in literature.

	Type	Principle	LOD	Advantages	Disadvantages	Ref.
1	DNA-DNA bond	Absorbance λ 260 nm	\sim 100 nM	Basic photo-spectrometer	No sequence specific detection	
2	q-PCR DNA amplification	Specific amplification	1 target strand	World wide accepted	Dedicated apparatus with fluorescent probes	
3	Flow through microarray	Fluorescent	1.6×10^4 cfu/ml	PCR free	Fluorescent probes	19
4	13 nm GNP aggregation	Standard Absorbance	\sim 100 pM	Analyte specific	Large sample volume	43
5	13 nm GNP aggregation	Standard Absorbance	100 pM	Basic photo-spectrometer	Large sample volume	16
6	50 and 100 nm GNP aggregation	Standard Absorbance	50 pM	Basic photo-spectrometer	Large sample volume	45
7	Site specific GNP aggregation	Dipstick / lateral flow	500 pM	Simple analysis method	Requires PCR step	17
8	Site specific carbon aggregation	Dipstick / lateral flow	10^4 cfu/ml	Simple analysis method	Requires PCR step	48,49
9	GNP capture + barcode amplification	Biobarcode scanner	7 aM	PCR free, very sensitive	Complex multistep procedure	52
10	Specific mRNA hybridisation (Cy3 + biotin labelled)	Gene expression microarray (GNP amplification)	1 ng (16 pg / μ l)	GNPs were able to detect $300 \times$ more compared to Cy3 at low concentration	Gene expression assay, less suitable for diagnostics Single colour only	53
11	Specific DNA-DNA hybridisation	Imaging SPR	10 nM	Label-free	Dedicated complex apparatus	58
12	Specific DNA-DNA hybridisation	Amplified Imaging SPR	10 pM	Simple and sensitive SPR DNA detection	Dedicated complex apparatus	70
13	Specific PNA-DNA hybridisation	Amplified Imaging SPR	1 fM	Simple and sensitive SPR DNA detection	Dedicated complex apparatus	69
14	Specific DNA-DNA hybridisation	Individual Biobarcode	8.3 pM	Simple method, simple microscope	Not fully developed	28
15	Specific DNA-DNA hybridisation	2 GNP close proximity	fM range	sub-fM possible, simple microscope	Not label-free	82
16	Specific DNA-DNA-hairpin hybridisation	2 GNP close proximity	\sim 10 pM	Label-free method, simple microscope	Limit of detection might be limited	84

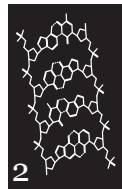
2.5 Bibliography

- (1) Watson J.D., Crick F.H.C. Molecular structure of nucleic acids: A structure for deoxyribose nucleic acid. *Nature* **1953**; *171*: 737-8.
- (2) Griffiths A.J.F., Gelbart W.M., Lewontin R.C., Miller J.H. *Modern Genetic Analysis*. 2nd ed. W.H. Freeman & Co Ltd: New York, **2002**. p. 736.
- (3) Mandelkern M. The dimensions of DNA in solution. *Journal of Molecular Biology* **1981**; *152*: 153-61.
- (4) Yoo O.J., Agarwal K.L. Cleavage of single strand oligonucleotides and bacteriophage phi X174 DNA by Msp I endonuclease. *Journal of Biological Chemistry* **1980**; *255*: 10559-62.
- (5) Roberts R.J. How restriction enzymes became the workhorses of molecular biology. *Proceedings of the National Academy of Sciences of the United States of America* **2005**; *102*: 5905-8.
- (6) Roberts R.J., Murray K. Restriction endonuclease. *Critical Reviews in Biochemistry & Molecular Biology* **1976**; *4*: 123-64.
- (7) Sanger F., Nicklen S., Coulson A.R. DNA sequencing with chain-terminating inhibitors. *Proceedings of the National Academy of Sciences of the United States of America* **1977**; *74*: 5463-7.
- (8) Kleppe K., Ohtsuka E., Kleppe R., Molineux I., Khorana H.G. Studies on polynucleotides: XCVI. Repair replication of short synthetic DNA's as catalyzed by DNA polymerases. *Journal of Molecular Biology* **1971**; *56*: 341-61.
- (9) Mullis K. *Dancing Naked in the Mind Fields*. Pantheon Books: New York, **1998**.
- (10) Saiki R., Gelfand D., Stoffel S., Scharf S., Higuchi R., Horn G., Mullis K., Erlich H. Primer-directed enzymatic amplification of DNA with a thermostable DNA polymerase. *Science* **1988**; *239*: 487-91.
- (11) NCBI. GenBank sequences from pandemic (H1N1) 2009 viruses. <http://www.ncbi.nlm.nih.gov/genomes/FLU/SwineFlu.html> (accessed Oct 1, 2010)
- (12) World Health Organisation. CDC protocol of realtime RTPCR for influenza A (H1N1). *Pandemic Control* **2009**; Document 1: 7.
- (13) Klostranec J.M., Chan W.C.W. Quantum dots in biological and biomedical research: Recent progress and present challenges. *Advanced Materials* **2006**; *18*: 1953-64.
- (14) Mirkin C.A., Letsinger R.L., Mucic R.C., Storhoff J.J. A DNA-based method for rationally assembling nanoparticles into macroscopic materials. *Nature* **1996**; *382*: 607-9.
- (15) Chan M. (World Health Organisation) *World now at the start of 2009 influenza pandemic* **2009**. p. 3.
- (16) Elghanian R., Storhoff J.J., Mucic R.C., Letsinger R.L., Mirkin C.A. Selective colorimetric detection of polynucleotides based on the distance-dependent optical properties of gold nanoparticles. *Science* **1997**; *277*: 1078-81.
- (17) Kalogianni D.P., Goura S., Aletras A.J., Christopoulos T.K., Chanos M.G., Christofidou M., Skoutelis A., Ioannou P.C., Panagiotopoulos E. Dry reagent dipstick test combined with 23S rRNA PCR for molecular diagnosis of bacterial infection in arthroplasty. *Analytical Biochemistry* **2007**; *361*: 169-75.
- (18) Gibson U.E., Heid C.A., Williams P.M. A novel method for real time quantitative RT-PCR. *Genome Research* **1996**; *6*: 995-1001.
- (19) Anthony R.M., Schuitema A.R.J., Oskam L., Klatser P.R. Direct detection of *Staphylococcus aureus* mRNA using a flow through microarray. *Journal of Microbiological Methods* **2005**; *60*: 47-54.



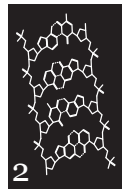
- 
- (20) Small J., Call D.R., Brockman F.J., Straub T.M., Chandler D.P. Direct detection of 16S rRNA in soil extracts by using oligonucleotide microarrays. *Applied & Environmental Microbiology* **2001**; 67: 4708-16.
- (21) Ginzinger D. Gene quantification using real-time quantitative PCR: An emerging technology hits the mainstream. *Experimental Hematology* **2002**; 30: 503-12.
- (22) Rouet F., Ekouevi D.K., Chaix M.L., Burgard M., Inwoley A., Tony T.D.A., Danel C., Anglaret X., Leroy V., Msellati P., Dabis F., Rouzioux C. Transfer and evaluation of an automated, low-cost real-time reverse transcription-PCR test for diagnosis and monitoring of human immunodeficiency virus type 1 infection in a West African resource-limited setting. *Journal of Clinical Microbiology* **2005**; 43: 2709-17.
- (23) Southern E. Detection of specific sequences among DNA fragments separated by gel electrophoresis. *Journal of Molecular Biology* **1975**; 98: 503-17.
- (24) Song L., Ahn S., Walt D.R. Fiber-optic microsphere-based arrays for multiplexed biological warfare agent detection. *Analytical Chemistry* **2006**; 78: 1023-33.
- (25) Ferguson J.A., Boles T.C., Adams C.P., Walt D.R. A fiber-optic DNA biosensor microarray for the analysis of gene expression. *Nature Biotechnology* **1996**; 14: 1681-4.
- (26) Azek F., Grossiord C., Joannes M., Limoges B., Brossier P. Hybridization assay at a disposable electrochemical biosensor for the attomole detection of amplified human cytomegalovirus DNA. *Analytical Biochemistry* **2000**; 284: 107-13.
- (27) Lucarelli F., Marrazza G., Mascini M. Enzyme-based impedimetric detection of PCR products using oligonucleotide-modified screen-printed gold electrodes. *Biosensors & Bioelectronics* **2005**; 20: 2001-9.
- (28) Schultz S., Smith D.R., Mock J.J., Schultz D.A. Single-target molecule detection with nonbleaching multicolor optical immunolabels. *Proceedings of the National Academy of Sciences of the United States of America* **2000**; 97: 996-1001.
- (29) Oldenburg S.J., Schultz D. Optically detectable colloidal metal labels: properties, methods, and biomedical applications. *Topics in Fluorescent Spectroscopy* **2005**; 8: 333-51.
- (30) Lalander C.H., Zheng Y., Dhuey S., Cabrini S., Bach U. DNA-directed self-assembly of gold nanoparticles onto nanopatterned surfaces: controlled placement of individual nanoparticles into regular arrays. *ACS Nano* **2010**; 4: 6153-61.
- (31) Shlyapnikov Y.M., Shlyapnikova E.A., Morozova T.Y., Beletsky I.P., Morozov V.N. Detection of microarray-hybridized oligonucleotides with magnetic beads. *Analytical Biochemistry* **2010**; 399: 125-31.
- (32) Mannelli I., Minunni M., Tombelli S., Wang R., Michela Spiriti M., Mascini M. Direct immobilisation of DNA probes for the development of affinity biosensors. *Bioelectrochemistry* **2005**; 66: 129-38.
- (33) Yao X., Li X., Toledo F., Zurita-Lopez C., Gutova M., Momand J., Zhou F. Subattomole oligonucleotide and p53 cDNA determinations via a high-resolution surface plasmon resonance combined with oligonucleotide-capped gold nanoparticle signal amplification. *Analytical Biochemistry* **2006**; 354: 220-8.
- (34) Taton T.A., Mirkin C.A., Letsinger R.L. Scanometric DNA array detection with nanoparticle probes. *Science* **2000**; 289: 1757-60.
- (35) Yguerabide J., Yguerabide E.E. Light-scattering submicroscopic particles as highly fluorescent analogs and their use as tracer labels in clinical and biological applications. *Analytical Biochemistry* **1998**; 262: 157-76.
- (36) Liu X., Atwater M., Wang J., Huo Q. Extinction coefficient of gold nanoparticles with different sizes and different capping ligands. *Colloids & Surfaces B: Biointerfaces* **2007**; 58: 3-7.

- (37) Jain P.K., Lee K.S., El-Sayed I.H., El-Sayed M.A. Calculated absorption and scattering properties of gold nanoparticles of different size, shape, and composition: applications in biological imaging and biomedicine. *The Journal of Physical Chemistry B* **2006**; *110*: 7238-48.
- (38) Liandris E., Gazouli M., Andreadou M., Comor M., Abazovic N., Sechi L.A., Ikononopoulos J. Direct detection of unamplified DNA from pathogenic mycobacteria using DNA-derivatized gold nanoparticles. *Journal of Microbiological Methods* **2009**; *78*: 260-4.
- (39) Zhu X., Liu Y., Yang J., Liang Z., Li G. Gold nanoparticle-based colorimetric assay of single-nucleotide polymorphism of triplex DNA. *Biosensors & Bioelectronics* **2010**; *25*: 2135-9.
- (40) Storhoff J.J., Elghanian R., Mucic R.C., Mirkin C.A., Letsinger R.L. One-pot colorimetric differentiation of polynucleotides with single base imperfections using gold nanoparticle probes. *Journal of the American Chemical Society* **1998**; *120*: 1959-64.
- (41) Ding C., Wang Z., Zhong H., Zhang S. Ultrasensitive chemiluminescence quantification of single-nucleotide polymorphisms by using monobase-modified Au and CuS nanoparticles. *Biosensors & Bioelectronics* **2010**; *25*: 1082-7.
- (42) Cao Y.C., Jin R., Thaxton C.S., Mirkin C.A. A two-color-change, nanoparticle-based method for DNA detection. *Talanta* **2005**; *67*: 449-55.
- (43) Chen S.H., Lin K.I., Tang C.Y., Peng S.L., Chuang Y.C., Lin Y.R., Wang J.P., Lin C.S. Optical detection of human papillomavirus type 16 and type 18 by sequence sandwich hybridization with oligonucleotide-functionalized Au nanoparticles. *IEEE Transactions on Nanobioscience* **2009**; *8*: 120-31.
- (44) Bai X., Shao C., Han X., Li Y., Guan Y., Deng Z. Visual detection of sub-femtomole DNA by a gold nanoparticle seeded homogeneous reduction assay: toward a generalized sensitivity-enhancing strategy. *Biosensors & Bioelectronics* **2010**; *25*: 1984-8.
- (45) Reynolds R.A., Mirkin C.A., Letsinger R.L. Homogeneous, nanoparticle-based quantitative colorimetric detection of oligonucleotides. *Journal of the American Chemical Society* **2000**; *122*: 3795-6.
- (46) Toubanaki D.K., Christopoulos T.K., Ioannou P.C., Flordellis C.S. Identification of single-nucleotide polymorphisms by the oligonucleotide ligation reaction: a DNA biosensor for simultaneous visual detection of both alleles. *Analytical Chemistry* **2009**; *81*: 218-24.
- (47) Elenis D.S., Ioannou P.C., Christopoulos T.K. A nanoparticle-based sensor for visual detection of multiple mutations. *Nanotechnology* **2011**; *22*: 155501-10.
- (48) Noguera P., Posthuma-Trumpie G., van Tuil M., van der Wal F.J., de Boer A., Moers A.P.H.A., van Amerongen A. Carbon nanoparticles in lateral flow methods to detect genes encoding virulence factors of Shiga toxin-producing *Escherichia coli*. *Analytical & Bioanalytical Chemistry* **2011**; *399*: 831-8.
- (49) Posthuma-Trumpie G., Korf J., van Amerongen A. Lateral flow (immuno)assay: its strengths, weaknesses, opportunities and threats. A literature survey. *Analytical & Bioanalytical Chemistry* **2009**; *393*: 569-82.
- (50) Nam J.M., Stoeva S.I., Mirkin C.A. Bio-bar-code-based DNA detection with PCR-like sensitivity. *Journal of the American Chemical Society* **2004**; *126*: 5932-3.
- (51) Hill H.D., Mirkin C.A. The bio-barcode assay for the detection of protein and nucleic acid targets using DTT-induced ligand exchange. *Nature Protocols* **2006**; *1*: 324-36.
- (52) Thaxton C.S., Hill H.D., Georganopoulou D.G., Stoeva S.I., Mirkin C.A. A bio-bar-code assay based upon dithiothreitol-induced oligonucleotide release. *Analytical Chemistry* **2005**; *77*: 8174-8.



- (53) Bao P., Frutos A.G., Greef C., Lahiri J., Muller U., Peterson T.C., Warden L., Xie X. High-sensitivity detection of DNA hybridization on microarrays using resonance light scattering. *Analytical Chemistry* **2002**; *74*: 1792-7.
- (54) Schasfoort R., Tudos A. *Handbook of Surface Plasmon Resonance*. Royal Society of Chemistry: Cambridge, **2008**. p. 403.
- (55) Samoc A., Miniewicz A., Samoc M., Grote J.G. Refractive-index anisotropy and optical dispersion in films of deoxyribonucleic acid. *Journal of Applied Polymer Science* **2007**; *105*: 236-45.
- (56) Davis T.M., Wilson W.D. Determination of the refractive index increments of small molecules for correction of surface plasmon resonance data. *Analytical Biochemistry* **2000**; *284*: 348-53.
- (57) Lao A.I.K., Su X., Aung K.M.M. SPR study of DNA hybridization with DNA and PNA probes under stringent conditions. *Biosensors & Bioelectronics* **2009**; *24*: 1717-22.
- (58) Nelson B.P., Grimsrud T.E., Liles M.R., Goodman R.M., Corn R.M. Surface plasmon resonance imaging measurements of DNA and RNA hybridization adsorption onto DNA microarrays. *Analytical Chemistry* **2001**; *73*: 1-7.
- (59) Jin-Lee H., Goodrich T.T., Corn R.M. SPR imaging measurements of 1-D and 2-D DNA microarrays created from microfluidic channels on gold thin films. *Analytical Chemistry* **2001**; *73*: 5525-31.
- (60) Wark A.W., Lee H.J., Corn R.M. Long-range surface plasmon resonance imaging for bioaffinity sensors. *Analytical Chemistry* **2005**; *77*: 3904-7.
- (61) Jordan C.E., Corn R.M. Surface plasmon resonance imaging measurements of electrostatic biopolymer adsorption onto chemically modified gold surfaces. *Analytical Chemistry* **1997**; *69*: 1449-56.
- (62) Besselink G.A.J., Kooyman R.P.H., van Os P.J.H.J., Engbers G.H.M., Schasfoort R.B.M. Signal amplification on planar and gel-type sensor surfaces in surface plasmon resonance-based detection of prostate-specific antigen. *Analytical Biochemistry* **2004**; *333*: 165-73.
- (63) Goodrich T.T., Lee H.J., Corn R.M. Enzymatically amplified surface plasmon resonance imaging method using RNase H and RNA microarrays for the ultrasensitive detection of nucleic acids. *Analytical Chemistry* **2004**; *76*: 6173-8.
- (64) Brockman J.M., Frutos A.G., Corn R.M. A multistep chemical modification procedure to create DNA arrays on gold surfaces for the study of protein-DNA interactions with surface plasmon resonance imaging. *Journal of the American Chemical Society* **1999**; *121*: 8044-51.
- (65) McFarland A.D., Haynes C.L., Mirkin C.A., van Duyne R.P., Godwin H.A. Color my nanoworld. *Journal of Chemical Education* **2004**; *81*: 544A.
- (66) Kimling J., Maier M., Okenve B., Kotaidis V., Ballot H., Plech A. Turkevich method for gold nanoparticle synthesis revisited. *The Journal of Physical Chemistry B* **2006**; *110*: 15700-7.
- (67) Willets K., van Duyne R.P. Localized surface plasmon resonance spectroscopy and sensing. *Annual Review of Physical Chemistry* **2007**; *58*: 267-97.
- (68) D'Agata R., Corradini R., Grasso G., Marchelli R., Spoto G. Ultrasensitive detection of DNA by PNA and nanoparticle-enhanced surface plasmon resonance imaging. *ChemBioChem* **2008**; *9*: 2067-70.
- (69) D'Agata R., Corradini R., Ferretti C., Zanolli L., Gatti M., Marchelli R., Spoto G. Ultrasensitive detection of non-amplified genomic DNA by nanoparticle-enhanced surface plasmon resonance imaging. *Biosensors & Bioelectronics* **2010**; *25*: 2095-100.

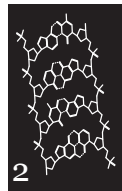
- (70) He L., Musick M.D., Nicewarner S.R., Salinas F.G., Benkovic S.J., Natan M.J., Keating C.D. Colloidal Au-enhanced surface plasmon resonance for ultrasensitive detection of DNA hybridization. *Journal of the American Chemical Society* **2000**; *122*: 9071-7.
- (71) Brockman J.M., Nelson B.P., Corn R.M. Surface plasmon resonance imaging measurements of ultrathin organic films. *Annual Review of Physical Chemistry* **2000**; *51*: 41-63.
- (72) Li Y., Wark A.W., Lee H.J., Corn R.M. Single-nucleotide polymorphism genotyping by nanoparticle-enhanced surface plasmon resonance imaging measurements of surface ligation reactions. *Analytical Chemistry* **2006**; *78*: 3158-64.
- (73) Brinkers S., Dietrich H.R.C., de Groote F.H., Young I.T., Rieger B. The persistence length of double stranded DNA determined using dark field tethered particle motion. *The Journal of Chemical Physics* **2009**; *130*: 215105.
- (74) Ungureanu F., Wasserberg D., Yang N., Verdoold R., Kooyman R.P.H. Immunosensing by colorimetric darkfield microscopy of individual gold nanoparticle-conjugates. *Sensors & Actuators: B Chemical* **2010**; *150*: 529-36.
- (75) Ungureanu F., Halamek J., Verdoold R., Kooyman R.P.H. The use of a colour camera for quantitative detection of protein-binding nanoparticles. *Proceedings of SPIE* **2009**; *7192*: 71920O.
- (76) Oldenburg S.J., Genick C.C., Clark K., Schultz D. Base pair mismatch recognition using plasmon resonant particle labels. *Analytical Biochemistry* **2002**; *309*: 109-16.
- (77) Taton T.A., Lu G., Mirkin C.A. Two-color labeling of oligonucleotide arrays via size-selective scattering of nanoparticle probes. *Journal of the American Chemical Society* **2001**; *123*: 5164-5.
- (78) Sannomiya T., Sahoo P.K., Mahcicek D.I., Solak H.H., Hafner C., Grieshaber D., Vörös J. Biosensing by densely packed and optically coupled plasmonic particle arrays. *Small* **2009**; *5*: 1889-96.
- (79) Verdoold R., Ungureanu F., Wasserberg D., Kooyman R.P.H. Gold nanoparticle assays: towards single molecule unamplified DNA detection. *Proceedings of SPIE* **2009**; *7312*: 73120N.
- (80) Sönnichsen C., Reinhard B.M., Liphardt J., Alivisatos A.P. A molecular ruler based on plasmon coupling of single gold and silver nanoparticles. *Nature Biotechnology* **2005**; *23*: 741-5.
- (81) Sannomiya T., Hafner C., Voros J. In situ sensing of single binding events by localized surface plasmon resonance. *Nano Letters* **2008**; *8*: 3450-5.
- (82) Xiao L., Wei L., He Y., Yeung E.S. Single molecule biosensing using color coded plasmon resonant metal nanoparticles. *Analytical Chemistry* **2010**; *82*: 6308-14.
- (83) Reinhard B.M., Siu M., Agarwal H., Alivisatos A.P., Liphardt J. Calibration of dynamic molecular rulers based on plasmon coupling between gold nanoparticles. *Nano Letters* **2005**; *5*: 2246-52.
- (84) Chen J.I.L., Chen Y., Ginger D.S. Plasmonic nanoparticle dimers for optical sensing of DNA in complex media. *Journal of the American Chemical Society* **2010**; *132*: 9600-1.
- (85) Mock J.J., Hill R.T., Degiron A., Zauscher S., Chilkoti A., Smith D.R. Distance-dependent plasmon resonant coupling between a gold nanoparticle and gold film. *Nano Letters* **2008**; *8*: 2245-52.
- (86) Knight M.W., Wu Y., Lassiter J.B., Nordlander P., Halas N.J. Substrates matter: influence of an adjacent dielectric on an individual plasmonic nanoparticle. *Nano Letters* **2009**; *9*: 2188-92.
- (87) Lee S.W., Lee K.S., Ahn J., Lee J.J., Kim M.G., Shin Y.B. Highly sensitive biosensing



using arrays of plasmonic Au nanodisks realized by nanoimprint lithography. *ACS Nano* **2011**; *5*: 897-904.

- (88) Chen S., Svedendahl M., Duyne R.P.V., Käll M. Plasmon-enhanced colorimetric ELISA with single molecule sensitivity. *Nano Letters* **2011**; *11*: 1826-30.
- (89) Hall W.P., Ngatia S.N., Van Duyne R.P. LSPR biosensor signal enhancement using nanoparticle-antibody conjugates. *The Journal of Physical Chemistry C* **2011**; *115*: 1410-4.







Chapter 3

Chemistry in DNA sensing



In physics we can model, calculate and/or approximate; this is not the case with immobilisation/functionalisation chemistry. In order to get the chemistry working, a lot of trial and error is required and sometimes luck and coincidence. A number of practical aspects are now under control, not only because of luck and coincidence, but above all because we kept trying. With this knowledge it was possible to assemble a functioning sensing system, as well as to teach others, in order to avoid re-inventing the wheel.

In this chapter the chemical components of a biosensor are explained. In particular, we describe how these components can be put together in a working manner. First, various surface coatings and modifications are described. Subsequently, we describe how gold nanoparticles (GNPs) can be functionalised and used for sensing. Finally, various incubation methods are outlined for use with an optical microscope system. We present in each section protocols describing the basics for surface modifications, gold nanoparticle functionalisation, and flow-cell fabrication, respectively.

Parts of the results from this chapter have been published in Proceedings of SPIE, *Proceedings of SPIE* **2009**; 7312: 73120N; DOI:10.1117/12.818120

3.1 Introduction

Every type of chemical sensor has to contain a specific receptor molecule which should remain active towards a specific target ('analyte') molecule, once immobilised on the sensor surface. Additionally, many detection systems need a special surface suitable for the method of detection. Liquid handling is necessary in order to guide the sample, containing the analyte, over the sensor surface. This chapter describes in more detail a few relevant aspects of constructing a biosensor focussing mainly on gold nanoparticle based biosensing. Surface plasmon resonance (SPR) is an alternative detection method that can be used. The planar gold SPR sensor allows studying surface cross-linking methods which could work on the surface of gold nanoparticles as well.

Biomolecular interactions take place on the surface of the sensor. The sensor generally consists of four basic components: (a) the substrate, (b) linker layer, (c) immobilisation matrix and (d) the receptor molecules. The immobilisation matrix is not always present or is sometimes incorporated in the linkage layer. These layers are illustrated in Figure 3-1. Each of these components must be selected with great care, otherwise the detection assay might not work at all or not work optimally. In gold nanoparticle (GNP) based sensors, multiple layers are present which will be described in this chapter.

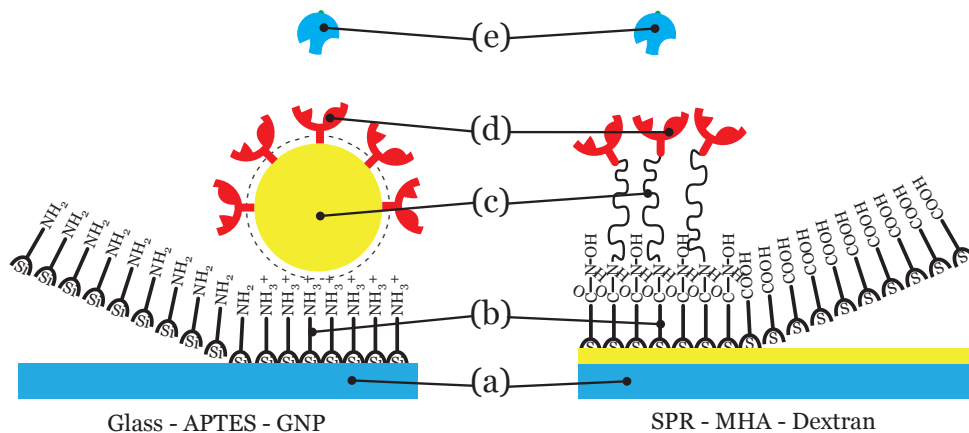


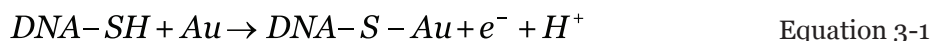
Figure 3-1: The components of a biosensor: (a) the substrate with a self-assembled monolayer (SAM) of (b) the linker, followed by (c) the matrix on which (d) the receptor is immobilised. The receptor is oriented for optimal binding to (e) the analyte. In the left panel, a gold nanoparticle is used as matrix on APTES coated glass. On the right, a SPR sensor surface is coated with 6-mercaptopropionic acid (MHA) followed by a dextran matrix on which the receptors are immobilized.

3.2 Sensing surfaces

3.2.1 Active triethoxy-silane surfaces

A transparent substrate is preferred for microscope based measurements, but is not necessary when working with a reflection setup. For darkfield GNP measurements on a surface, we could work either in transmission or reflection mode, therefore standard microscope slides were used as a substrate. Various linker layers were considered for immobilisation of the GNPs. 3-Aminopropyl-triethoxy-silane (APTES)¹⁻⁴ and 3-Mercaptopropyl-triethoxy-silane (MPTES)^{5,6} are both triethoxy-silane based linkers which can be silanised to a surface which presents hydroxyl groups. These groups can be found on glass, mica and metal-oxide surfaces. Cleaning the surface with a strong acid and hydrogen peroxide will result in a hydroxyl active surface. The silanisation process (Figure 3-2) results in a self-assembled monolayer (SAM) of the triethoxy-silane molecules.^{1,7} SAMs are highly organised single molecule layers. The difference between the linkers is the reactive end group: amine for APTES and thiol for MPTES. Both APTES and MPTES are suitable for the immobilisation of citrate capped GNPs. The amine end-groups from an APTES layer will have a positive charge upon positive ionization ($-\text{NH}_3^+$), while the citrate cap on the GNP will remain negatively charged to prevent aggregation. The GNPs can therefore attach non-specifically using electrostatic interactions with the surface.⁸ The free amine groups can be capped by acetyl groups to reduce non-specific binding of other molecules at a later stage in the surface modification or during the assay.^{9,10}

The thiol groups of a MPTES layer can bind GNPs via chemisorption,⁵ resulting in a near-covalent bond as shown in Equation 3-1.



This general approach is widely used for functionalisation of gold surfaces.^{11,12} The silanisation of a glass surface in wet phase is described in Protocol 3-1.



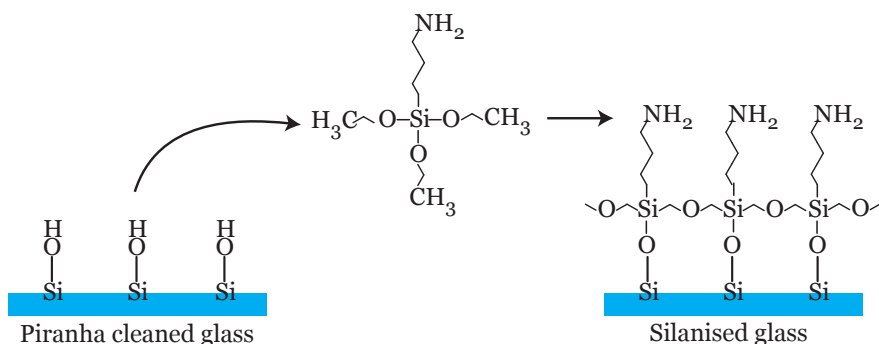


Figure 3-2: Silanisation process of APTES to glass. After cleaning of glass by piranha the $-\text{OH}$ groups are activated. Triethoxy-silanes, such as APTES, can form a SAM and after a baking step the cross-linking is finalised. The reactive group of APTES as illustrated here is $-\text{NH}_2$, and a $-\text{SH}$ group in MPTES.

Protocol 3-1: Wet phase silanisation of glass surface

1. Place the glass slides in a holder and sonicate them for 15 minutes in MilliQ water. This is done to remove small insoluble debris from glass fabrication.
2. Prepare a piranha solution by mixing 1 part cold H_2O_2 (35%) to 3 parts H_2SO_4 (>96%). The temperature will increase to 95 °C (Caution! Piranha solution is highly corrosive). Rest the solution for five minutes and then incubate the slides in it for 15 minutes.
3. Sonicate the slides again for 15 minutes in MilliQ water.
4. Prepare a 5% APTES or MPTES solution in pure ethanol and transfer the slides from the water to the APTES or MPTES solution without drying and incubate for 15 minutes.
5. Wash the slides with MilliQ water and sonicate with MilliQ water for 15 minutes.
6. Rinse the slides with MilliQ water and place them in oven at 120 °C for two hours.

Silanised slides can be used up to two days after preparation; it is advised to use them immediately after baking. Slides can be cooled in a flow of filtered nitrogen gas.

Random immobilisation of GNPs on a fresh APTES layer is easy.¹³ The GNPs in this sensor approach also act as immobilisation matrix since they will support the receptor molecules. However, for the immobilisation of the receptor molecules they appear as the substrate, thus a multiple layer sensor system has to be constructed. The number of GNPs on the surface is regulated by the concentration of the GNP solution and the time of incubation. The optimal average distribution of GNPs for darkfield microscope imaging at 40× magnification is one particle per 20 to 70

μm^2 . This results in a field of view with 500 to 2,000 particles that can easily be distinguished individually, which consequently facilitates further image analysis. The step-by-step procedure for GNP immobilisation on APTES and MPTES surfaces is described in Protocol 3-2. After immobilisation of GNPs the remaining surface can be blocked with APTES-reactive molecules. Acetic anhydride will deprotonate the surface resulting in covalently bound acetyl groups.⁹ Alternatively, bovine serum albumin (BSA) can be used, although it also adsorbs non-specifically to the surface of the GNPs; thus it is not suited for application after the immobilisation step of bare GNPs. After immobilisation on the surface, bare GNPs are ready for functionalisation with receptor molecules.

Protocol 3-2: Immobilisation of GNPs on APTES and MPTES

• APTES surface

1. Prepare a 25 ml diluted GNP solution in a petri dish by diluting citrate capped GNPs in MilliQ water to a concentration of 4.0×10^{-13} M for 60 and 80 nm GNPs.
2. Place a fresh APTES slide in the petri dish and submerge it, incubate for ten minutes on an orbital shaker.
3. Wash the slide with MilliQ water and dry with filtered nitrogen gas.

The remaining amine groups should be blocked to reduce non-specific binding. This can be done with various molecules, e.g., acetic anhydride, BSA or other protein.

4. Incubate the surface with 10% v/v acetic anhydride for ten minutes.
5. Wash with MilliQ water and dry the surface with filtered nitrogen gas.

• MPTES surface

1. Prepare a 25 ml diluted GNP solution in a petri dish by diluting citrate capped GNPs in MilliQ water to a concentration of 4.0×10^{-13} M for 60 and 80 nm GNPs.
2. Place a fresh MPTES slide in the petri dish and submerge it, incubate for 24 hours on an orbital shaker.
3. Wash the slide with MilliQ water and dry with filtered nitrogen gas.

The remaining -S groups should be blocked to reduce non-specific binding by incubating with BSA or other protein.

4. Incubate the surface with 10% w/v BSA for one hour.
5. Wash with MilliQ water and dry the surface with filtered nitrogen gas.

Gold coated slides can be stored under vacuum or nitrogen gas.



3.2.2 Active streptavidin based surface

As an alternative to the APTES or MPTES surfaces, *pre-functionalised* GNPs can be immobilised onto a streptavidin surface. Streptavidin is a tetrameric protein with a molecular mass of ~ 53 kDa and has an extraordinarily high affinity of $\sim 1 \times 10^{14}$ M⁻¹ for biotin.¹⁴⁻¹⁶ In addition to the high affinity, the streptavidin-biotin complex is resistant to denaturants and detergents often used in biological sensors. Moreover, it is also stable at high temperatures and over a wide range of pH.^{17,18} However, the bond with biotin is reversible at elevated temperatures.¹⁹ Traditionally streptavidin is immobilised on a surface via a linker to obtain a homogeneous monolayer.²⁰ A single streptavidin protein can be bound by four biotin molecules; therefore, when streptavidin is immobilised on a surface there is a high probability that at least one binding site is active. The method of applying biotinylated receptor molecules or functionalised GNPs to a streptavidin surface is described in Protocol 3-3. The streptavidin ‘Lego’ chemistry is depicted in Figure 3-3.

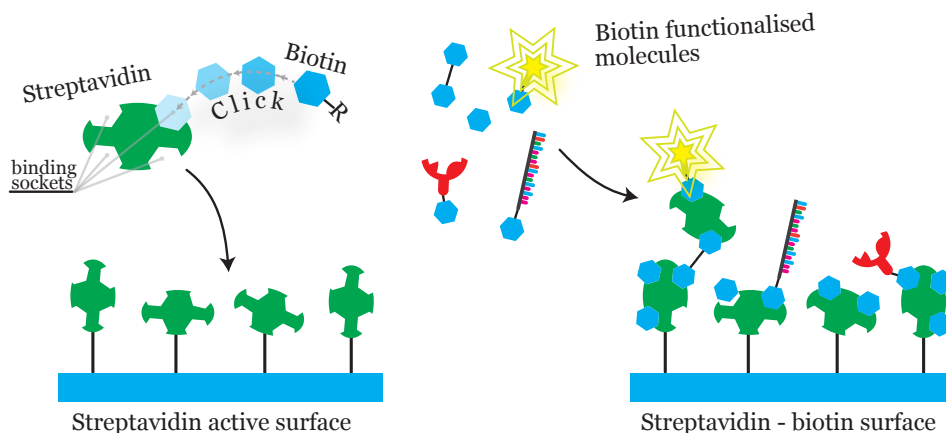


Figure 3-3: Streptavidin as functional receptor for immobilising any biotin labelled molecule, e.g., proteins, fluorophores and DNA. Each streptavidin has four binding sites for biotin. Not all binding sites might be available when immobilised on a surface. Free biotin molecules are used to fill the empty locations.

By using a biotin or streptavidin surface, it is possible to immobilise functionalised GNPs.^{21,22} An advantage of this approach over bare GNP immobilisation (as in APTES) is the storage possibility in a dry state. This is a desirable property for commercialisation of the assembled sensor chips.

Protocol 3-3: Binding of biotinylated molecules or GNPs on streptavidin surface

1. Prior to use, bring the (commercial) streptavidin slide to room temperature.
2. Rinse the surface with the sample buffer. In order to reduce the surface tension of the buffer, 0.01% of a detergent such as Tween-20 or SDS may be added (if the samples allow the use of detergents).
3. Add the biotin samples on the slide using a flow cell, spotter or microwells and incubate for 15 minutes at room temperature.
4. Wash the slide with the sample buffer.

The free streptavidin sites should be blocked to reduce any non-specific binding. This can be done with various biotinylated molecules, e.g., biotin-BSA, biotin-PEG or biotin.

5. Incubate the biotinylated blocking molecule at a concentration of $<1 \mu\text{M}$ for 15 minutes.
6. Wash with the sample buffer. If necessary (possible), dry the surface with filtered nitrogen gas.

Note that the biotin-streptavidin is non-covalent, therefore a high concentration of the blocking agent might replace the immobilised samples.

**3.2.3 Gold coated surface**

A planar gold surface forms the basis of the surface plasmon resonance (SPR) sensor. The gold layer usually has a thickness of ~ 50 nm, which is still transparent and therefore suitable for microscopy. An advantage of the gold layer is the possibility to use thiol based linkers such as cysteamine,²³⁻²⁵ 6-mercapto-hexanoic acid (MHA) and longer mercapto acid based molecules.^{26,27} Incubation with cysteamine results in a monolayer similar to APTES with free amine end groups. Onto this monolayer bare GNPs can be immobilised as on APTES. However, an intermediate linker, e.g., glutaraldehyde (GA), is needed to immobilise protein or amine-functionalised DNA strands directly.^{28,29} Incubation with MHA results in a monolayer with carboxylic acid end groups that are suitable for covalent coupling of proteins or amine-functionalised DNA strands via EDC/NHS chemistry (1-ethyl-3-(3-dimethylaminopropyl) carbodiimide) / N-hydroxysuccinimide).^{30,31} The linkage of streptavidin onto a functionalised gold surface enables simple immobilisation of antibodies and DNA strands.^{32,33} Various surface modifications are illustrated in Figure 3-4. A planar gold surface is very versatile and it is an ideal reaction surface for SPR. In Protocol 3-4 the thiol chemistry based functionalisation of a planar gold surface is described.

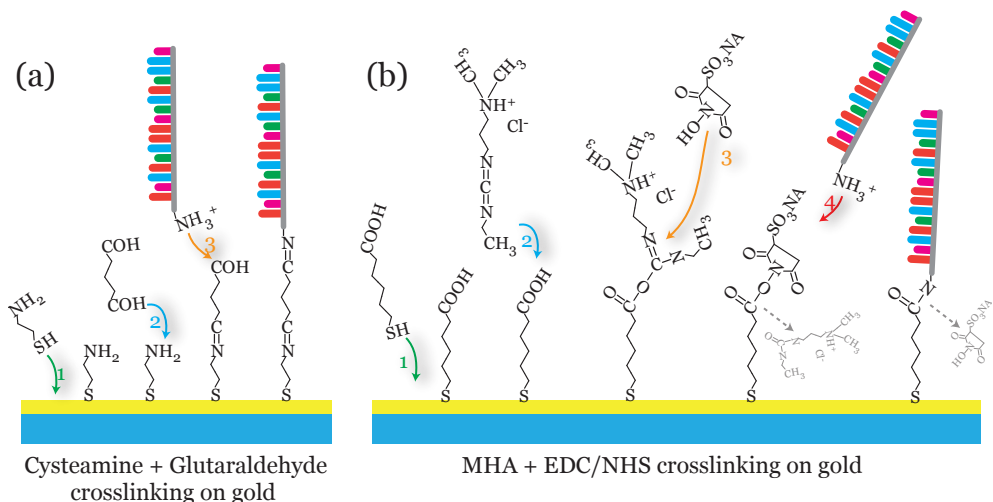


Figure 3-4: (a) Immobilisation of an amine functionalised DNA receptor molecule onto a planar gold surface via cysteamine and glutaraldehyde cross-linking. (b) Immobilisation strategy using MHA and EDC/NHS chemistry. Usually step 2 and 3 are combined in a single incubation step. Any molecule with free $-NH_2$ groups can be covalently bound to the surface, like the amine functionalised DNA strand.

Protocol 3-4: Planar gold functionalisation with thiol-molecules

1. Wash the sensor slide with MilliQ water.
2. Prepare a piranha solution by mixing 1 part cold H_2O_2 (35%) to 3 parts H_2SO_4 (>96%) the temperature will increase to 95 °C (Caution! Piranha solution is highly corrosive). Rest the solution for 5 minutes and then incubate the slides in it for one minute. Alternatively, oxygen plasma can be used for one minute to clean the slide.
3. Wash the sensor with MilliQ water and check hydrophobicity: the surface should be very hydrophilic. Dry the surface with nitrogen gas.
4. Prepare a 1 μM MHA solution in 10% ethanol or 1 μM cysteamine solution in PBS and incubate overnight in a humidity chamber.
5. Wash the surface with the desired buffer or MilliQ water.

The MHA monolayer can be used for EDC/NHS coupling and the cysteamine for GNP immobilisation or further coupling via glutaraldehyde. Step 4 can be replaced with 1 μM thiol-DNA 1 M KH_2PO_4 , pH 3.8, with one hour incubation step at room temperature.

For GNP based sensors the following procedure can be used: GNPs are immobilised on the APTES surface, followed by GNP functionalisation with thiolated DNA strands. This is the opposite for the streptavidin surfaces: in this case, prior to immobilisation on the surface, GNPs are functionalised in solution of DNA with and without biotin. Both approaches are illustrated in Figure 3-5. In passing, we note that planar gold

surfaces were used in SPR assays to check the binding affinity of molecules and to check the chemical approaches since the surface is similar to that of a GNP. This approach is depicted in Figure 3-5c. In addition, the use of GNPs in an SPR assay can drastically improve the sensitivity. The mass of a single GNP is many times higher compared to that of the molecule of interest. Using GNPs as mass labels in a SPR assay will especially improve the detection of low molecular weight molecules.

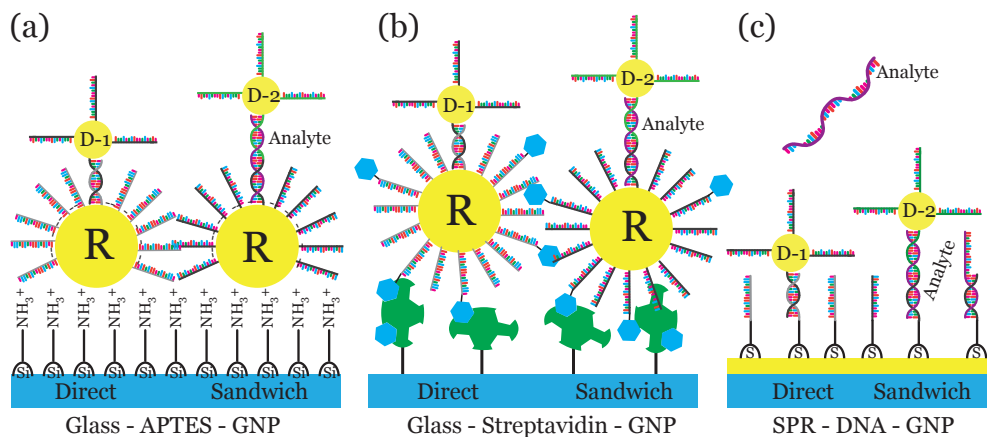


Figure 3-5: Illustration of various sensing approaches: (a) GNP scattering via APTES immobilisation, (b) GNP scattering via streptavidin immobilisation and (c) amplified SPR analysis of DNA. All assays can be performed directly or as sandwich using a target strand. The large GNP (R) is the receptor and the smaller GNP (D-1 and D-2) is the developer. D-1 directly binds the receptor and D-2 binds the analyte captured by the receptor. In a direct assay the quality of the receptor GNP (or molecule) is tested, whereas in a sandwich assay an analyte or target strand can be detected. (Note: the two GNP detection assay is further described in Chapters 4 and 6).

3.2.4 Surface modification experiments

3.2.4.1 Glass-APTES surface results

The APTES coating procedure was developed and improved. The sonication step prior to piranha cleaning was essential to remove debris and large dust particles from the glass substrate. The piranha solution removes smaller contaminants and activates the $-OH$ groups on the glass surface. The second sonication step dilutes the piranha residues before APTES coating. It was found that the washing steps after coating ensure a good APTES monolayer and therefore are essential to the procedure. In Figure 3-6 APTES coated glass slides with GNPs are shown by various imaging methods. Under darkfield conditions the APTES layer can be seen as a homogeneous black background when submerged in an aqueous solution. Rapid

chilling of an APTES coated glass slide resulted in damage of the layer, which was visible as large, bright flaky structures in the coating. Additionally, scanning electron microscopy (SEM) and atomic force microscopy (AFM) analysis were performed to study the APTES surface with GNPs.

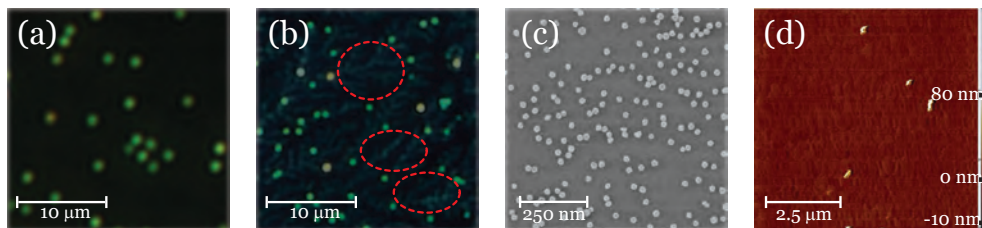


Figure 3-6: (a) Darkfield image of 80 nm GNPs on APTES, (b) darkfield image of 60 nm GNPs on damaged APTES (damaged APTES is indicated by red circles), (c) HR-SEM image of high density 60 nm GNPs on APTES and (d) AFM image of 80 nm GNPs on APTES.

The electrostatic immobilisation of citrate capped GNPs on the APTES surface could be controlled by varying the incubation time and the GNP concentration. Aggregation of GNPs occurred when the incubation time was too long. Most aggregates present on the APTES surface were already aggregated in solution.

As an alternative to functionalisation in solution, GNPs were immobilised on an APTES surface followed by functionalisation with thiol-DNA molecules. An advantage of this approach is the reduced aggregation. Immobilised GNPs remained on the surface even when incubated with NaCl concentrations of up to 1 M NaCl.

We also considered immobilisation on a MPTES coated substrate. However, the binding of bare GNPs on such a surface was significantly slower compared to that on an APTES coated surface. An advantage of the MPTES surface would be a near-covalent bond between the GNP and the surface which ensures the position of the GNP. But also on an APTES coated substrate we found that immobilised GNPs remained on the surface, even after incubation with high ionic strength buffers and during SEM measurements. A second drawback of MPTES is that thiol-DNA molecules can bind with the MPTES surface by forming disulphide bridges. This effect is not desired, the DNA should be only present on the GNPs and not on the surface. Therefore we decided to only focus on an optimization of the APTES approach.

EDC/NHS chemistry was utilized in an indirect immobilisation approach. First, EDC/NHS was used to covalently link BSA to the APTES surface. Then GNPs, previously functionalised in bulk with thiol-DNA-amine, could be added on this surface by EDC/NHS linking. The BSA layer functioned as a spacer and surface blocking agent simultaneously, reducing non-specific binding of other molecules during incubation of the target and developer GNP.

Conclusion

The APTES layer on glass turned out to be very versatile, reproducible, and stable during the measurement. It was very suitable for immobilising GNPs and proteins and it remained stable during the analysis using darkfield microscopy, electron microscopy (SEM) and atomic force microscopy (AFM). The surface structure was smooth and homogeneous when not exposed to rapid temperature changes. Unfortunately, the main drawback of the surface was the inability to store slides after coating. Freshly coated slides could be used up to two days; it was found that for longer storage periods the immobilisation of GNPs could not be controlled. On the other hand, once GNPs were immobilised they remained on the surface; however, they could lose the ability to bind thiol-DNA strands. It is likely that the GNP surfaces were covered with free thiol molecules from the air.³⁴ Therefore, directly after immobilisation on the surface bare GNPs should be immediately functionalised with thiol-DNA or other thiol molecules.

Glutaraldehyde was used to covalent couple amino-DNA to the APTES surface. However, covalently coupling of thiol-DNA to a thin gold layer required fewer steps and was therefore preferred. Additionally, EDC/NHS chemistry was used to covalently couple BSA to the APTES surface followed by EDC/NHS coupling of antibody functionalised GNPs. By immobilising antibody-GNPs on to BSA the surface was well blocked to reduce non-specific binding in protein assays.³¹

3.2.4.2 Streptavidin surface results

Commercial streptavidin slides from a company named Array-it were chosen over in-house fabrication of a streptavidin surface. With this approach a research and optimisation track was avoided. The commercial slides are developed for biotin-DNA microarrays spots and are functionalised at one side. It was expected that commercial slides were homogeneously functionalised with streptavidin. An assay where the streptavidin was filled with a fluorescently labelled biotin-Alexa488 showed that this was not the case, as shown in Figure 3-7d,e. Also, it showed that incubation with Tween-20 as surfactant did not influence the binding capability. Later this was also confirmed by binding biotin-DNA functionalised GNPs. Similar clustered structures were visible in both darkfield microscopy and SEM.



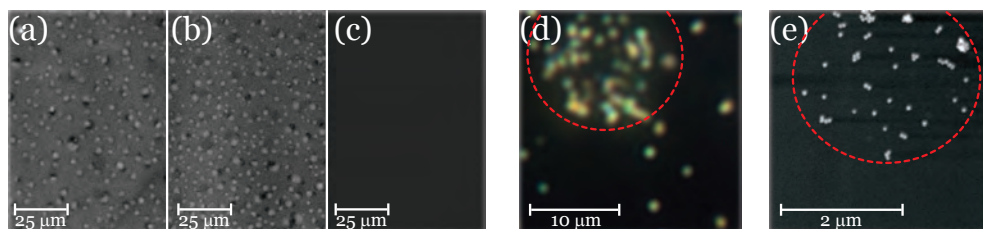


Figure 3-7: Confocal fluorescence images of streptavidin coated glass slide incubated with (a) biotin-alexa488, (b) biotin-alexa488 in presence of Tween-20 and (c) control, incubated with buffer. Uneven distribution of GNPs shown in (d) Darkfield of 60 nm GNP–DNA–biotin immobilised on the streptavidin surface and (e) Environmental SEM image of 60 nm GNP–DNA–biotin on the surface.

For the immobilisation of DNA receptor strands biotin-DNA strands were commercially obtained to construct a sensor as illustrated before (Figure 3-5b). Unfortunately the functionalised DNA strands were unreliable and did not show the expected biotin-streptavidin interaction.

Conclusion

The streptavidin surface was seen as the solution to the storage problems of APTES-glass slides. GNPs functionalised in buffer in which they can be stored, in combination with an active surface (streptavidin) on which they can bind, could yield more stable sensor slides. Unfortunately, the commercially available streptavidin slides showed poor surface homogeneity. However, the surface was active and fluorescent biotin-Alexa488 did bind specifically. Immobilised DNA-biotin GNPs remained on the surface with a similar distribution as was seen in the confocal images of the biotin-Alexa488, suggesting that the binding occurred specifically. However the control experiment with GNP-DNA showed randomly immobilised GNPs indicating that non-specific binding occurs. It is hard to distinguish between specific and non-specific binding since the amount of GNPs in both assays is similar, therefore we conclude that the binding was non-specific. The incubation with fluorescent DNA or bare GNPs did not show any significant signal. However, addition of GNP-streptavidin resulted in high numbers of GNPs on the surface. It is likely that the commercial slides are constructed by immobilising streptavidin over a biotin monolayer, but this is not described by the manufacturer.

Overall, at this stage the use of APTES slides was preferred because the immobilisation of GNPs on APTES slides was easier to control. The short shelf-life of APTES slides had to be taken for granted. However, in the future more efforts should be put into the realization of the practical use of streptavidin surfaces.

3.2.4.3 Planar gold surface

Conventional SPR experiments were done to investigate the efficacy of various blocking agents. The planar gold surface could be used directly as a sensor surface for SPR experiments, in contrast to the APTES/glass and streptavidin/glass systems where the immobilised GNPs are the sensors. In the SPR approach, an ensemble measurement is performed of a selected area of the sensor surface, whereas immobilised GNPs can be individually monitored. As a consequence, surface heterogeneity did not directly result in measuring artefacts. The SPR instrument was based on the Kretschmann imaging configuration, and the sensor surfaces consisted of a large gold layer on which spots could be made. In order to make spotting and orientation easier, parts of the gold layer were etched resulting in four or six gold patches on one sensor chip. Incubation could then be done on individual patches without leaking of droplets into other patches. Each patch was visible in the SPR imaging camera as a separate sensor. The flow conditions on all patches were identical allowing the simultaneous analysis of the response of various concentrations and reducing the amount of required conjugates.

Functionalisation of thiol-DNA on the gold surface resulted in active receptor layers which could be bound by other DNA strands or GNP-DNA. The surface was functionalised with thiol-DNA-D (GGATTACATTAGATTAGTTC-thiol 3') at a concentration of 1 μM in 1 M KH_2PO_4 , pH 3.8, for one hour. It was followed by incubation with 30 pM target DNA-M2 (ACTAATCTAATGTAATCCGGTTGGCGCGAATTCCAAGTCT) for one hour. Eventually, the binding of the developer GNP-DNA-A (5' thiol-GCAGACTTGGAATTCGCGCC) at a concentration of 1.0×10^{-10} M to the target DNA-M2 was monitored in SPR. In this type of assay the target strand is sandwiched between the receptor DNA strand and the strand on the GNP.

A part of the response originated from non-specific surface binding of the developer GNP-DNA. In order to reduce the non-specific binding various blocking molecules were compared; these are shown in Figure 3-8a. In these experiments the surface was functionalised not with thiol-DNA-D but with various blocking agents to monitor the binding of the developer GNP-DNA to the surface itself. The blocking agents were salmon sperm DNA (spDNA), 1-Amino-11-undecanethiol (AT), BSA, thiol-polyethylene glycol 1600 (tPEG), 6-mercapto hexanol (MH) and 11-mercapto undecanol (MU) and were all incubated at a concentration of 1 mM in 100 mM phosphate buffer pH 7.4 for one hour. In Figure 3-8a a bar graph shows the results of these experiments. Results are expressed in the initial SPR-angle shift per second. This approach allows comparing the results for different measurements as shown in the table of Figure 3-8b.



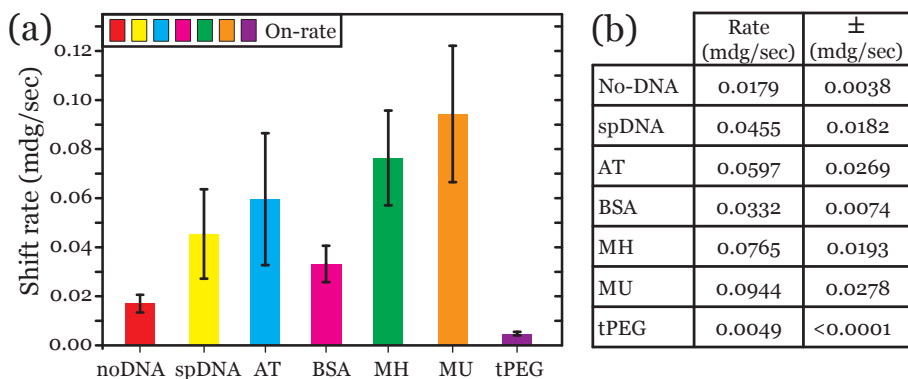


Figure 3-8: (a) Various blocking strategies as compared to the non-blocked DNA sample. (b) On-rate values measured for the blocking agents.

Conclusion

SPR measurements showed that it was possible to follow hybridisation of DNA and GNP–DNA over time. The gold sensor surface could be modified and functionalised without problems.

Non-specific binding of molecules to the surface should be reduced to the minimum. In the blocking experiment (Figure 3-8a,b) only tPEG showed significant reduction of non-specific binding of the developer GNP–DNA-A to the planar gold surface. Compared to the non-specific GNP–DNA-A binding rate to planar gold, nearly all tested blocking agents had a binding rate higher than the blank, meaning that non-specific binding was not reduced. In an additional experiment tPEG (1600) was combined with the specific thiol-DNA-D strand but it prevented the desired hybridisation of the target strand. Probably tPEG can be used but the polymer should be shorter than the hybridisation area of the DNA receptor strands. It is also possible to use a long spacer on the surface attachment side of the DNA strand, e.g., poly-A, poly-T strands or even a PEG spacer.¹¹

3.3 Gold nanoparticle functionalisation

GNPs should be able to specifically bind analytes, therefore DNA receptor strands have to be immobilised on the surface of the GNP. In the present context an important property of reporter molecules (e.g., fluorescent probes, radioactive probes, etc.) is their functionalisation capability. To avoid aggregation, GNPs should have either a positive or negative surface charge. Commonly used are negatively charged citrate capped GNPs and positively charged cetyltrimethylammonium bromide (CTAB) capped GNPs. In view of their commercial availability, we will focus on the use of

citrate capped GNPs that possess a high grade of monodispersity (<8% CV). Literature describes several approaches for immobilising DNA molecules on GNPs.^{3,11,21,22,35-38} Both DNA and GNP are negatively charged and would normally repel each other unless their charges are screened by, e.g., increasing the ionic strength of the solution. Unfortunately, as soon as the negatively charged citrate cap of the GNP is screened the particles will have a strong tendency to aggregate irreversibly; this can be reduced by using a high concentration of thiol labelled DNA and a surfactant.^{11,39-41} Thiol-DNA can form dimers via the thiol group; this property affects the functionalisation efficiency. Therefore dimerisation has to be reduced by using dithiothreitol (DTT).^{11,42} After DTT-treatment the DTT is removed by desalting. DTT treated DNA has a limited stability and it is recommended to use it immediately for functionalisation of gold surfaces. The necessity of DTT treatment for the binding of thiol-DNA to gold is shown by an SPR measurement (Figure 3-9).

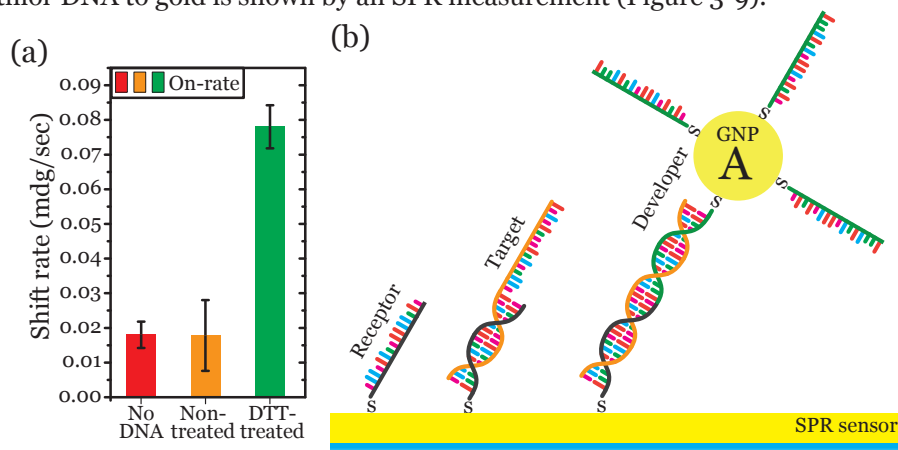


Figure 3-9: (a) The effect of DTT treatment can be seen as an increased specific binding rate. Normal non-specific binding of the developer GNP to a planar gold surface occurred at a rate of 0.0179 ± 0.0038 mdg/sec, which is practically the same as the rate of 0.0177 ± 0.0102 mdg/sec for non-treated thiol-DNA. Freshly DTT treated thiol-DNA shows a binding rate of 0.0779 ± 0.0062 mdg/sec, indicating that non-DTT treated thiol-DNA does not bind very good to a gold surface. (b) The amplified SPR assay: first a receptor strand is immobilised followed by the hybridisation of the target strand. Due to the low molecular weight of the target strand the presence can be amplified by hybridising a high molecular weight DNA functionalised GNP (GNP-DNA-A).

The two main approaches for functionalising GNPs are either mixing the GNPs with the DNA and gradually increasing the NaCl concentration¹¹ or first mixing the DNA with NaCl followed by adding the GNPs.³ The latter is a simpler approach. The loading efficiency of DNA on the GNP is determined by the DNA and the NaCl concentrations.^{11,42} As noted earlier, a high NaCl concentration reduces the charge of

DNA. DNA strands become more stretched or straight at a high NaCl concentration which allows closer packing on the GNP surface.¹¹ Additionally a sonication step in the GNP–DNA production procedure improves the packing density.¹¹ However, as already mentioned an increased NaCl concentration promotes GNP aggregation. The use of small surfactants, such as sodium dodecyl sulphate (SDS),¹¹ bis-(p-sulfonatophenyl) phenylphosphine (BSPP)^{39,40} or zonyl-FSN-100,⁴¹ helps to mask the ‘damaged’ citrate cap until replaced with a bound thiol-DNA strand. After the DNA functionalisation the remaining empty spots on the GNP can be covered with short chains of thiol-polyethylen glycol (tPEG).⁴³ If the GNP is not fully covered with DNA strands, this backfilling is necessary to reduce the aggregation of functionalised GNPs during hybridisation with the analyte. The thiol bond between gold and DNA is reversible at temperatures above 100 °C and will therefore not have any major influence in a melting curve analysis that is done below this temperature.⁴⁴

The functionalisation process of GNPs in bulk using the single step approach is described in Protocol 3-5, whereas the functionalisation of immobilised GNPs is outlined in Protocol 3-6. The main difference is the probability of aggregation: immobilised GNPs will not aggregate as a result of the high ionic strength. Following this protocol also large immobilised GNPs can be functionalised with DNA, despite their increased tendency to aggregate.⁴⁵ Additionally centrifugation washing steps are not necessary, a simple exchange of washing buffer is sufficient.

Protocol 3-5: Functionalising GNPs with thiol-DNA in buffer

1. Reduce DNA dimers by incubating equal volumes of stock DNA (100 µM) with 100 mM DTT in 180 mM PB pH 8.0 for one hour at room temperature.
2. Remove the DTT by using a NAP-5 desalting spin column and heat the sample to 96 °C for five minutes followed by cooling to room temperature.
3. Prepare DNA solution in high NaCl buffer: 0.5 µM DNA in 9 ml of 11 mM PB pH 7.4, 555 mM NaCl and 0.1% SDS. Incubate for 15 minutes.
4. Add 1 ml of stock GNP solution ($\sim 1.0 \times 10^{-10}$ M) and incubate at room temperature for 48 hours. Sonicate ten times for 30 seconds with 15 minute resting intervals.
5. Wash the samples with 10 ml washing solution (0.05% SDS in MilliQ water) after one hour centrifugation at 3,900× *g*. Repeat twice. In the last step resuspend in 1 ml of washing solution and transfer to 1.5 ml Eppendorf tube. To resuspend the pellet sonicate the sample while shaking for 10 seconds.
6. Wash by centrifugation at 8,000× *g* for ten minutes, repeat three times.
7. Measure the absorbance from $\lambda = 450$ nm to 700 nm using washing buffer as blank reference and analyse for absorbance peak shift compared to the bare GNPs.

This protocol was tested for particles ranging in size from 20 to 80 nm. Sonication in step 4 will improve the loading on the GNPs. Note that the end concentration is 500 mM of NaCl which will not result in fully loaded GNPs. Backfilling with tPEG 300 (at 1 µM for 30 minutes) after step 4 will further stabilise GNPs.



Protocol 3-6: On APTES immobilised GNP functionalisation with thiol-DNA

1. Reduce DNA dimers by incubating equal volumes of stock DNA (100 μM) with 100 mM DTT in 180 mM PB pH 8.0 for one hour at room temperature.
2. Remove the DTT by using a NAP-5 desalting spin column and heat the sample to 96 $^{\circ}\text{C}$ for five minutes followed by cooling to room temperature.
3. Prepare a 1 ml solution consisting of 5 μM thiol-DNA, 10 mM PB pH 7.4, 500 mM NaCl and 0.1% SDS and pipet the necessary volume in the flow-cell or cover-well with immobilised GNPs on APTES and incubate for two hours.
4. Wash the samples 5 \times with washing solution (10 mM phosphate buffer pH 7.4, 300 mM NaCl and 0.1% SDS).

Additionally:

5. Measure the absorbance for individual GNPs under darkfield conditions using a fibre spectrometer from $\lambda = 450$ nm to 700 nm with dark background as reference. (The fibre spectrometer procedure is described in Chapter 6.2)

This protocol was tested for particles sizes of 60 and 80 nm. Note that the NaCl end concentration is 500 mM which will not result in fully loaded GNPs.

This protocol can be adapted for immobilisation of thiol-DNA on planar gold (SPR-sensor) by using 1 μM thiol-DNA in step 3 instead of 5 μM .



Measuring the extinction spectrum of the functionalised batch of GNPs serves to monitor the functionalisation quality. The position of the extinction peak of GNPs in a bulk solution shifts towards the red upon binding of molecules. The amount of peak shift in nanometers is an indication for the number of molecules bound on the surface of GNP.^{3,45-47} Upon binding of DNA molecules ($n \sim 1.5$) water molecules ($n \sim 1.33$) are replaced, and the shell around the GNP will attain a slightly increased refractive index, which translates into a red-shifted extinction maximum.⁴⁸⁻⁵⁰ Additionally, the GNP spectrum indicates the presence of aggregated GNPs in the sample: a stable GNP solution presents a single absorbance peak, while the presence of two or more peaks indicates the presence of aggregates. However, the extinction peak shift can only indicate the presence of DNA strands but not its biochemical activity.

In the hybridisation assay two types of particles are mixed together. Two batches of GNPs are functionalised with mutually complementary DNA strands.³⁵⁻⁵¹ At a sufficiently high ionic strength and temperature below the DNA strand melting point temperature (T_m) the functionalized GNPs will hybridise. At T_m 50% of the DNA solution has the double strand conformation and the other 50% is still single stranded. The hybridisation properties of DNA strands are affected by many variables, e.g., the presence of mono- and bivalent ions, pH, concentration, neighbouring nucleotides and more.⁵²⁻⁵³ This hybridisation process results in cross-linking of both GNPs and can be monitored as a change in absorbance at a fixed wavelength of $\lambda = 260$ nm (or

at the plasmon peak position of the GNP solutions). Cross-linking occurs only if the functionalised GNPs are still biochemically active, and can be reversed by increasing the temperature above the T_m . This specific GNP cross-linking (aggregation) has been used to measure target DNA in a solution using a standard spectrometer.^{54,55}

3.3.1 Functionalised gold nanoparticle experiments

3.3.1.1 DNA conjugation

Two sets of ssDNA strands were functionalised to 60 nm GNPs: DNA-A (thiol-GCA GAC TTG GAA TTC GCG CC) and the complementary strand DNA-A' (ACG GCG CGA ATT CCA AGT CT -thiol). DNA-A is 5' thiol modified and the DNA-A' complementary to DNA-A over 18 bases, has a 3' thiol modification. The change in extinction peak as a result of DNA binding to 60 nm GNPs is shown in Figure 3-10. As already mentioned, a high ionic strength buffer of 500 mM NaCl is necessary to successfully conjugate ssDNA to GNPs. However, GNPs are instable in high ionic strength solutions. A high concentration of ssDNA ($> 30,000$ copies per GNP) in a large volume was used to reduce GNP aggregation. Under these conditions aggregation was minimal as determined from the shape of the curve in Figure 3-10. GNP aggregation can be seen as a second peak at $\lambda > 600$ nm. The peak shift that we obtained with coupling of 20-mer ssDNA was ~ 7 nm which corresponds to a theoretical amount of ~ 900 ssDNA molecules per GNP.^{31,56} An increased length of the ssDNA resulted in a larger shift, because in that case the DNA shell thickness is larger.⁵⁷

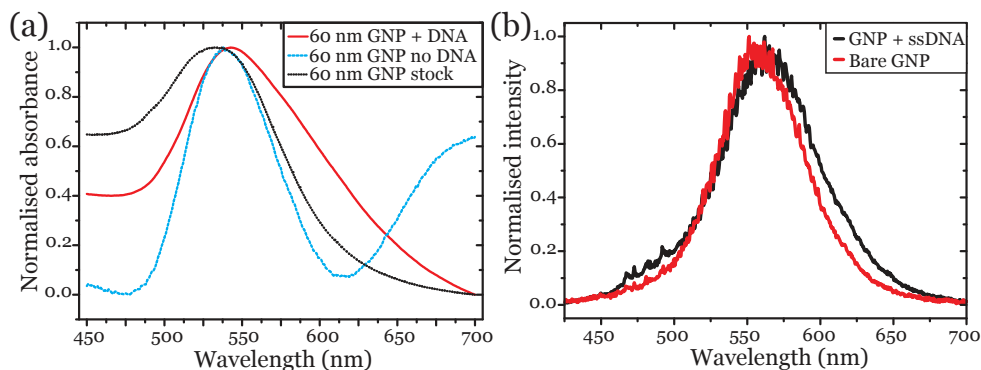


Figure 3-10: (a) Absorbance curves of GNPs: the 20-mer ssDNA (~ 7 nm shell length) conjugation (red) shows a shift when compared to the stock GNP solution (black). The control sample without ssDNA (blue) shows aggregation of GNPs as observed by increase of absorbance at $\lambda > 600$ nm. (b) Single particle scattering spectrum shifts upon binding of ssDNA to an 80 nm particle.

For immobilised GNPs the scattering spectra of individual particles were measured. Binding of ssDNA was observed as a red-shift of ~ 6 nm for the 80 nm GNPs, corresponding to an estimated amount of 700 DNA molecules per GNP.⁵⁸

Conclusion

The functionalisation of GNPs in colloidal suspension with thiol-DNA strands was successful; the average loading on each GNP could be determined using a spectrophotometer. The shape of the spectra of functionalised GNPs gave a good indication of the quality of the GNP-DNA samples.

3.3.1.2 Ionic strength and hybridisation behaviour

The hybridisation behaviour of DNA depends on the ionic strength of the buffer.^{52,53} At an increasing NaCl concentration the melting temperature also increased. The melting behaviour of DNA-A and DNA-A' was analysed by measuring the increase in absorbance at $\lambda = 260$ nm upon breaking of the hybridisation bond. In Figure 3-11 DNA-A and DNA-A' are hybridised (without GNP) at various NaCl concentrations. 1 μ M of both DNA-A and DNA-A' were mixed with 10 mM PB at pH 7.4. The concentration of NaCl varied from 0 to 1,000 mM.

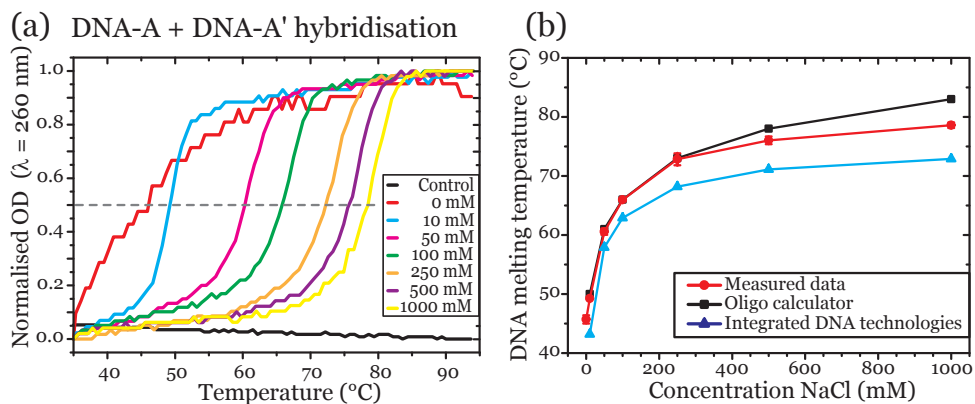


Figure 3-11: (a) Increase in melting temperature (T_m) of dsDNA samples due to an increased NaCl concentration. (b) T_m plotted against the NaCl concentration (red) comparing measured data with two online oligonucleotide property calculators.^{52,53}

We already noted that an increased ionic strength is necessary to overcome the repelling forces of DNA functionalised GNPs for hybridisation. If the NaCl concentration is too low, hybridisation will not occur. On the other hand, if the concentration is too high then also non-hybridised particles can aggregate resulting in false-positives. This hybridisation effect was analysed by measuring the decrease



in absorbance at $\lambda = 260$ nm upon formation of double stranded DNA. To assess the decrease in absorbance by hybridisation, the extinction at $\lambda = 260$ nm was measured. The samples consisted of the hybridisation pair GNP–DNA-A and GNP–DNA-A' ($\sim 2.5 \times 10^{-11}$ M each) mixed with 0.01% SDS to stabilise the suspension and 10 mM PB to maintain a stable pH at 7.4. Just before the measurement NaCl was added to obtain final NaCl concentrations ranging from 0 to 500 mM. Thereafter the samples were mixed and measured for 30 minutes. Additionally, a control experiment was performed without the complementary particle GNP–DNA-A' to observe self-aggregation of GNP–DNA-A. The hybridisation process is shown in Figure 3-12; the GNP–DNA-A and GNP–DNA-A' hybridise resulting in aggregation of the colloidal solution. Aggregation is seen as a decrease in absorbance, but could only be measured from NaCl concentrations > 200 mM. The control samples stabilised within 30 minutes and did not aggregate. This indicates that the decrease in absorbance measured for the GNP–DNA-A and GNP–DNA-A' is caused by hybridisation and not self-aggregation.

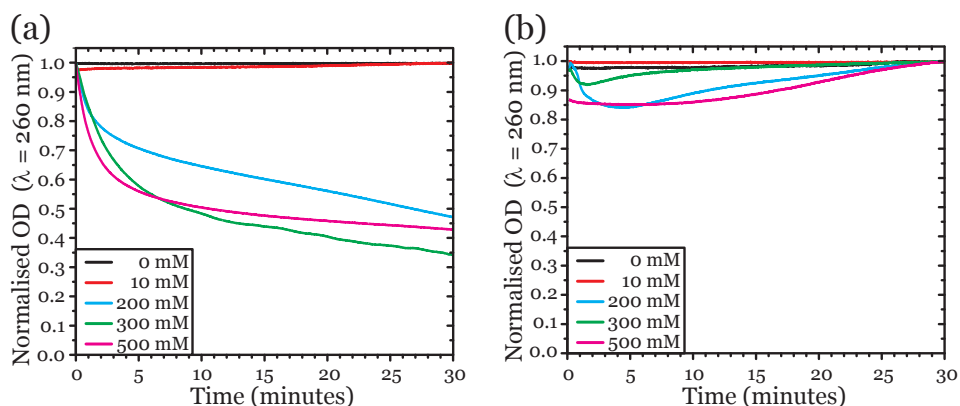


Figure 3-12: (a) Comparison between ionic strengths necessary to hybridise GNP-DNA-A and GNP-DNA-A'. A decrease in OD indicates hybridisation. In the control experiment (b) self-aggregation of GNP-DNA-A under influence of high NaCl concentrations was measured.

Conclusion

It was found that the NaCl concentration needed for specific hybridisation had to be higher than 200 mM. At concentrations above 200 mM the repelling forces of the GNP–DNA particles are low enough for the DNA strands to hybridise. A disadvantage of a high NaCl concentration is the non-specific hybridisation or hybridisation over a few nucleotides compared to the 18 nucleotides available. Non-specific hybridisation (self-aggregation) was seen as a decrease in absorbance for the control samples. However, the samples stabilised over time and the absorbance increased back to

the base level. Therefore, a NaCl concentration of 250 mM can safely be used for hybridisation assays.

3.3.1.3 Temperature and hybridisation/melting behaviour

As concluded from earlier experiments a NaCl concentration of 250 mM was sufficient to hybridise GNP–DNA-A and GNP–DNA-A'. In further experiments the temperature induced changes in hybridisation of a colloidal suspension containing GNP–DNA-A and GNP–DNA-A' were monitored. Measurements were performed with both increasing and decreasing temperatures. Prior to the hybridisation and melting analysis of the GNP–DNA pairs the T_m was determined for free DNA-A and DNA-A' as shown in Figure 3-11. The T_m of the free DNA pair was found to be ~ 73 °C at the optimal NaCl concentration (250 mM) for hybridising a GNP–DNA pair. The hybridisation induced changes in extinction were measured at $\lambda = 260$ nm. During the measurement the temperature of the samples was increased from 4 °C to 96 °C at a rate of 0.2 °C per minute. Thereafter the temperature was kept at 96 °C for ten minutes and it was followed by decreasing the temperature to 4 °C at a rate of 0.2 °C per minute. The absorbance was measured at 0.5 °C intervals. The samples consisted of the hybridisation pair GNP–DNA-A and GNP–DNA-A' ($\sim 2.5 \times 10^{-11}$ M each) with 0.01% SDS to stabilise the suspension and 10 mM PB to maintain a stable pH at 7.4, NaCl was added to the final concentration of 250 mM. Prior to the measurement, the samples were left to hybridise in the cuvettes at room temperature for two hours. The GNP–DNA hybridisation pair A and A' aggregated at temperatures below T_m . This was visible as a change from an intense red coloured suspension to almost colourless as shown in Figure 3-13a. Upon heating the colourless suspension regained the intense red colour indicating that GNPs were free in suspension. The melting of the pairs GNP–DNA-A and GNP–DNA-A' is shown in Figure 3-13b. The pairs remain hybridised until T_m is reached. Subsequently, hybridisation was monitored as shown in Figure 3-13c. These processes of melting and annealing were reversible and could be repeated several times.



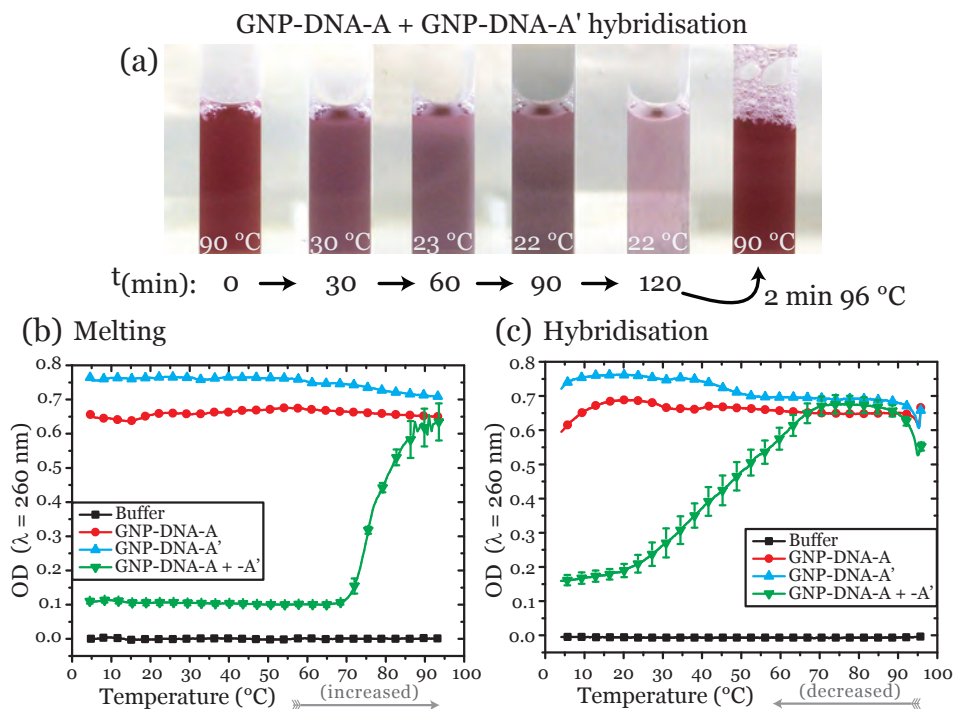


Figure 3-13: (a) Reversible aggregation of DNA functionalised GNPs over time. The GNP-DNA-A and complementary GNP-DNA-A' hybridise resulting in cross-linked complexes. Upon heating the strands de-hybridise and GNPs are free in the suspension. (b) Increasing the temperature results in melting of DNA; from T_m the DNA strands de-hybridise and GNPs return to the suspension. (c) Decreasing temperatures result in hybridisation of DNA strands attached to GNPs. GNP-DNA mixtures are a combination of 50% GNP-DNA-A and 50% GNP-DNA-A'. Each data point represents the mean of triplicate measurement \pm standard deviation.

Conclusion

The temperature induced changes measured at $\lambda = 260 \text{ nm}$ originate from the combined effects of (de)hybridising DNA and precipitating/resuspending GNPs. The melting temperature measured with the GNP-DNA-A and -A' hybridisation assay was $77.0 \pm 0.6^\circ\text{C}$ which is close to the $72.8 \pm 1.0^\circ\text{C}$ from free DNA measurement as shown in Figure 3-11. This might indicate that the hybridisation and dehybridisation occurs between GNP-DNA-A and GNP-DNA-A'; however, there could be an additional contribution towards T_m by the addition of GNPs. An explanation for this could be the locally concentrated DNA on the GNP surface. The T_m is affected not only by the concentration of NaCl but also by the concentration of DNA itself. A high concentration of hybridising DNA strands increases the T_m . Due to the highly organised spacing of ssDNA on the surface of a GNP, the local concentration of

hybridising strands can be very high because of the low volume between the two GNPs. In conclusion, these experiments show that ssDNA molecules can be conjugated to GNPs and are still capable of reacting with the complementary ssDNA molecule.

3.4 Incubation methods

Most biochemical interaction assays are performed in aqueous conditions. This includes static incubations or continuous flow incubations; additionally, the reactants are also stored in aqueous solutions. Because of the low atmospheric humidity it is necessary to perform static incubations in a closed or high humid environment, such as a humidity incubation chamber. Moreover, it is an advantage to perform multiple reactions on the same surface in parallel, which eliminates variations in sensor chip preparations. Commercially available cover-wells allow 24 parallel experiments on a standard microscope slide. Experiments performed using cover-wells are static, thus in order to change the buffer or sample the solution has to be removed before the next one is added. This approach can be compared with experiments performed in microtiter plates or small containers. Under a microscope with a programmable motorised microscope stage each well can be analyzed quickly and repeatedly by programming the coordinates of each well.

An alternate approach to static incubation is to perform measurements under flow conditions. The receptors are immobilised on the surface of the flow-cell and sample buffers are perfused over the surface. It is important that the rate at which the molecules are passing the surface is not too high. The analytes cannot interact with the receptors immobilised on the surface if the flow rate is too high. On the other hand, the buffer with analytes becomes depleted if the flow rate is too low. Both too fast and too slow flow rates result in measuring inaccurate receptor-analyte binding kinetics.⁵⁹ The optimal flow rate varies per analyte and depends mostly on the size of the analyte. Usually a larger analyte benefits from a lower flow rate. There are various methods to create a flow-cell on a microscope slide. In essence, it is a tunnel with an inlet and outlet making contact with the surface of the microscope slide itself. Two versatile and easy methods generally used are a setup of glass-spacer-glass or a moulded polymer, e.g., a moulded plastic or polydimethylsiloxane (PDMS) to create hollow chambers on a sensor surface.⁶⁰ In Protocol 3-7, the fabrication of a glass-spacer-glass flow-cell is described and it is illustrated in Figure 3-14. An example of a fabricated flow-cell fixed to a microscope translation table base plate is shown in Figure 3-15. The protocol describes the use of Parafilm, which melts two slides together and has the function of the spacer. An advantage of Parafilm over adhesives is the chemical resistance to solvents or salts in aqueous solutions. Moreover, it is present in nearly any laboratory.



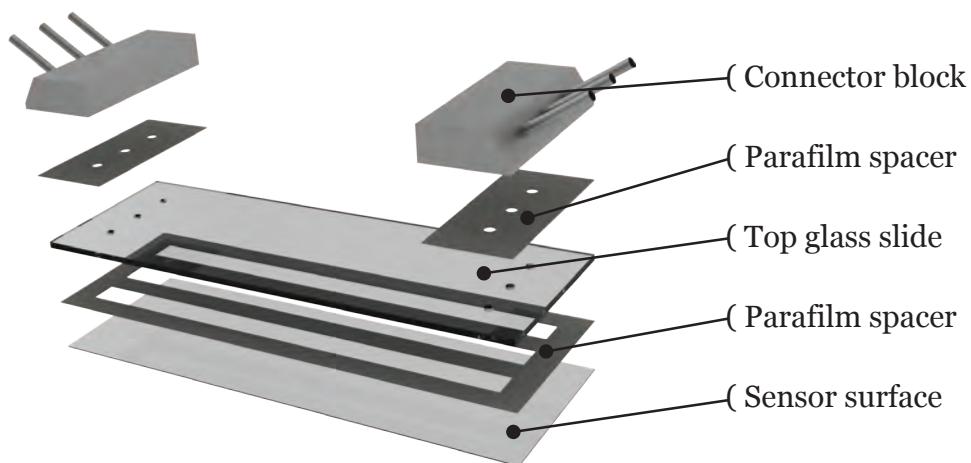


Figure 3-14: Components of the Parafilm flow-cell. The sensor surface can be pre-coated with APTES and GNPs.

Protocol 3-7: Glass-spacer-glass flow cell

1. Prepare the sensor surface as usual (APTES + GNPs) and cut the desired shape of the flow cell from Parafilm keeping at least 3 mm from the edge free. Place the Parafilm on top of the sensor slide.
2. Place the connector slide on top of the Parafilm and heat the constructed flow cell to 120 °C for one minute. The Parafilm will melt and can be used to adhere the glass slides together by applying pressure with the blunt end of a pen on the top glass slide.
3. Allow the flow cell to cool down slowly and connect tubing to the connector slide before use.

As an alternative to Parafilm, a double sided tape or other adhesive can be used. This allows construction without heating the sensor, however taking the flow cell apart might be a problem.

3.4.1 Incubation method experiments

The static incubation in cover-wells proved to be very useful; usually eight measurements were performed in triplicate on the same sensor surface. The adhesive backing of the strip resulted in a very good attachment to APTES coated glass slides, to Array-it streptavidin slides as well as to self made or commercial 50 nm gold slides (1 nm Cr adhesion layer + 49 nm Au by vacuum coating). The height of each well was 2 mm and the reaction volume was 10 μ l. Because of this low volume it was important to perform each incubation step in a humidity chamber. During washing it was essential to prevent drying of the surface otherwise it could lead to “coffee stain” effects, seen as higher density of GNPs near the edge of the well.⁶¹ Washing

steps were done using a vacuum needle to aspirate the sample and simultaneously adding the buffer with a pipette. For imaging, it was only possible to use the darkfield microscope in reflection mode due to the small working distance of the transmission darkfield condenser. The sample slide was mounted onto the removable base plate of the microscope translation stage. This allowed performing incubations in a humidity chamber away from the microscope. The self-aligning base plate ensured that the sample was placed back at exactly the same position on the microscope translation stage after each incubation step. A disadvantage of the darkfield system was the out of focus scattering of the buffer surface while measuring at the sensor-buffer interface. This was reduced to the minimum by filling each well with 14.5 μl buffer followed by placing a cover slip on top of the cover-wells. As a result, each well was sealed with a glass slide improving microscopy and reducing evaporation of the samples at the same time.

The Parafilm was cut using a steel mould that created three channels of 4×68 mm with a height of 100 μm (~ 28 μl volume). The bottom slide was either a 1 mm thick standard 26×76 mm object slide or a 0.17 mm thin slide with the same dimensions. Before construction of the flow-cell the bottom slide was coated with APTES and used to immobilise GNPs. The top slide was a 1 mm standard thickness object slide with three holes on each end which were used as in- and outlets. The spacing of the holes made it nearly impossible to create them by drilling because of the risk of breaking the slide. Consequently, the holes were made using powder blasting with 29 μm aluminium oxide particles at a pressure of 415 kN/m^2 for ten minutes. For powder blasting, Ordyl BF410 photoresist material (Tokyo Oga Kogyo, Japan) was used for soft lithography of the mask. The photoresist material was deposited on the glass. At the location of the holes the photoresist material was not developed and washed away, thus allowing the particles to hit the glass and form a hole after a few minutes of powder blasting. Steel connector blocks were connected to the top slide by Parafilm. The connector blocks allowed connection of tubing and secure mounting on the (microscope translation stage) base plate, as shown in Figure 3-15. The flow-rate was controlled by pushing or pulling the samples using a peristaltic or syringe pump. Flow-rates up to 1 ml/min were possible without leaking; higher flow-rates in push mode resulted in leakage through the Parafilm.



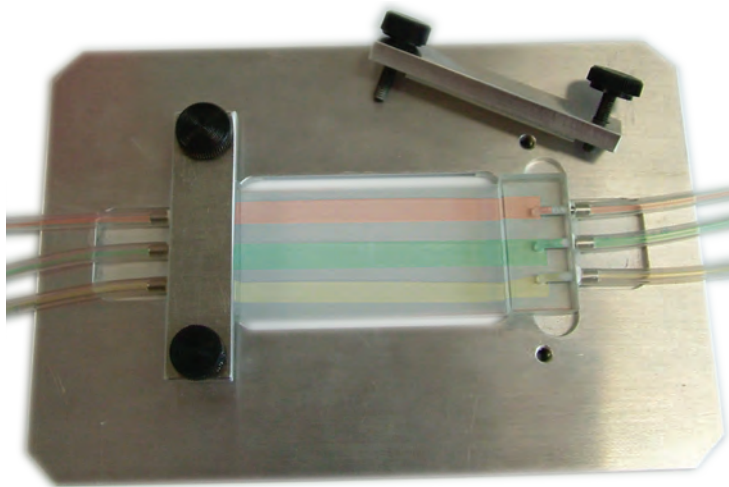


Figure 3-15: Parafilm flow-cell with glass connector blocks on the translation stage base plate, filled with chromophores. The base plate with flow-cell could be removed and placed back on the microscope translation stage keeping the position within 10 μm .

Conclusion

For static incubation conditions a cover-well is a good method. The 10 μl sample incubation volume allows pipetting of samples without significant evaporation. In addition, the cover-wells prevent cross-contamination of the samples. On the other hand, the fluid meniscus reflects light into all directions under darkfield conditions. This back-scattering prevents good image acquisition. However, placing a cover-slip on top of the cover-well eliminates this problem. Moreover, the cover-well method allows performing 24 experiments in a small volume on the same surface under the same conditions, making it an excellent method for rapid testing of various biochemical approaches.

For the flow-cell experiments, the Parafilm flow-cell constructed for our measurements worked well and was easy to adapt. A few advantages and disadvantages will be discussed here. The flow-cell is based on the standard 26 \times 76 mm microscope slide which is versatile and accepted by all microscope systems. The connector blocks allow to having a maximum of three channels in a single microscope slide. A stainless steel cutting mould results in high reproducibility of the 3-channel flow-cells made within 15 minutes. Any other shape of flow-cell that fits within the size of the microscope slide can be cut out from the Parafilm and used as well. On the other hand, Parafilm flow-cells cannot withstand rapid temperature changes; particularly at temperatures

below 4 °C the Parafilm becomes hard and loses its adhesive strength resulting in a leaking flow-cell. Additionally, the system cannot be used with protein functionalised surfaces since it requires heating to at least 70 °C to cure the Parafilm and the glass slides together. However, with carefully planned surface modifications this is not a problem. Overall, the Parafilm flow-cell is a very useful and easy system for sample incubations under flow conditions.

3.5 Overview

In this chapter we have described several chemical approaches that might provide an answer to the central question: *How can a gold nanoparticle be immobilized on a coated glass surface, functionalised with receptors and perform a target detection assay?* Many other approaches and experiments have been tested, but the APTES surface with immobilised bare GNPs followed by DNA functionalisation in a Parafilm flow-cell or cover-wells was the best approach for this project. Results of these experiments are described in chapters 5 & 6 and also used in chapter 7.

3.6 Bibliography

- (1) Möller R., Csáki A., Köhler J.M., Fritzsche W. DNA probes on chip surfaces studied by scanning force microscopy using specific binding of colloidal gold. *Nucleic Acids Research* **2000**; *28*: E91.
- (2) Li Y.T., Liu H.S., Lin H.P., Chen S.H. Gold nanoparticles for microfluidics-based biosensing of PCR products by hybridization-induced fluorescence quenching. *Electrophoresis* **2005**; *26*: 4743-50.
- (3) Verdoold R., Ungureanu F., Wasserberg D., Kooyman R.P.H. Gold nanoparticle assays: towards single molecule unamplified DNA detection. *Proceedings of SPIE* **2009**; *7312*: 73120N.
- (4) Liu S., Zhu T., Hu R., Liu Z. Evaporation-induced self-assembly of gold nanoparticles into a highly organized two-dimensional array. *Physical Chemistry Chemical Physics* **2002**; *4*: 6059-62.
- (5) Chen J.I.L., Chen Y., Ginger D.S. Plasmonic nanoparticle dimers for optical sensing of DNA in complex media. *Journal of the American Chemical Society* **2010**; *132*: 9600-1.
- (6) He L., Smith E.A., Natan M.J., Keating C.D. The distance-dependence of colloidal Au-amplified surface plasmon resonance. *The Journal of Physical Chemistry B* **2004**; *108*: 10973-80.
- (7) Fritzsche W. DNA-gold conjugates for the detection of specific molecular interactions. *Journal of Biotechnology* **2001**; *82*: 37-46.
- (8) Bhat R., Genzer J. Using spectroscopic ellipsometry for quick prediction of number density of nanoparticles bound to non-transparent solid surfaces. *Surface Science* **2005**; *596*: 187-96.
- (9) Fuentes M., Mateo C., García L., Tercero J.C., Guisán J.M., Fernández-Lafuente R. Directed covalent immobilization of aminated DNA probes on aminated plates. *Biomacromolecules* **2004**; *5*: 883-8.
- (10) Kouassi G.K., Irudayaraj J. Magnetic and gold-coated magnetic nanoparticles as a



- DNA sensor. *Analytical Chemistry* **2006**; *78*: 3234-41.
- (11) Hurst S.J., Lytton-Jean A.K.R., Mirkin C.A. Maximizing DNA loading on a range of gold nanoparticle sizes. *Analytical Chemistry* **2006**; *78*: 8313-8.
- (12) Pavlov V., Xiao Y., Gill R., Dishon A., Kotler M., Willner I. Amplified chemiluminescence surface detection of DNA and telomerase activity using catalytic nucleic acid labels. *Analytical Chemistry* **2004**; *76*: 2152-6.
- (13) Bhat R.R., Fischer D.A., Genzer J. Fabricating planar nanoparticle assemblies with number density gradients. *Langmuir* **2002**; *18*: 5640-3.
- (14) Green N.M. Avidin. *Advances in Protein Chemistry* **1975**; *29*: 85-133.
- (15) Wilchek M., Bayer E. The avidin-biotin complex in bioanalytical applications. *Analytical Biochemistry* **1988**; *171*: 1-32.
- (16) Green N.M. Avidin and streptavidin. *Methods in Enzymology* **1990**; *184*: 51-67.
- (17) Savage D., Mattson G., Desai S., Nielander G., Morgensen S., Conklin E. *Avidin-Biotin Chemistry: A Handbook*. Pierce Chemical Company: Rockford, IL, USA, **1992**. p. 1-23.
- (18) Tong X., Smith L.M. Solid-phase method for the purification of DNA sequencing reactions. *Analytical Chemistry* **1992**; *64*: 2672-7.
- (19) Holmberg A., Blomstergren A., Nord O., Lukaacs M., Lundeborg J., Uhlén M. The biotin-streptavidin interaction can be reversibly broken using water at elevated temperatures. *Electrophoresis* **2005**; *26*: 501-10.
- (20) Pollet J., Delpont F., Janssen K.P.F., Jans K., Maes G., Pfeiffer H., Wevers M., Lammertyn J. Fiber optic SPR biosensing of DNA hybridization and DNA-protein interactions. *Biosensors & Bioelectronics* **2009**; *25*: 864-9.
- (21) Reinhard B.M., Siu M., Agarwal H., Alivisatos A.P., Liphardt J. Calibration of dynamic molecular rulers based on plasmon coupling between gold nanoparticles. *Nano Letters* **2005**; *5*: 2246-52.
- (22) Sönnichsen C., Reinhard B.M., Liphardt J., Alivisatos A.P. A molecular ruler based on plasmon coupling of single gold and silver nanoparticles. *Nature Biotechnology* **2005**; *23*: 741-5.
- (23) Wirde M., Gelius U., Nyholm L. Self-assembled monolayers of cystamine and cysteamine on gold studied by XPS and voltammetry. *Langmuir* **1999**; *15*: 6370-8.
- (24) Thanh N.T.K., Green L.A.W. Functionalisation of nanoparticles for biomedical applications. *Nano Today* **2010**; *5*: 213-30.
- (25) Duan R., Zhou X., Xing D. Electrochemiluminescence biobarcode method based on cysteamine-gold nanoparticle conjugates. *Analytical Chemistry* **2010**; *82*: 3099-103.
- (26) Bain C.D., Whitesides G.M. Formation of monolayers by the coadsorption of thiols on gold: variation in the length of the alkyl chain. *Journal of the American Chemical Society* **1989**; *111*: 7164-75.
- (27) Nuzzo R.G., Allara D.L. Adsorption of bifunctional organic disulfides on gold surfaces. *Journal of the American Chemical Society* **1983**; *105*: 4481-3.
- (28) Wang Z.H., Jin G. Covalent immobilization of proteins for the biosensor based on imaging ellipsometry. *Journal of Immunological Methods* **2004**; *285*: 237-43.
- (29) Anthony R.M., Schuitema A.R.J., Oskam L., Klatser P.R. Direct detection of *Staphylococcus aureus* mRNA using a flow through microarray. *Journal of Microbiological Methods* **2005**; *60*: 47-54.
- (30) Teramura Y., Arima Y., Iwata H. Surface plasmon resonance-based highly sensitive immunosensing for brain natriuretic peptide using nanobeads for signal amplification.

- Analytical Biochemistry* **2006**; *357*: 208-15.
- (31) Ungureanu F., Wasserberg D., Yang N., Verdood R., Kooyman R.P.H. Immunosensing by colorimetric darkfield microscopy of individual gold nanoparticle-conjugates. *Sensors & Actuators: B Chemical* **2010**; *150*: 529-36.
- (32) O'Shannessy D.J., Brigham-Burke M., Peck K. Immobilization chemistries suitable for use in the BIAcore surface plasmon resonance detector. *Analytical Biochemistry* **1992**; *205*: 132-6.
- (33) Nilsson P., Persson B., Uhlén M., Nygren P.A. Real-time monitoring of DNA manipulations using biosensor technology. *Analytical Biochemistry* **1995**; *224*: 400-8.
- (34) Bramanti E., D'Ulivo L., Lomonte C., Onor M., Zamboni R., Raspi G., D'Ulivo A. Determination of hydrogen sulfide and volatile thiols in air samples by mercury probe derivatization coupled with liquid chromatography-atomic fluorescence spectrometry. *Analytica Chimica Acta* **2006**; *579*: 38-46.
- (35) Storhoff J.J., Elghanian R., Mucic R.C., Mirkin C.A., Letsinger R.L. One-pot colorimetric differentiation of polynucleotides with single base imperfections using gold nanoparticle probes. *Journal of the American Chemical Society* **1998**; *120*: 1959-64.
- (36) Elghanian R., Storhoff J.J., Mucic R.C., Letsinger R.L., Mirkin C.A. Selective colorimetric detection of polynucleotides based on the distance-dependent optical properties of gold nanoparticles. *Science* **1997**; *277*: 1078-81.
- (37) Mucic R.C., Storhoff J.J., Mirkin C.A., Letsinger R.L. DNA-directed synthesis of binary nanoparticle network materials. *Journal of the American Chemical Society* **1998**; *120*: 12674-5.
- (38) Yang L., Wang H., Yan B., Reinhard B.M. Calibration of silver plasmon rulers in the 1-25 nm separation range: experimental indications of distinct plasmon coupling regimes. *The Journal of Physical Chemistry C* **2010**; *114*: 4901-8.
- (39) Suzuki K., Hosokawa K., Maeda M. Controlling the number and positions of oligonucleotides on gold nanoparticle surfaces. *Journal of the American Chemical Society* **2009**; *131*: 7518-9.
- (40) Sauthier M.L., Carroll R.L., Gorman C.B., Franzen S. Nanoparticle layers assembled through DNA hybridization: Characterization and optimization. *Langmuir* **2002**; *18*: 1825-30.
- (41) Zu Y., Gao Z. Facile and controllable loading of single-stranded DNA on gold nanoparticles. *Analytical Chemistry* **2009**; *81*: 8523-8.
- (42) Hill H.D., Millstone J.E., Banholzer M.J., Mirkin C.A. The role radius of curvature plays in thiolated oligonucleotide loading on gold nanoparticles. *ACS Nano* **2009**; *3*: 418-24.
- (43) Xiao L., Wei L., He Y., Yeung E.S. Single molecule biosensing using color coded plasmon resonant metal nanoparticles. *Analytical Chemistry* **2010**; *82*: 6308-14.
- (44) Büttner M., Belser T., Oelhafen P. Stability of thiol-passivated gold particles at elevated temperatures studied by X-ray photoelectron spectroscopy. *The Journal of Physical Chemistry B* **2005**; *109*: 5464-7.
- (45) Reynolds R.A., Mirkin C.A., Letsinger R.L. Homogeneous, nanoparticle-based quantitative colorimetric detection of oligonucleotides. *Journal of the American Chemical Society* **2000**; *122*: 3795-6.
- (46) Ungureanu F., Halamek J., Verdood R., Kooyman R.P.H. The use of a colour camera for quantitative detection of protein-binding nanoparticles. *Proceedings of SPIE* **2009**; *7192*: 71920O.



- (47) Samoc A., Miniewicz A., Samoc M., Grote J.G. Refractive-index anisotropy and optical dispersion in films of deoxyribonucleic acid. *Journal of Applied Polymer Science* **2007**; *105*: 236-45.
- (48) Yguerabide J., Yguerabide E.E. Light-scattering submicroscopic particles as highly fluorescent analogs and their use as tracer labels in clinical and biological applications. *Analytical Biochemistry* **1998**; *262*: 157-76.
- (49) Liu X., Atwater M., Wang J., Huo Q. Extinction coefficient of gold nanoparticles with different sizes and different capping ligands. *Colloids & Surfaces B: Biointerfaces* **2007**; *58*: 3-7.
- (50) Jain P.K., Lee K.S., El-Sayed I.H., El-Sayed M.A. Calculated absorption and scattering properties of gold nanoparticles of different size, shape, and composition: applications in biological imaging and biomedicine. *The Journal of Physical Chemistry B* **2006**; *110*: 7238-48.
- (51) Thaxton C.S., Georganopoulou D.G., Mirkin C.A. Gold nanoparticle probes for the detection of nucleic acid targets. *Clinica Chimica Acta* **2006**; *363*: 120-6.
- (52) Kibbe W.A. OligoCalc: an online oligonucleotide properties calculator. *Nucleic Acids Research* **2007**; *35*: W43-6.
- (53) Owczarzy R., You Y., Moreira B.G., Manthey J.A., Huang L., Behlke M.a., Walder J.A. Effects of sodium ions on DNA duplex oligomers: improved predictions of melting temperatures. *Biochemistry* **2004**; *43*: 3537-54.
- (54) Hurst S.J., Hill H.D., Mirkin C.A. "Three-dimensional hybridization" with polyvalent DNA-gold nanoparticle conjugates. *Journal of the American Chemical Society* **2008**; *130*: 12192-200.
- (55) Hurst S.J., Hill H.D., Macfarlane R.J., Wu J., Dravid V.P., Mirkin C.A. Synthetically programmable DNA binding domains in aggregates of DNA-functionalized gold nanoparticles. *Small* **2009**; *5*: 2156-61.
- (56) Draine B.T., Flatau P.J. Discrete-dipole approximation for scattering calculations. *Journal of the Optical Society of America A* **1994**; *11*: 1491-9.
- (57) Liu G.L., Yin Y., Kunchakarra S., Mukherjee B., Gerion D., Jett S.D., Bear D.G., Gray J.W., Alivisatos A.P., Lee L.P., Chen F.F. A nanoplasmonic molecular ruler for measuring nuclease activity and DNA footprinting. *Nature Nanotechnology* **2006**; *1*: 47-52.
- (58) Verdoold R., Gill R., Ungureanu F., Molenaar R., Kooyman R.P.H. Femtomolar DNA detection by parallel colorimetric darkfield microscopy of functionalized gold nanoparticles. *Biosensors & Bioelectronics* **2011**; *27*: 77-81.
- (59) Tran T.H., Chang W.J., Kim Y.B., Koo Y.M., Kim E.K., Yoon J.Y., Kim J. The effect of fluidic conditions on the continuous-flow bioluminescent detection of ATP in a microfluidic device. *Biotechnology & Bioprocess Engineering* **2007**; *12*: 470-4.
- (60) McDonald J.C., Duffy D.C., Anderson J.R., Chiu D.T., Wu H., Schueller O.J., Whitesides G.M. Fabrication of microfluidic systems in poly(dimethylsiloxane). *Electrophoresis* **2000**; *21*: 27-40.
- (61) Kajiya T., Kaneko D., Doi M. Dynamical visualization of "coffee stain phenomenon" in droplets of polymer solution via fluorescent microscopy. *Langmuir* **2008**; *24*: 12369-74.







Chapter 4

Physics of surface plasmon based sensing

In this chapter we discuss surface plasmon resonance based sensor systems. Sensing strategies based on planar surface plasmon resonance (SPR) and local surface plasmon resonance (LSPR) rely on the detection of changes in the refractive index in the immediate vicinity of the sensing surface. We also discuss the methods to analyze data and calculate affinity constants from experimentally obtained data.



4.1 Introduction

Surface plasmon resonance (SPR) is a physical phenomenon first predicted by Ritchie, in 1957.¹ Previously, in the beginning of the twentieth century, Wood had observed surface plasma waves on diffraction gratings.² Approximately ten years after the publication of Ritchie, optical excitation of surface plasmons could be experimentally demonstrated in an attenuated total reflection setup. Both Kretschmann and Otto developed a method to excite surface plasmons.^{3,4} This provided the basis for the development of SPR based sensing strategies.⁵ The SPR method proved itself to be a useful tool for molecule interaction sensing at an interface; with SPR it is possible to follow in real-time the association and dissociation kinetics between proteins.⁶⁻⁸ The potential of label-free and sensitive molecule interaction sensing was soon understood, and the Biacore was introduced as the first commercial SPR based biosensor system.⁹ The Biacore was followed by many other SPR systems;¹⁰ however, all these systems were able to monitor only a few types of receptors simultaneously in real-time. This was changed by the introduction of the imaging SPR systems where the photodiode was replaced by a CCD-camera.¹¹ The CCD-camera allowed the monitoring of multiple spots on the sensor surface simultaneously and in real-time.¹² It is also possible to observe local surface plasmon resonance (LSPR) on the surface of metal nanoparticles.^{13,14} Already at the beginning of the twentieth century Mie gave a full quantitative description of the optics of (spherical) nanoparticles, although the concept of surface plasmons was unknown to him.¹⁵ Recent developments show the possibility to use gold and silver nanoparticles as reporters for immunosensing and the detection of specific DNA strands.¹⁶ These nanoparticles can be analyzed either individually or in bulk, as described in Chapter 2.

4.1.1 Surface plasmons

Surface plasmons (SPs) are collective conduction electron oscillations at the interface between a metal and a dielectric. SPs can be excited by p-polarized light that enters a thin metal layer (~50 nm) under total internal reflectance conditions (see Figure 4-1). At a certain angle of incidence (the 'resonance angle'), dictated by the applied wavelength, the type of metal used, and the refractive index of the various layers involved, a SP can be excited, resulting in a strong electromagnetic field, the so-called evanescent field, that extends to about half a wavelength (a few hundred nm) from the metal-dielectric interface. The build-up of this field manifests itself as a sharp minimum of the reflectance, as illustrated in Figure 4-1b.^{10,12,17}

The sensing potential of SPR becomes clear if one realizes that attachment of a monolayer of molecules to the metal results in a changed refractive index profile leading to a changed resonance angle.



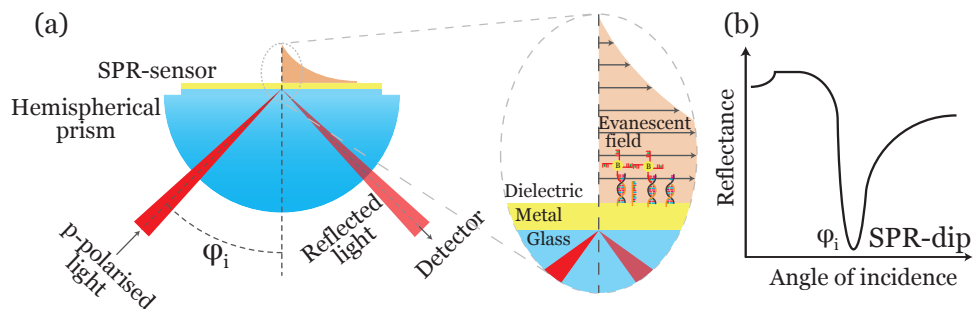


Figure 4-1: (a) Schematic representation of the SPR principle based on the Kretschmann configuration. (b) Reflectance curve of a typical SPR response. Upon changing the angle of incidence, the reflectance passes through a minimum known as SPR-dip.

Various types of metal layers can be used in the visible light spectrum, e.g., gold, copper, silver and aluminium.^{17,18} However, the metal should be free of oxides and not react with ions from a buffer which eliminates the use of copper, aluminium and silver. Gold is therefore commonly used and allows easy modifications, as described in Chapter 3.

For metal nanoparticles the principle is similar;^{19,20} however, the light is usually not coupled through a prism under TIR conditions, although this is still possible,²¹ but instead darkfield illumination is used.^{20,22-24} When the conduction electrons of GNPs are excited (with visible light for gold and silver), they coherently oscillate with high amplitude as shown in the inset in Figure 4-2a. This effect is known as local surface plasmon resonance: when a GNP is illuminated with white light the scattering efficiency passes through a maximum as shown in Figure 4-2a.²⁴⁻²⁷ This scattering plasmon peak position (λ_{\max}) can be used for sensing of biomolecules since the peak position changes upon binding of molecules similarly as in planar SPR.²⁶ The λ_{\max} position varies on many external factors such as shape, material, size of the nanoparticles, as well as polarisation of the coupling light.²⁴ A comparison between various sized silver and gold spherical nanoparticles is illustrated in Figure 4-2b.



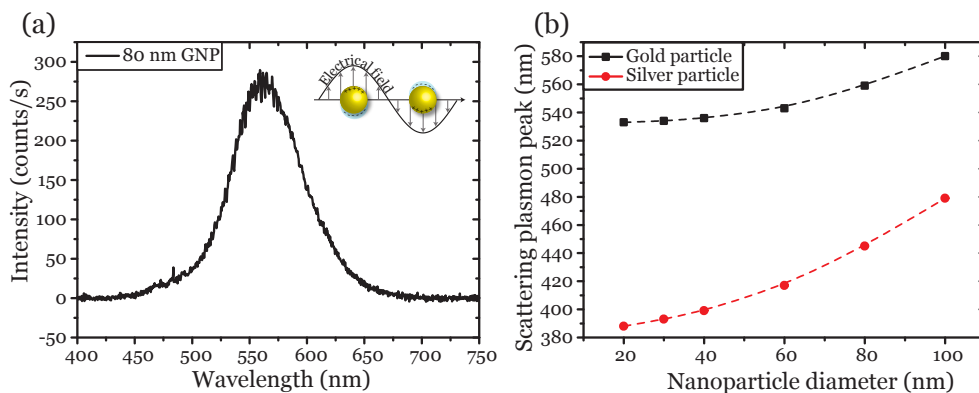


Figure 4-2: (a) Light scattering signal from a single 80 nm GNP excited with a xenon light source in darkfield illumination. The inset shows the coherent oscillation of the conduction electrons. The scattering plasmon peak position for this particular GNP is ~ 565 nm; at this wavelength the white light scattering efficiency is at a maximum. (b) Simulated data of variations in scattering plasmon peak positions for various sizes of silver and gold nanoparticles.²⁸

4.2 GNP detection

The light scattering of individual GNPs can easily be observed by a charged coupled device (CCD) -camera or even by a naked human eye at 200 to 400 times magnification. A convenient way of observing this phenomenon is to illuminate GNPs with white light under darkfield conditions. A darkfield condition is created by focussing ring-shaped light through a condenser lens on the sample. Most of the light is transmitted following its original light path, missing the objective lens and resulting in a black sample background. Some of the light is scattered by objects in the sample plane. This scattered light is collected by the objective lens and visualised on the dark background; hence the name darkfield illumination as illustrated in Figure 4-3a. As shown in Figure 4-3b,c, the scattering colour can vary per particle.^{24,29} From the data in Figure 4-3b we conclude that various particle sizes are present and that a batch of GNPs contains a distribution of sizes.

In addition to a CCD-camera a spectrometer can be used to analyse the exact scatter spectrum of each individual GNP. This allows a precise monitoring of the changes in the scattering plasmon peak position (λ_{\max}). Moreover, it enables calibration of a colour camera for darkfield GNP detection.³⁰

The colour of scattering GNPs is expressed as a ratio between the signal intensities from the red and green channels of the CCD-camera (r/g). Changes of the local refractive index result in a shift of the λ_{\max} (λ_{\max} shift is explained in more detail in Figure 4-6); this shift towards red can be observed as an increase of the r/g ratio, as shown in Figure 4-3c.^{30,31}

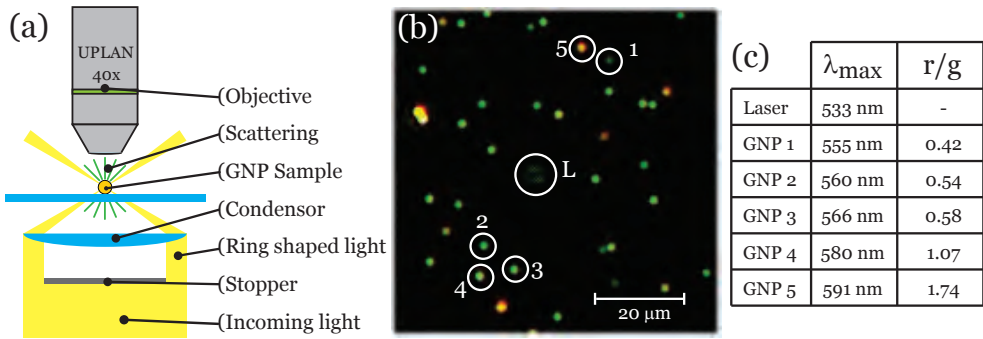


Figure 4-3: (a) Schematic representation of darkfield illumination. Only the scattering of the object (GNP) is observed via the microscope objective. (b) Darkfield image of GNPs on a glass surface. The laser (L) is the internal calibrator for the single particle fibre spectrometer. (c) Scattering peak position (as measured by a spectrometer) and the corresponding ratio between red and green channel (as measured by a colour CCD-camera) of the marked GNPs.

4.3 Detection of refractive index changes

SPR and LSPR can both be used for measuring changes in the net refractive index (n_{net}) in the near vicinity of the surface of the planar gold layer or around a nanoparticle, respectively. This enables both methods to be used for detection of biomolecules, such as proteins, DNA, or other molecules. A simplified principle of n_{net} sensing is illustrated in Figure 4-4. In short, water molecules with a refractive index of $n = 1.33$ are replaced with protein or DNA molecules ($n \sim 1.5$). This results in an increase of n_{net} in the sensing area.

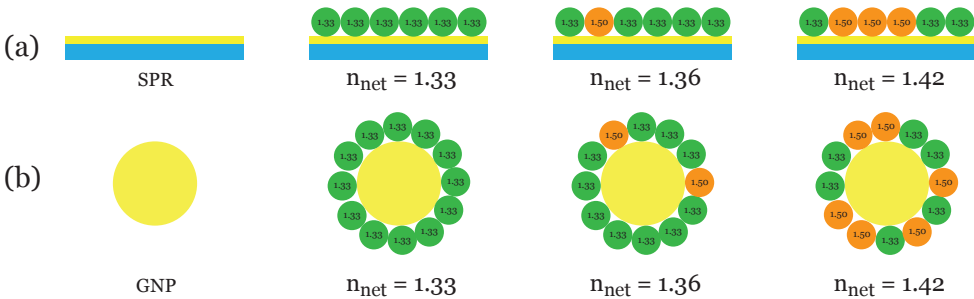


Figure 4-4: Sensing of biomolecules based on change of n_{net} . The water molecules (green) are replaced with the binding of biomolecules (orange), thus increasing the n_{net} . The illustration is given for both planar SPR (a) and GNPs (b). Note: the weighted averaging of refractive indices as done here is for illustrative purposes only. A more accurate approximation of n_{net} can be obtained by applying, e.g., Maxwell-Garnett theory.³²



The dynamic range of the sensor is important for the targeted field of use, i.e., gas phase or liquid phase. The scattering of gold nanoparticles can be monitored within a refractive index range from $n = 1$ up to $n = > 1.5$ without modifying the system, and is therefore suitable for both gases and liquids.^{27,33} With planar SPR, the dynamic range is determined by the scanning angle range of the system. Most SPR instruments are optimised for analysing protein interactions in aqueous solutions and can scan the angle of the incident light over a few degrees using a scanning mirror or a linear diode array.^{10,34,35} The SPR-dip for an aqueous solution with $n = 1.33$ appears at $\varphi \sim 69^\circ$ (for $\lambda = 670$ nm, with gold as metal surface). Protein optimized SPR sensor systems can analyse angular changes of approximately 0.005 degrees, which corresponds to refractive index steps of $n \sim 7 \times 10^{-5}$ and are therefore very sensitive over their scan range.^{10,35,36} On the other hand some instruments are able to scan over a range of 38° to 78° and are therefore capable of measuring a dielectric from $n = 1.0$ to $n = 1.4$.^{10,36}, thereby sacrificing angular resolution. Compared to GNPs, where the λ_{\max} change as a result from changing the dielectric is directly visible as a change in scattering colour in the visible light, planar SPR is somewhat limited, as far as it concerns their dynamic range.

Solutions with known refractive indices, e.g., calibrated oils or calibrated glucose solutions can be used to analyse the instrument response ($\Delta\varphi$ or $\Delta\lambda_{\max}$) to a changing refractive index. In its turn, the changed index is a measure for the number of molecules that have bound to the sensing surface. For GNPs this relationship is shown in Figure 4-5. In this particular measurement the average λ_{\max} shift of 80 nm gold nanoparticles was monitored while changing the refractive index using solutions with various glucose concentrations. The $\Delta\lambda_{\max}$ shift varies for the size, shape and composition of GNPs.³⁷⁻⁴⁰ In order to make an average measurement of multiple GNPs, only the GNPs with the same λ_{\max} at the beginning of the measurement are included in the averaging procedure.



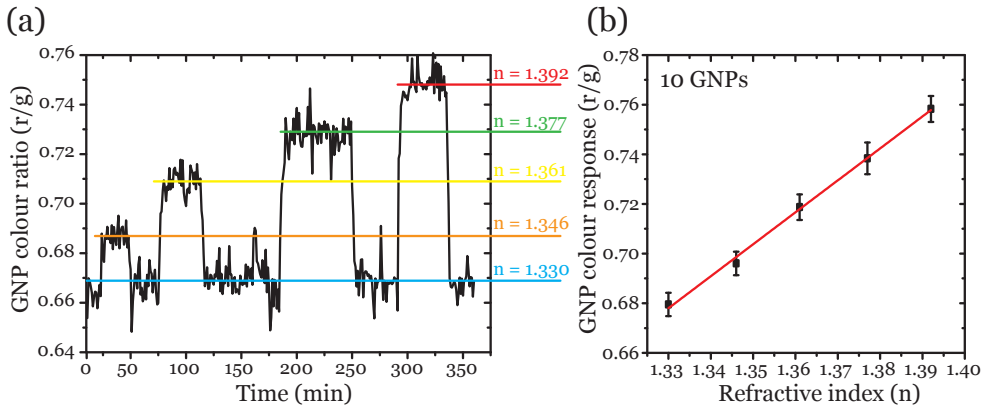


Figure 4-5: (a) Relation between refractive index and the scattering colour of 80 nm GNPs (average of 350 GNPs) in the sensing area; the change in refractive index changes the scattering colour of the GNPs and is expressed as a ratio between the red and green channel (r/g). (b) Refractive index response of 10 similar-sized GNPs (similar r/g at beginning of the measurement). The change in refractive index results in a proportional change in r/g of the GNPs.

4.4 Biomolecular interaction

4.4.1 Analyte – receptor interaction

The essence of a biosensor is to monitor the interaction between a receptor [A] and an analyte [B] to form a complex [AB]. In most assays the receptor molecules are immobilised on a support. This support can be planar as in conventional SPR, or curved as in GNPs, or three-dimensional using a hydrogel matrix in which the receptors are absorbed. The interaction between receptor and analyte can be described as a first order reaction for which we assume that: (1) all receptors are equally accessible for analytes; (2) a receptor is either free or occupied, there is no partial binding; (3) the binding between receptor and analyte is reversible and (4) the binding of the analyte does not change the receptor. The interaction rate for any given time point is expressed as

$$\frac{d[AB]}{dt} = k_{on} [A][B] - k_{off} [AB] \quad \text{Equation 4-1}$$

The brackets, e.g., [AB], indicate the molar concentrations of molecules. The association rate k_{on} is a measure of how fast the complex AB is formed and is expressed in $M^{-1}s^{-1}$. The dissociation rate k_{off} is a measure for how fast the complexes AB break and is expressed in s^{-1} .

In a real-time measurement a sensorgram typically visualises the increase of signal



as a result from the formation of AB in time, as shown in Figure 4-6. The sensorgram gives valuable information about the interaction between A and B. Here, we will only describe the equilibrium behaviour, as the experimentally determined rates are largely determined by instrument geometry.

The mutual affinity of the molecules is described by the equilibrium association constant K_A and is expressed in M^{-1} . For the type of molecular interactions as considered here the Langmuir binding isotherm (Equation 4-2) gives a fairly accurate description of the equilibrium situation.^{41,42}

$$\Gamma = \frac{K_A [B]}{1 + K_A [B]} \quad \text{Equation 4-2}$$

Here, Γ is the fractional coverage of the receptor A, and $[B]$ the concentration of free analyte B.

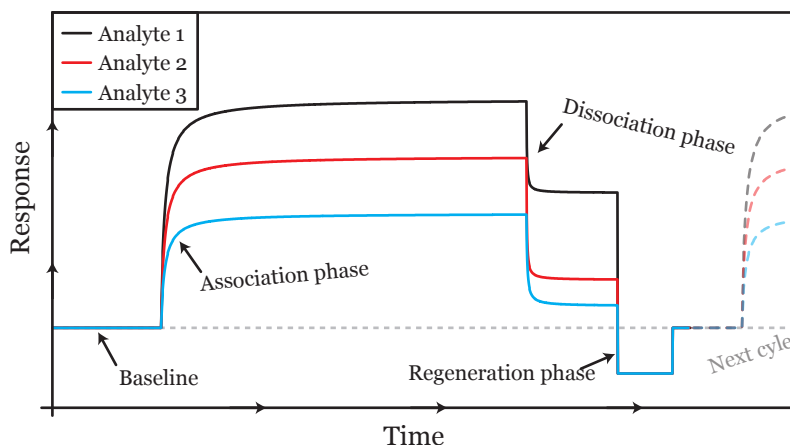


Figure 4-6: Schematic representation of a typical sensorgram of molecule interaction for three analyte concentrations. The baseline shows the ‘zero’ response of the system and indicates if the system is stable. During the association phase the analytes are introduced and interact with the surface; the response varies depending on the analyte concentration and affinity for the receptor. During the dissociation phase the weakly bound or adsorbed analytes are washed away and the analytes are removed completely during the regeneration step. After regeneration the receptors are ready for the next cycle of analyte interaction.

For a known K_A the coverage Γ can be determined in a SPR experiment. From eq. 4-2 the concentration $[B]$ follows. Alternatively, of course, from a known $[B]$ and measured Γ we can determine K_A . However, in a GNP assay the receptors are spread over many GNPs which respond differently compared to planar SPR. In the assay that

we developed, a single occupied receptor on a single GNP will result in a measurable signal change from that individual GNP, as is described in more detail in section 4.4.2. Each GNP has single molecule sensitivity, but we cannot discriminate whether one or more analytes are bound to a single GNP. Therefore we require a different strategy to analyze the binding response. In order to describe the equilibrium response a Monte Carlo simulation adapted to the assays can be used. The Monte Carlo method is based on repeated random sampling and results in an approximate result. In a particular field of view (FOV) there are N_1 GNPs, all evenly occupied with N_2 active receptors. This gives $(N_1 \cdot N_2)$ as the total amount of active receptors in FOV. The total number of occupied receptors N_{tot} can be calculated with Equation 4-3 for any Γ , where Γ is again determined by the Langmuir isotherm (eq. 4-2).

$$N_{tot} = \Gamma \cdot N_1 \cdot N_2 \quad \text{Equation 4-3}$$

In this Monte Carlo simulation procedure analyte molecules are randomly placed on the receptors distributed over the GNPs until the condition in Equation 4-3 is met. One result of this procedure is that we know the number of GNPs that have at least one analyte bound. In the experiment we count the number of GNPs that changed their colour and, subsequently, with the Γ and K_D the corresponding analyte concentration can be calculated using Equation 4-2. This enables the use of the GNP assay as a sensor for sensitive analyte detection as is described in more detail in section 4.4.2 and Chapter 6.

4.4.2 Gold nanoparticles for biomolecular interaction sensing

As already explained, changes of the local refractive index of a GNP can be detected as a shift of the scattering plasmon peak position (λ_{max}). Using a colour camera this shift is seen as a change in colour; in this way a plasmon peak shift as small as 1 nm can be detected.³⁰ However, the sensitivity depends on the sizes of both the binding molecules and the individual GNPs, as illustrated in Figure 4-7.



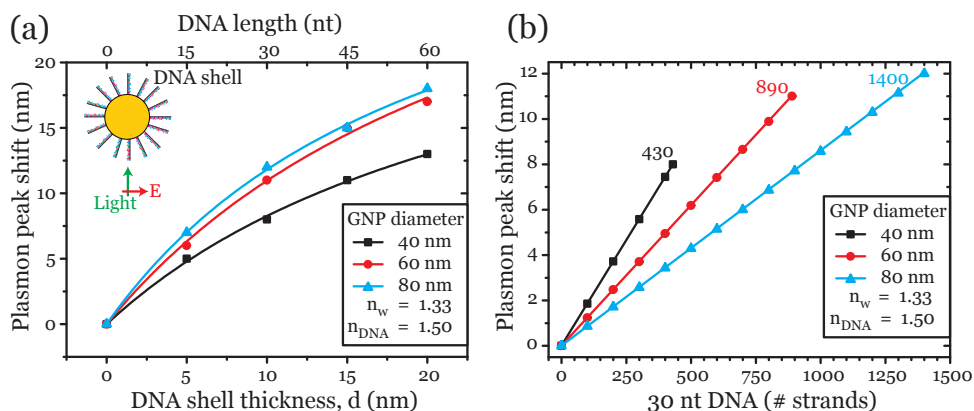


Figure 4-7: Simulations on the plasmon peak shift as a function of the binding of DNA molecules on various sized GNPs. (a) The various sized GNPs were simulated with DNA shells of increasing thickness ($n = 1.50$) in an aqueous environment ($n = 1.33$). The differential sensitivity decays with the distance from the particle's surface, as indicated by the non-linear increase in plasmon peak shift. At a maximum loading we assume that a 40 nm GNP can accommodate 430 strands, 60 nm - 890 strands and 80 nm - 1,400 strands. (b) The spectral response for various sized GNPs in aqueous environment, upon binding increasing amounts of 30 nt long DNA molecules (10 nm).

The advantage of the colour camera is that each individual particle in the field of view (FOV) can be monitored for a colour change. However, the λ_{max} shift is not very sensitive, according to simulations shown in Figure 4-7. It is necessary to bind at least 81 DNA strands on a 60 nm GNP to obtain a plasmon peak shift of 1 nm. This is the threshold for the camera.

Moreover, the amount of receptors that can be placed on an individual GNP is limited. The spherical GNP is supported on a glass surface; therefore the lower hemisphere of the particle cannot be fully functionalised. Additionally, in order to reduce steric hindrance the receptor strands should not be tightly packed. Therefore a GNP should host approximately half of the maximum possible coverage.²³ This significantly limits the minimal detectable ratio between number of covered receptors and total number of receptors available (Γ_{min}). Γ_{min} in combination with the affinity constant can be used to estimate the limit of detection (LOD) of an assay. The minimum detectable coverage for a LSPR assay based on a 60 nm GNP with 445 (half of maximum) DNA receptors (30 nt, ~10 nm) and a detection threshold of 81 occupied receptors results in a $\Gamma_{min} = 0.18$. For conventional SPR and the same DNA strand length Γ_{min} is approximately 0.1. Additionally, for LSPR the size of the GNP is directly linked with the surface area. The sensitivity of various GNP sizes compared with conventional SPR are shown in Table 4-1. The theoretical limit of detection (LOD) was calculated

using an affinity constant of $0.25 \times 10^{10} \text{ M}^{-1}$ for an 18-mer ssDNA hybridisation³¹ and assuming Langmuir type behaviour.

Table 4-1: The theoretical sensitivity of SPR techniques

Sensor system	Max coverage	DNA strands/ 1 nm shift λ_{max}	$\Gamma_{\text{min}}^{\text{a}}$	Detection limit ^b [M]
Planar SPR		-	0.1	4.0×10^{-11}
40 nm GNP LSPR	430	54	0.25	1.0×10^{-10}
60 nm GNP LSPR	890	81	0.18	7.2×10^{-11}
80 nm GNP LSPR	1,400	117	0.17	6.8×10^{-11}
80 – 40 two GNP LSPR ^c	$1,000 \times 700^{\text{d}}$	1	$\sim 1.4 \times 10^{-6}$	$\sim 5.7 \times 10^{-16}$

^a The binding ratio Γ is based on only half the maximum coverage due to immobilised GNPs.

^b Affinity constant: $0.25 \times 10^{10} \text{ M}^{-1}$.³¹

^c Distance between GNPs is 15 nm (~ 45 nt DNA distance); note that the shift is ~ 15 nm instead of 1 nm.

^d 1,000 GNPs with each 700 receptors.

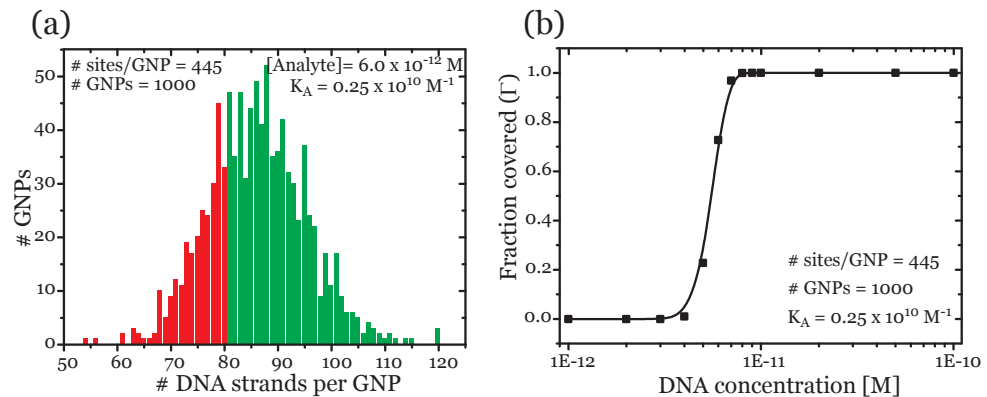


Figure 4-8: LSPR sensor response for using individual GNPs as sensors. (a) Distribution of number of DNA strands per GNP at an analyte concentration of $6.0 \times 10^{-12} \text{ M}$ (affinity constant $0.25 \times 10^{10} \text{ M}^{-1}$). A $\Delta\lambda_{\text{max}}$ shift threshold of ≥ 1 nm means that every particle with shift ≥ 1 nm can be detected with the colour camera. For a 60 nm GNP with max 445 receptors this threshold is exceeded when 81 or more analytes hybridise with the receptors. At an analyte concentration of $6.0 \times 10^{-12} \text{ M}$, as in panel (a), 727 GNPs (of 1,000) have 81 or more analytes, thus exceeding the $\Delta\lambda_{\text{max}}$ shift threshold and therefore can be detected. These are indicated by the green bars, while the GNPs that do have $\Delta\lambda_{\text{max}}$ shift < 1 nm are shown red and are rejected. (b) Theoretical concentration dependence for a single GNP system, where 1,000 GNPs with 445 receptors each are monitored. A Γ of 1 indicates that all 1,000 GNPs have bound more than 81 target strands (for a detectable shift of 1 nm). At $\Gamma = 0.5$ only 500 GNPs have bound 81 or more target strands.



The theoretical LOD of 7.2×10^{-11} M for 60 nm GNP (Table 4-1) does not correspond to the Monte Carlo simulations shown in Figure 4-8a,b. At a target concentration of 6.0×10^{-12} M, 727 GNPs still give a measurable signal ($\sim 70\%$ positive). This discrepancy arises from the fact that the LOD calculation is based on the response of one individual GNP, while in this particular case the simulation takes into account the statistical response from 1,000 GNPs in the FOV. From the total number of visible GNPs, only those with at least 81 bound target molecules, corresponding to a λ_{\max} shift of ≥ 1 nm, are selected and counted. Compared to planar SPR, the LSPR method does not provide a better sensitivity for label-free sensing. However, when a second GNP is hybridised in close proximity (< 30 nm) of the first particle the situation changes. The interaction between the particles as a result of a single target hybridisation event causes a large plasmon peak shift.^{31,43-45} The amount of λ_{\max} shift depends on many variables, such as the distance between both GNPs, as well as their size and shape. Using discrete dipole approximation scattering simulations^{46,47} the effect of the mutual distances in the range from 5 to 30 nm for various GNP pairs can be simulated (Figure 4-9). The results are averaged over all polarization angles since standard darkfield illumination uses unpolarised light. For the 80 – 40 nm GNP pair the λ_{\max} shift ranges from ~ 30 nm at 5 nm inter-particle distance to ~ 7 nm at 30 nm inter-particle distance. The close proximity particle interaction shows a significant shift of λ_{\max} upon binding of one particle within the plasmon field of another particle.⁴⁸⁻⁵⁰ Thus, if we would be able to observe 1,000 GNPs simultaneously, each of them accommodating 700 active receptors, we could theoretically detect one binding event out of 700,000 binding sites. In short, this detection strategy allows detection of single binding events out of thousands of receptor molecules resulting in a very low theoretical detection limit as shown in Table 4-1.

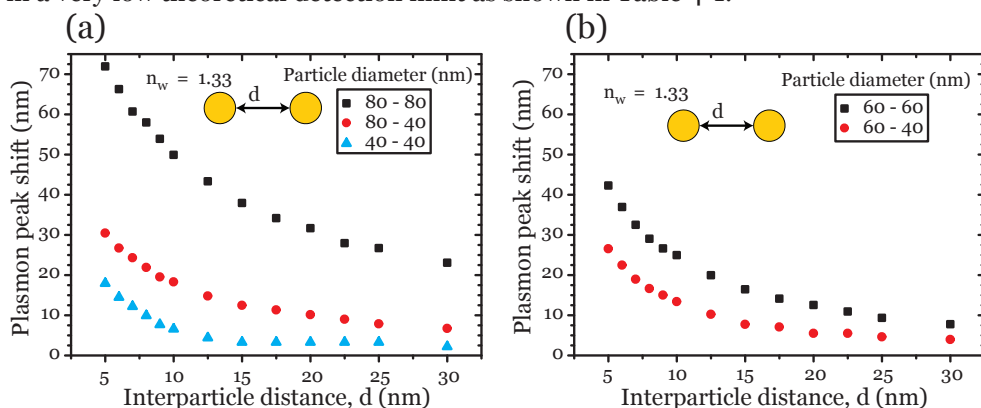


Figure 4-9: Theoretical plasmon peak shifts from discrete dipole approximation (DDA) simulations. 80 nm (a) or 60 nm (b) GNPs coupled with different nanoparticle sizes with various inter-particle distances. The obtained results are shown for a particle pair under unpolarised light conditions.

The comparison between both assays is shown in Figure 4-10a. The sensitivity of the close proximity assay relies both on the affinity constant of the analyte for the receptor pair as well as on the total amount of receptors in the FOV as shown in Figure 4-10b. The amount of receptors in the FOV can be increased by using larger particles which are able to host more receptors or by a more efficient use of the surface area by organising GNPs in an array.

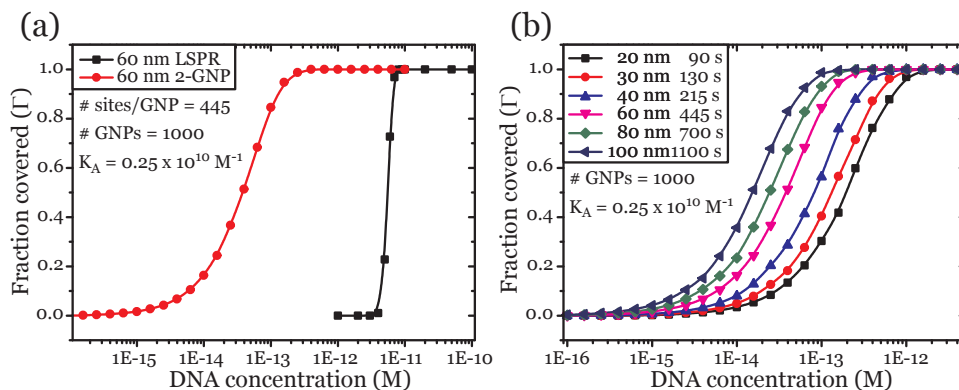


Figure 4-10: (a) Sensitivity comparison simulated for the basic LSPR assay with 60 nm GNPs or for the two GNP close proximity assay. (b) Sensitivity simulation of the two GNP close proximity assay comparing various sized GNPs which translates to increasing numbers of receptors sites.

4.5 Conclusion

The use of gold nanoparticles (GNPs) for biomolecule detection is very versatile. The excitation of surface plasmons on GNPs (LSPR) can easily be achieved by a standard darkfield microscope, rather than requiring a complex apparatus for conventional planar surface plasmon resonance (SPR). Both SPR and LSPR have the advantage of using a gold surface, which allows modification with receptor molecules via the strong thiol-gold interaction (see Chapter 3). The use of individual 60–80 nm GNPs as sensor results in a sensitivity comparable to that of SPR. However, the large shift in λ_{max} when two GNPs approach each other at a distance < 30 nm allows detection of a single hybridisation event. Using a camera this allows monitoring thousands of GNPs simultaneously to identify which GNP has undergone a single binding event. An advantage of this approach is the possibility to use a high number of receptors in the whole field of view and still be able to identify one binding event, thus making it possible to detect very low concentrations of target strands. Additionally, as seen from Figure 4-10a, the dynamic range of the two GNP close proximity assay is wider when compared to that of the single GNP assay. However, it is fair to remark that in such a sensor system we give up the label-free approach.



GNPs are highly suitable for a simple and easy to build biosensor for DNA or other analytes. GNPs are easy to detect using simple optical techniques: a standard microscope equipped with a darkfield condenser and a colour camera is sufficient to detect molecule interaction induced GNP scattering colour changes. The interaction between the receptor and analyte can be interpreted using the well-understood Langmuir binding model. In conclusion, the use of GNPs could change the future of nano-based biosensing technology, allowing small sensors and needing only a single droplet to be analysed in a short time period.

4.6 Bibliography

- (1) Ritchie R. Plasma losses by fast electrons in thin films. *Physical Review* **1957**; *106*: 874-81.
- (2) Wood R.W. XLII. On a remarkable case of uneven distribution of light in a diffraction grating spectrum. *Philosophical Magazine Series 6* **1902**; *4*: 396-402.
- (3) Otto A. Excitation of nonradiative surface plasma waves in silver by the method of frustrated total reflection. *Zeitschrift fur Physik* **1968**; *216*: 398-410.
- (4) Kretschmann E. Decay of non radiative surface plasmons into light on rough silver films. Comparison of experimental and theoretical results. *Optics Communications* **1972**; *6*: 185-7.
- (5) Liedberg B., Nylander C., Lunström I. Surface plasmon resonance for gas detection and biosensing. *Sensors & Actuators* **1983**; *4*: 299-304.
- (6) Kooyman R.P.H., Kolkman H., van Gent J., Greve J. Surface plasmon resonance immunosensors: sensitivity considerations. *Analytica Chimica Acta* **1988**; *213*: 35-45.
- (7) Andrade J.D., Vanwagenen R.A., Gregonis D.E., Newby K., Lin J.N. Remote fiber-optic biosensors based on evanescent-excited fluoro-immunoassay: Concept and progress. *IEEE Transactions on Electron Devices* **1985**; *32*: 1175-9.
- (8) Malmqvist M. Biospecific interaction analysis using biosensor technology. *Nature* **1993**; *361*: 186-7.
- (9) Jönsson U., Fägerstam L., Ivarsson B., Johnsson B., Karlsson R., Lundh K., Löfås S., Persson B., Roos H., Rönnerberg I. Real-time biospecific interaction analysis using surface plasmon resonance and a sensor chip technology. *BioTechniques* **1991**; *11*: 620-7.
- (10) Schasfoort R., Tudos A. *Handbook of Surface Plasmon Resonance*. Royal Society of Chemistry: Cambridge, **2008**. p. 403.
- (11) Rothenhäusler B., Knoll W. Surface plasmon microscopy. *Nature* **1988**; *332*: 615-7.
- (12) Berger C.E.H., Beumer T.A.M., Kooyman R.P.H., Greve J. Surface plasmon resonance multisensing. *Analytical Chemistry* **1998**; *70*: 703-6.
- (13) Nath N., Chilkoti A. A colorimetric gold nanoparticle sensor to interrogate biomolecular interactions in real time on a surface. *Analytical Chemistry* **2002**; *74*: 504-9.
- (14) Haes A.J., Hall W.P., Chang L., Klein W.L., van Duyne R.P. A localized surface plasmon resonance biosensor: First steps toward an assay for Alzheimer's disease. *Nano Letters* **2004**; *4*: 1029-34.
- (15) Mie G. Beiträge zur Optik trüber Medien, speziell kolloidaler Metallösungen. *Annalen der Physik* **1908**; *330*: 377-445.



- (16) Merkoçi A. Nanoparticles-based strategies for DNA, protein and cell sensors. *Biosensors & Bioelectronics* **2010**; *26*: 1164-77.
- (17) De Bruijn H.E., Kooyman R.P.H., Greve J. Choice of metal and wavelength for surface-plasmon resonance sensors: some considerations. *Applied Optics* **1992**; *31*: 440_1-2.
- (18) Rhodes C., Franzen S., Maria J.P., Losego M., Leonard D.N., Laughlin B., Duscher G., Weibel S. Surface plasmon resonance in conducting metal oxides. *Journal of Applied Physics* **2006**; *100*: 054905.
- (19) Ghosh S.K., Pal T. Interparticle coupling effect on the surface plasmon resonance of gold nanoparticles: from theory to applications. *Chemical Reviews* **2007**; *107*: 4797-862.
- (20) Schultz D. Plasmon resonant particles for biological detection. *Current Opinion in Biotechnology* **2003**; *14*: 13-22.
- (21) Sönnichsen C., Geier S., Hecker N.E., von Plessen G., Feldmann J., Ditzlacher H., Lamprecht B., Krenn J.R., Aussenegg F.R., Chan V.Z.H., Spatz J.P., Möller M. Spectroscopy of single metallic nanoparticles using total internal reflection microscopy. *Applied Physics Letters* **2000**; *77*: 2949.
- (22) Sannomiya T., Vörös J. Single plasmonic nanoparticles for biosensing. *Trends in Biotechnology* **2011**; *29*: 343-51.
- (23) Schultz S., Smith D.R., Mock J.J., Schultz D.A. Single-target molecule detection with nonbleaching multicolor optical immunolabels. *Proceedings of the National Academy of Sciences of the United States of America* **2000**; *97*: 996-1001.
- (24) Willets K., van Duyne R.P. Localized surface plasmon resonance spectroscopy and sensing. *Annual Review of Physical Chemistry* **2007**; *58*: 267-97.
- (25) Lee S.E., Lee L.P. Biomolecular plasmonics for quantitative biology and nanomedicine. *Current Opinion in Biotechnology* **2010**; *21*: 489-97.
- (26) Haes A.J., van Duyne R.P. A unified view of propagating and localized surface plasmon resonance biosensors. *Analytical & Bioanalytical Chemistry* **2004**; *379*: 920-30.
- (27) Okamoto T., Yamaguchi I., Kobayashi T. Local plasmon sensor with gold colloid monolayers deposited upon glass substrates. *Optics Letters* **2000**; *25*: 372-4.
- (28) Juluri B.K., Huang J., Jensen L. Extinction, scattering and absorption efficiencies of multilayer nanoparticles. <http://nanohub.org/resources/nmie> (DOI: 10254/nanohub-r8228.2) **2010**.
- (29) Mock J.J., Smith D.R., Schultz S. Local refractive index dependence of plasmon resonance spectra from individual nanoparticles. *Nano Letters* **2003**; *3*: 485-91.
- (30) Ungureanu F., Halamek J., Verdoold R., Kooyman R.P.H. The use of a colour camera for quantitative detection of protein-binding nanoparticles. *Proceedings of SPIE* **2009**; *7192*: 71920O.
- (31) Verdoold R., Gill R., Ungureanu F., Molenaar R., Kooyman R.P.H. Femtomolar DNA detection by parallel colorimetric darkfield microscopy of functionalized gold nanoparticles. *Biosensors & Bioelectronics* **2011**; *27*: 77-81.
- (32) Barnett A., Goldys E.M. Modeling of the SPR resolution enhancement for conventional and nanoparticle inclusive sensors by using statistical hypothesis testing. *Optics Express* **2010**; *18*: 9384-97.
- (33) McFarland A.D., Van Duyne R.P. Single silver nanoparticles as real-time optical sensors with zeptomole sensitivity. *Nano Letters* **2003**; *3*: 1057-62.
- (34) Beusink J.B., Lokate A.M.C., Besselink G.A.J., Pruijn G.J.M., Schasfoort R.B.M. Angle-scanning SPR imaging for detection of biomolecular interactions on microarrays.



Biosensors & Bioelectronics **2008**; *23*: 839-44.

- (35) Lokate A.M.C., Beusink J.B., Besselink G.A.J., Pruijn G.J.M., Schasfoort R.B.M. Biomolecular interaction monitoring of autoantibodies by scanning surface plasmon resonance microarray imaging. *Journal of the American Chemical Society* **2007**; *129*: 14013-8.
- (36) Liang H., Miranto H., Granqvist N., Sadowski J.W., Viitala T., Wang B., Yliperttula M. Surface plasmon resonance instrument as a refractometer for liquids and ultrathin films. *Sensors & Actuators: B Chemical* **2010**; *149*: 212-20.
- (37) Hu M., Novo C., Funston A., Wang H., Staleva H., Zou S., Mulvaney P., Xia Y., Hartland G.V. Dark-field microscopy studies of single metal nanoparticles: understanding the factors that influence the linewidth of the localized surface plasmon resonance. *Journal of Materials Chemistry* **2008**; *18*: 1949-60.
- (38) Haes A.J., Haynes C.L., McFarland A.D., Schatz G.C., van Duyne R.P., Zou S. Plasmonic materials for surface-enhanced sensing and spectroscopy. *MRS Bulletin* **2011**; *30*: 368-75.
- (39) Haynes C.L., van Duyne R.P. Nanosphere lithography: A versatile nanofabrication tool for studies of size-dependent nanoparticle optics. *The Journal of Physical Chemistry B* **2001**; *105*: 5599-611.
- (40) Kelly K.L., Coronado E., Zhao L.L., Schatz G.C. The optical properties of metal nanoparticles: The influence of size, shape, and dielectric environment. *The Journal of Physical Chemistry B* **2003**; *107*: 668-77.
- (41) Langmuir I. The constitution and fundamental properties of solids and liquids. Part 1. Solids. *Journal of the American Chemical Society* **1916**; *38*: 2221-95.
- (42) Langmuir I. The constitution and fundamental properties of solids and liquids. II Liquids. *Journal of the American Chemical Society* **1917**; *39*: 1848-906.
- (43) Krenn J.R., Ditlbacher H., Schider G., Hohenau A., Leitner A., Aussenegg F.R. Surface plasmon micro- and nano-optics. *Journal of Microscopy* **2003**; *209*: 167-72.
- (44) Reinhard B.M., Siu M., Agarwal H., Alivisatos A.P., Liphardt J. Calibration of dynamic molecular rulers based on plasmon coupling between gold nanoparticles. *Nano Letters* **2005**; *5*: 2246-52.
- (45) Chen J.I.L., Chen Y., Ginger D.S. Plasmonic nanoparticle dimers for optical sensing of DNA in complex media. *Journal of the American Chemical Society* **2010**; *132*: 9600-1.
- (46) Draine B.T., Flatau P.J. Discrete-dipole approximation for scattering calculations. *Journal of the Optical Society of America A* **1994**; *11*: 1491.
- (47) Draine B.T., Flatau P.J. Discrete-dipole approximation for periodic targets: theory and tests. *Journal of the Optical Society of America A* **2008**; *25*: 2693-703.
- (48) Sönnichsen C., Reinhard B.M., Liphardt J., Alivisatos A.P. A molecular ruler based on plasmon coupling of single gold and silver nanoparticles. *Nature Biotechnology* **2005**; *23*: 741-5.
- (49) Sannomiya T., Hafner C., Vörös J. In situ sensing of single binding events by localized surface plasmon resonance. *Nano Letters* **2008**; *8*: 3450-5.
- (50) Xiao L., Wei L., He Y., Yeung E.S. Single molecule biosensing using color coded plasmon resonant metal nanoparticles. *Analytical Chemistry* **2010**; *82*: 6308-14.



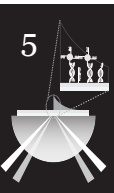




Chapter 5

Gold nanoparticle amplified surface plasmon resonance: the effect of size

Recently the research interest in conventional surface plasmon resonance (SPR) has been accompanied by interest in local surface plasmon resonance (LSPR) based sensing strategies. This is mainly due to the increased sensitivity compared to SPR for the detection of low molecular weight targets. In this chapter we show that conventional SPR can still be improved to reach better sensitivity by amplifying the SPR signal using gold nanoparticles (GNPs) as mass labels. GNPs are an ideal label for amplified SPR because of the large mass and the high dielectric constant. In the experiments described hereafter we combine simulations with experimental data using 20 and 60 nm GNPs for amplification of the detection of low molecular weight DNA target strands.



5.1 Introduction

From numerous reports on surface plasmon resonance (SPR) assays it can be concluded that this technique in many cases provides sufficient sensitivity to determine low (down to nanomolar) concentrations of relatively large molecules, such as proteins.^{1,2} However, when the molecules of interest are relatively small (<10 kDalton) SPR fails to provide sufficient sensitivity.³ Still, an SPR assay for this type of molecules can be very attractive, mainly owing to its excellent multi-sensing capabilities.⁴

In this chapter we will make an estimate of the increase in sensitivity that can be obtained if we give up the label-free approach and use a mass label in a sandwich assay format as depicted in Figure 5-1. We also present experimental results on such a system. We will concentrate on the detection of a short (40 nucleotides) target DNA strand, depicted as Target M in Figure 5-1. To achieve this, a ssDNA receptor strand, with its nucleotide sequence complementary to part of Target M is immobilized on a surface of a thin gold layer. After a certain incubation time ssDNA conjugated gold nanoparticles (GNPs), depicted as GNP-E in Figure 5-1, specific to the remaining part of Target M, are added to detect the presence of Target M and thus ‘develop’ the assay. The added mass of the bound nanoparticles is expected to result in lower detection limits for the sandwiched Target M.



5.2 Sandwich assay - modelling

The sandwich assay depicted in Figure 5-1 can be modelled with a six layer system, each with its own thickness and dielectric constant. The optical properties of such a multilayer system can be conventionally analyzed by repeated application of Fresnel's equations;⁵ in particular the angle of minimum reflectance, characteristic for surface plasmon resonance, can be found.

The characteristics of the various layers are as follows:

Layer 1 is a half-infinite layer, representing the glass half-sphere, necessary to couple in light to excite surface plasmons. The refractive index n_1 is taken as 1.52.

Layer 2 corresponds to a 50 nm Au layer. The dielectric constant $\epsilon(\lambda)^a$, with λ the wavelength of the used light, is taken from an extrapolation of the tabulated data of Johnson and Cristy.⁶ We will use $\lambda = 840$ nm, corresponding to the wavelength in our experiments; $\epsilon_2(840) = -25.7 + j \times 1.72$.

a The dielectric constant ϵ and the refractive index n are related by: $n = \epsilon^{1/2}$

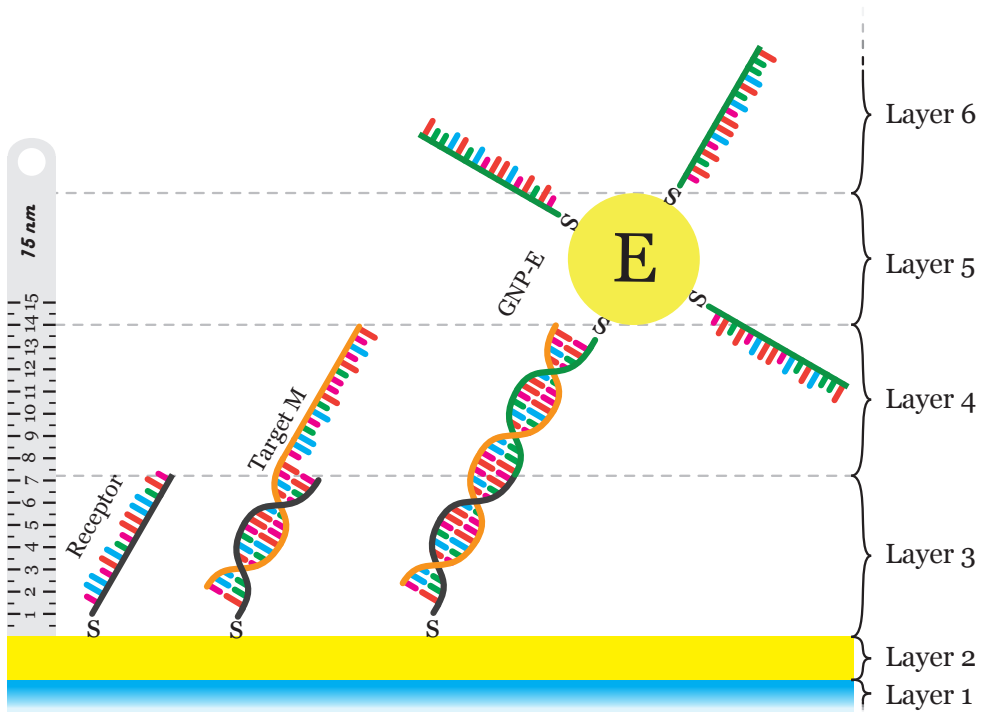


Figure 5-1: The basic amplified SPR detection strategy. A ‘Receptor’ DNA strand is immobilised on the surface, followed by hybridisation with the ‘Target M’ strand. Finally, the signal is amplified by ‘GNP-E’ which acts as a mass label. The amplified SPR consists of the following layers: 1st – glass, 2nd – 50 nm gold, 3rd – ssDNA receptors, 4th – hybridised target DNA strands and 5th – hybridised GNP–DNA. (Note: only the DNA is drawn to scale).

Layer 3 represents the DNA receptor layer. We assume that this is a dense layer. For such a layer it has previously been shown that $n_3 = 1.38$ is a realistic value.⁷ Taking into consideration the length of the DNA strand (25 nucleotides) and the fact that it is tilted we assume layer thickness $d_3 = 7$ nm.

Layer 4 is the layer where the binding DNA-E with Target M strand takes place. Since we are mainly interested in the characteristics of low concentrations for this layer we take somewhat arbitrarily the refractive index value close to that of water: $n_4 = 1.335$. For the layer thickness we assume $d_4 = 7$ nm.

Layer 5 is composed of a mixture of gold nanoparticles with diameter d and surrounding water. Thus, the layer thickness $d_5 = d$.

To obtain a value for the effective dielectric constant ϵ_5 (or refractive index) we have to determine an average of the polarizabilities of the several components of the mixture. Depending on the specific composition of such a layer, several models have been put forward (see, e.g., Sambles *et al.*⁸). In view of the approximate character



of our calculations we prefer the simplest model, which is in fact a volume averaged polarizability of a mixture of water and gold nanoparticles:

$$\frac{\epsilon_5 - 1}{\epsilon_5 + 2} = f_g \cdot \frac{\epsilon_g - 1}{\epsilon_g + 2} + (1 - f_g) \cdot \frac{\epsilon_w - 1}{\epsilon_w + 2} \tag{Equation 5-1}$$

Here, ϵ_g is the dielectric constant of gold: $\epsilon_g = \epsilon_2$, and $\epsilon_w = 1.77$, the dielectric constant of water ($n_w = 1.33$). The parameter f_g is the volume fraction of gold in layer 5.

We convert f_g to the number of gold particles per $(\text{nm})^2$ f_A :

$$f_g = f_A \cdot \frac{2}{3} \pi \cdot r^2 \tag{Equation 5-2}$$

where r is the radius of the gold nanoparticle.

Subsequently we solve eq. 5-1 for ϵ_5 , while substituting eq. 5-2:

$$\epsilon_5 (f_A) = \frac{2[(f_A \cdot \frac{2}{3} \pi r^2) \cdot (\frac{\epsilon_g - 1}{\epsilon_g + 2} - \frac{\epsilon_w - 1}{\epsilon_w + 2}) + \frac{\epsilon_w - 1}{\epsilon_w + 2}] + 1}{1 - [(f_A \cdot \frac{2}{3} \pi r^2) \cdot (\frac{\epsilon_g - 1}{\epsilon_g + 2} - \frac{\epsilon_w - 1}{\epsilon_w + 2}) + \frac{\epsilon_w - 1}{\epsilon_w + 2}]} \tag{Equation 5-3}$$

Note that in equation 5-3 there is a maximum f_A : $f_{A,max} = 1/\pi r^2$.

Finally, *layer 6* is the half-infinite layer representing the aqueous solution, with $n_6 = n_w = 1.33$. In Table 5-1 the layers of the simulation are summarised.

Table 5-1: Summary of layers of the multilayered nanoparticle SPR amplification simulation system at $\lambda = 840 \text{ nm}$.

Layer	Material	Thickness (nm)	Refractive index (n)	Dielectric constant (ε)
1	Prism (BK7)	∞	1.52	2.31
2	Gold	50	0.1695 + j×5.07	-25.7 + j×1.72
3	DNA receptor	7	1.38	1.90
4	DNA target	7	1.335	1.78
5	GNP	20 / 60	GNP density depending (variable)	
6	Water	∞	1.33	1.77



A complete physical characterization of a sensor system comprises three aspects; (1) limit of detection (LOD), (2) differential sensitivity and (3) dynamic range. Other aspects of a chemical sensor, such as specificity, sensitivity for non-specific interactions, etc, fall within the chemical domain, and will not be discussed in the present context.

In Figure 5-2a the dielectric constant of layer 5, ϵ_5 , is depicted as a function of the gold nanoparticle surface concentration for two nanoparticle dimensions^b. Not surprisingly, the dielectric constant of this layer increases faster with 60 nm particles than with 20 nm particles.

Figure 5-2b shows the results of a simulation of the SPR experiment as a function of ϵ_5 , using the above-defined parameters of the various layers. Of course, when measuring a real concentration dependence, also ϵ_4 changes its value, but this change is much smaller than the accompanying change of ϵ_5 . We therefore believe that varying only ϵ_5 in our simulations provides sufficient accuracy.

By combining the data in Figures 5-2a,b we have constructed Figure 5-2c where the shift of the reflectance minimum ($\Delta\phi$) is shown as a function of immobilized GNP surface density (σ). Note that for low analyte concentrations this corresponds to the bound analyte density.

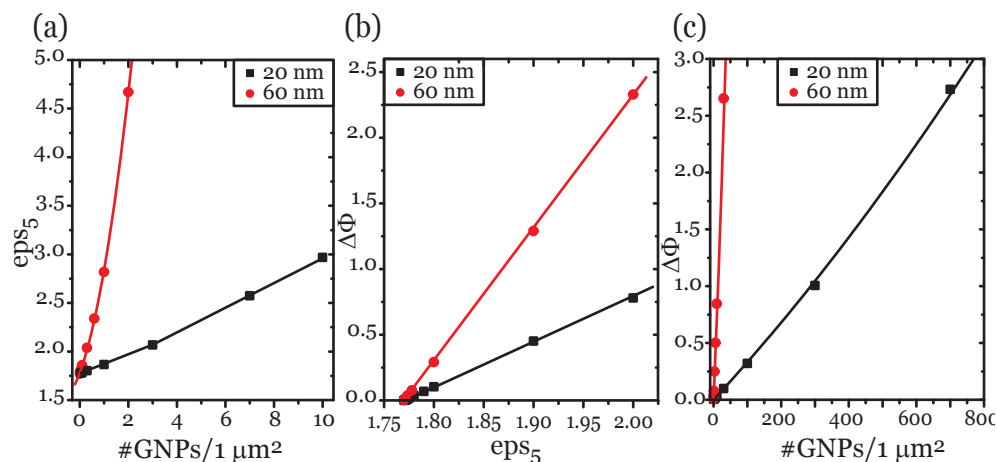


Figure 5-2: (a) Calculated ϵ_5 as a function of GNP surface density for two GNP dimensions. (b) Shift of the reflectance minimum ($\Delta\phi$) response as a function of ϵ_5 . (c) Calculated $\Delta\phi$ response as a function of GNP surface density.

^b Although, strictly spoken, ϵ_5 has also an imaginary component, it turned out that at low nanoparticle concentrations the inclusion of this imaginary part had no influence on the value of the resulting SPR minimum reflectance angle.



The angular resolution of modern SPR instruments in determining the $\Delta\phi$ is better than $\Delta\phi_{\text{SPR}} \sim 0.01$ degrees. With this number and the combination of the data in Figures 5-2a,b we can construct Table 5-2, where the covered fraction of receptor molecules, Γ , is estimated assuming a dense population of receptors which has previously been estimated at $\sim 20 \text{ nm}^2$ per molecule.⁹⁻¹¹

From Figure 5-2c we find the slope $\Delta\phi_{\text{SPR}} / \Delta\sigma_{\text{GNP}} = 3.9 \times 10^{-3} (\mu\text{m})^2$ for 20 nm GNPs. Additionally, from Table 5-2 we find the relation between Γ and σ_{GNP} : $\Gamma = 2 \times 10^{-6} \sigma_{\text{GNP}}$. For the low analyte concentrations involved we can simplify the Langmuir binding isotherm by $\Gamma = K \cdot C_{\text{analyte}}$ with K as the affinity constant.

Table 5-2: Expected limit of detection (at $\Delta\phi_{\text{SPR}} = 10$ mdegrees), differential sensitivity, and dynamic range for GNP amplified SPR at $\lambda=840 \text{ nm}$. The surface densities of GNPs (σ) are expressed in number/ μm^2 .

GNP \varnothing (nm)	$\sigma_{\text{min, GNP}}$	Γ_{min}	$\sigma_{\text{max, GNP}}$	Γ_{max}	$\Delta\phi_{\text{SPR}} / \Delta\Gamma$ at $\Gamma \sim 10^{-4}$
20	3	6×10^{-5}	3×10^3	0.06	196
60	0.1	2×10^{-6}	3×10^2	0.006	6×10^5

Adsorption experiments of receptor molecules result in $\Delta\phi_{\text{SPR}} \sim 0.13$ degrees for a dense layer (data not shown), implying that in the most favourable *not-amplified* case a target molecule concentration can be measured corresponding to $\Gamma \sim 0.1$. Comparison with the data in Table 5-2 suggests an enormous sensitivity enhancement if the SPR response is enhanced by GNPs. Also the dynamic range ($\Gamma_{\text{max}} / \Gamma_{\text{min}}$) then is significantly larger. The fact that $\Gamma_{\text{max}} \ll 1$ for the GNP amplified case comes solely from the fact that at higher Γ steric hindrance of GNPs prevents further GNP binding. Basically, there is no more space available on the surface. We also see that for the larger GNP diameter the differential sensitivity is much larger.

In the next section we will discuss experimental data on amplified SPR and compare them with the data in Table 5-2.

5.3 Experimental

5.3.1 Materials and reagents

Citrate capped gold nanoparticles (60 nm average size with $< 8\%$ CV (GNPs⁶⁰) and 20 nm average size with $< 7\%$ CV (GNPs²⁰)) were purchased from British Biocell International (Cardiff, UK). Thiolated oligonucleotides (DNA) were purchased from Biologio (Nijmegen, The Netherlands). Dithiothreitol (DTT), sodium dodecyl sulphate (SDS), salts and reagents were purchased from Sigma-Aldrich (St. Louis,



MO, USA). Illustra NAP-5 mini spin columns containing a Sephadex G-25 DNA grade matrix were purchased from G.E. Healthcare UK limited (Buckinghamshire, UK). Short thiol-PEG was purchased from Polypure (Oslo, Norway). All aqueous solutions were made with purified water (MilliQ) ($> 18.2 \text{ M}\Omega\cdot\text{cm}$) from a Millipore Academic purifier (Billerica, MA, USA). Aqueous solutions were degassed prior to use.

5.3.2 SPR surface fabrication, functionalisation and SPR set-up

SPR surfaces were prepared on BK7 glass slides ($16 \times 16 \times 1 \text{ mm}$). The slides were cleaned with freshly prepared piranha solution (1 part cold H_2O_2 (35%) to 3 parts H_2SO_4 ($>96\%$)) for 15 minutes followed by washing with MilliQ water and drying under a nitrogen flow. The slides were covered with deposition masks resulting in six individual circular sensor patches with a radius of 0.8 mm ($\sim 2 \text{ mm}^2$). Subsequently, a $\sim 15 \text{ \AA}$ Cr adhesion layer followed by a $\sim 490 \text{ \AA}$ Au layer were deposited using electron beam physical vapour deposition (Balzers BAK 600, Liechtenstein) at a rate of $\sim 1 \text{ \AA}/\text{sec}$ and base pressure of $2 \times 10^{-6} \text{ mbar}$.

Prior to DNA functionalisation the sensor slides were cleaned in piranha solution for one minute followed by washing with MilliQ water. Freshly DTT treated (see Chapter 3) thiolated DNA-D (see Table 5-3) was functionalised to all six sensor spots by incubating $1.5 \mu\text{l}$ $1 \mu\text{M}$ DNA-D in 1 M KH_2PO_4 , pH 3.8, in a humidity chamber for one hour. After incubation the sensor was washed with hybridisation buffer (HB) (300 mM NaCl, 10 mM PB, pH 7.4) followed by target strand hybridisation. The specific target DNA-M was incubated at concentrations of 30, 10, 3, 1, and 0.3 pM and the non-specific target DNA-Mx at 30 pM only. Hybridisation was conducted in HB with a total volume of $1.5 \mu\text{l}$ at room temperature in a humidity chamber for one hour followed by washing with HB. Washing was performed in such a way that individual samples were not mixed. Subsequently, the sensor slide was mounted onto the SPR prism using refractive index matching oil ($n = 1.518$) and placed in the IBIS-iSPR (IBIS, Netherlands) instrument using the Kretschmann configuration followed by incubation with GNP-DNA-E.^{12,13}

5.3.3 Functionalisation of DNA to GNPs

Table 5-3 contains the sequences of the oligonucleotides that were used in the experiments. Prior to functionalisation the protecting disulfide groups on the oligonucleotides were cleaved using a DTT solution. A volume of $100 \mu\text{M}$ DNA was mixed with an equal volume of 340 mM phosphate buffer at pH 8.0. Subsequently, DTT was added to a final concentration of 0.1 M . Samples were incubated on a



orbital shaker for two hours at room temperature followed by a purification step using a MilliQ water rinsed NAP-5 centrifuge column. The samples were diluted to 5 μM with MilliQ and heated to 96 $^{\circ}\text{C}$ for five minutes to ensure single strand conformation. The last step prior to functionalisation was rapid cooling to 4 $^{\circ}\text{C}$.

Table 5-3: Oligonucleotide sequences

Name	Linker (site)	Sequence 5' to 3'
DNA-D	Thiol (5')	GGA TTA CAT TAG ATT AGT TCT TTT T
DNA-E	Thiol (3')	GGG ATT AGG ATT AGG
TARGET M	None	GAA CTA ATC TAA TGT AAT CCG GTT CCT AAT CCT AAT CCC
TARGET M _x	None	GCA GCA GCA GCA GCA GCA GCA GCA GCA GCA GCA GCA GCA

Developer GNPs were constructed by conjugation of DNA-E to GNPs⁶⁰ and GNPs²⁰ in bulk by pre-incubating a 9 ml solution consisting of 0.5 μM DNA-E, 11 mM phosphate buffer (pH 7.4), 333 mM NaCl, 0.1% SDS at room temperature. After 15 minutes, 1 ml of stock GNPs solution (1.3×10^{-10} M) was added and incubated in a rotator at room temperature for 48 hours. After incubation short thiol-PEG at a concentration of 1 μM was incubated for one hour to fill the remaining area on the GNP surface. Subsequently, samples were washed by centrifugation for an hour at $3,900 \times g$ and replacing the supernatant by 10 ml washing solution (0.01% SDS in MilliQ water). This step was repeated twice. In the last step the samples were resuspended in 1 ml washing solution and transferred to 1.5 ml Eppendorf tubes. Subsequently, three more washing steps were done at $8,000 \times g$ for 10 minutes with 1 ml washing solution. To resuspend the pellet from the bottom, the samples were sonicated for 10 seconds while shaken. Due to the smaller size of the GNP²⁰, the centrifugation time was increased twofold. The GNP–DNA-E suspensions were stored at 4 $^{\circ}\text{C}$ until further use. The success of conjugation was assessed by recording extinction spectra.

5.3.4 Assay procedure

A flow-cell was mounted over the sensor surface and regions of interest (ROI) were defined for each sensor spot using the analysis software provided with the instrument. For each ROI the intensity was averaged; the lowest intensity is the SPR-dip (see Chapter 4). Scanning measurements were performed using the scanning mirror over a range of 4.5° with 0.025° intervals at a scan-rate of ~ 12 sec/deg. The flow-cell



temperature was kept constant at 25 °C during the measurement.

To ensure that the system is stable, first a baseline measurement was performed by incubating running buffer (RB) (10 mM phosphate, pH 7.4, 300 mM NaCl and 0.1% SDS) at a flow rate of 5 $\mu\text{l}/\text{min}$ for ten minutes. Subsequently, GNP–DNA-E was incubated at a concentration of 1.0×10^{-10} M in RB at a flow rate of 5 $\mu\text{l}/\text{min}$ for one hour. Incubation in flow ensures that there is no depletion of the GNP–DNA-E. The measurement was finished by a 30 minute washing step with RB to remove unbound GNPs. To ease data analysis, the moment of GNP–DNA-E injection is registered as $t = 0$.

5.4 Results and discussion

5.4.1 GNP functionalisation

The binding of DNA strands to the surface of the GNPs resulted in a change of local refractive index around the GNP. This change, expressed as a shift of the plasmon peak, could be determined using a conventional spectrophotometer for the GNPs²⁰–DNA-E and GNP⁶⁰–DNA-E. From the shape of the spectral curve, the shift of the peak as well as the presence of aggregates could be determined. In aqueous solution GNPs²⁰ have their plasmon peak at $\lambda \sim 524$ nm and GNPs⁶⁰ at $\lambda \sim 535$ nm, which shifts into the red upon binding of DNA-E. This shift is a direct indication for the number of receptors functionalized to the surface of the GNP.^{14,15} Aggregates can be seen as a second peak in the spectral curve, usually in the region $\lambda = 600$ to 700 nm (see Chapter 2). Samples were discarded if the absorbance of the second peak (aggregates) was $> 5\%$ of the absorbance of the primary peak. The extinction spectra of the functionalised GNPs were compared with the spectra of bare GNPs as shown in Figure 5-3. The DNA-E loading on the GNP surface can be estimated (see Chapter 4), using an estimated strand length of 7 nm and refractive index of 1.5. For the GNP²⁰ a shift of 1 nm corresponds to the presence of ~ 22 strands, for GNP⁶⁰ this indicates ~ 125 strands.

For the GNPs²⁰–DNA-E, the plasmon peak shifted from $\lambda \sim 524$ nm to $\lambda \sim 527$ nm; this shift of ~ 3 nm corresponds to approximately 70 receptor strands on the GNP surface. For the GNP⁶⁰–DNA-E, the observed shift was from $\lambda \sim 535$ nm to $\lambda \sim 538$ nm, which corresponds to the binding of ~ 400 strands. Additionally, the shape of the absorbance curve shows only one peak indicating that the presence of aggregates was very low.



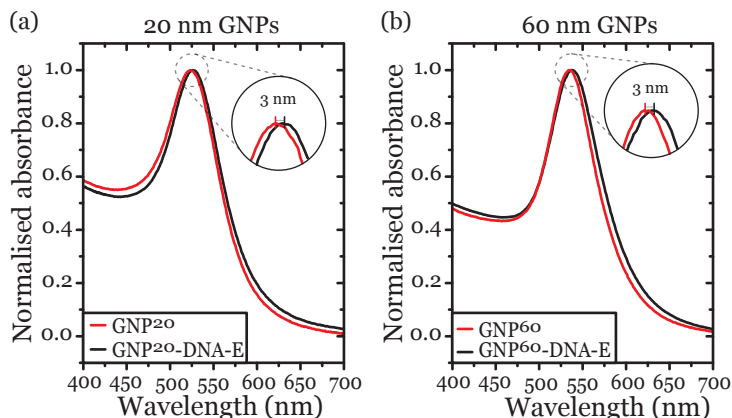


Figure 5-3: Absorbance spectra of bare citrate capped and functionalised 20 nm GNP (a) and 60 nm GNP (b). The inset shows magnified area of the plasmon peaks. The peak position shifted 3 nm into the red upon immobilisation of DNA-E.

5.4.2 Amplified SPR response

In the following experiments we evaluated the GNP amplification by incubating various target strand concentrations. First the data was zeroed to ease comparison (Figure 5-4), followed by concentration dependent responses shown in Figure 5-5.

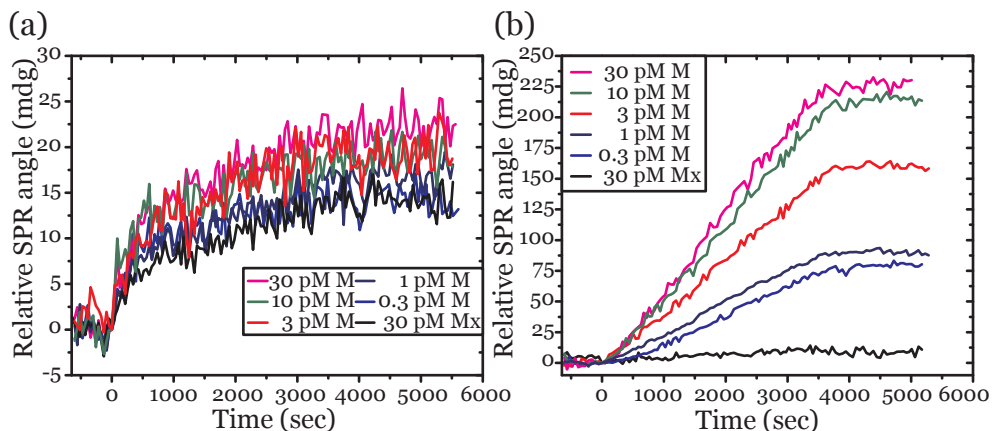


Figure 5-4: Typical concentration dependent results for SPR amplification using (a) 20 nm GNP and (b) 60 nm GNP. The washing started at $t = 3700$ sec. The relative SPR angle change over time is expressed in millidegrees.

The response for the 20 nm GNP amplification as shown in Figure 5-4 can be compared with conventional (label-free) SPR (as shown in Figure 4-6). The hybridisation shows exponential binding behaviour and saturates at a level of ~ 22 millidegrees (mdg).

For the analysis of the experimental data in Figure 5-4 it should be realized that we have to account for two binding processes: one is the binding of the analyte to the immobilized receptor, and another one is the binding of the developer to the hybridized analyte.

A 20 nm GNP accommodates ~ 70 DNA molecules. This implies that upon the approach of a GNP to a bound analyte molecule, the analyte experiences a very high concentration of developer DNA molecule. Thus, although the global developer DNA concentration is rather low ($\sim 10^{-8}$ M) it is reasonable to assume that *locally* there is an excess of developer DNA molecules, implying that *all* bound analytes are covered by GNPs.

The experimental data of Figure 5-4a are now relatively straightforward to analyze in view of the finding that here an equilibrium is reached.

From Figure 5-2c we find the slope $\Delta\phi_{\text{SPR}} / \Delta\sigma_{\text{GNP}} = 3.9 \times 10^{-3} \text{ mdg} \cdot (\mu\text{m})^2$ for 20 nm GNPs. Additionally, from Table 5-2 we find the relation between Γ and σ_{GNP} : $\Gamma = 2 \times 10^5 \sigma_{\text{GNP}}$. For the low analyte concentrations involved we can simplify the Langmuir binding isotherm by $\Gamma = K \cdot C_{\text{analyte}}$ with K as the affinity constant.

As already mentioned, Figure 5-4a exhibits an appreciable response from non-specific interactions. As for all analyte concentrations the same developer concentration was added, this is most probably a non-specific adsorption of GNPs to the receptor-covered surface. This is in line with the observation that for the lower analyte concentrations approximately the same final response is found. Therefore we interpret this non-specific response as a common-mode effect for all analyte concentrations, and the actual specific response is found by subtraction of the common-mode response.

To avoid possible effects due to depletion of the added analyte bulk concentration (*vide infra*), we select the 3 pM binding curve for further analysis as shown in Figure 5-5a. For this analyte concentration we then find the final net angular response as $\Delta\phi_{\text{SPR}} = 20.7 - 12.7 = 8 \text{ mdg}$ resulting in $K_A \sim 2 \times 10^7 \text{ M}^{-1}$, in line with the value found by the group of Corn for a similar DNA system.²

Compared with Figure 5-4a, amplification with 60 nm GNPs (Figure 5-4b) exhibits a much larger response. Applying a analyte concentration of, e.g., 3 pM results in a more than tenfold larger response from the GNP⁶⁰ assay compared to that from the GNP²⁰ assay. Also, not surprisingly, the response in the GNP⁶⁰ assay is much slower in time. From the model described in the appendix we expect that the angular change $\Delta\phi$ is both proportional to time and analyte concentration. A continuous flow of injected 60 nm GNPs indeed causes a linear increase in the signal; if not stopped, the signal reaches beyond the dynamic range of the instrument. At the moment the limit of the dynamic range is reached, the SPR-dip cannot be determined and the response curve stops.



However, the expected linear relation between $\Delta\phi$ and analyte concentration is not found: the response of 30 pM is almost the same as that found for 10 pM. The reason for this becomes clear by inspecting the number of analyte molecules that is available for binding at a receptor spot. For a spot size of $\sim 2 \text{ mm}^2$ and an occupied area of 20 nm^2 per receptor we have $\sim 10^{11}$ receptors on a spot. A $1.5 \mu\text{l}$ 10 pM analyte solution contains $\sim 9 \times 10^6$ analyte molecules. Thus, the maximum Γ that can be reached is $\Gamma_{\text{max}} = 9 \times 10^{-5}$. On the other hand, with $K_A = 2 \times 10^7 \text{ M}^{-1}$, as estimated from the GNP²⁰ experiments, we expect for the 10 pM analyte solution $\Gamma \sim 2 \times 10^{-4}$. Together with the circumstance that most probably not all receptors are active, this points to the situation that depletion plays an important role at higher analyte concentrations. In Figure 5-5b we have plotted $\Delta\phi$ at $t=1$ hour as a function of analyte concentration. It is seen that a linear fit through the origin, as predicted by the model, using only the lower concentrations, is of bad quality. One reason could be that already at the concentration of 3 pM depletion starts to affect the angular shifts found.

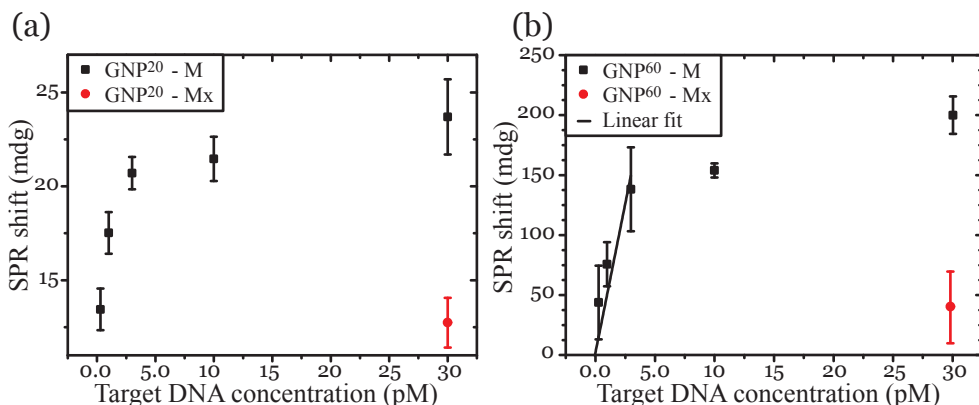


Figure 5-5: SPR-shift, millidegrees (mdg), after one hour incubation, as a function of analyte concentration, (a) for GNPs²⁰ and (b) for GNPs⁶⁰. For the GNPs⁶⁰, line represents a fit through the origin on the basis of the lower three datapoints.

In addition to the studied amplification by GNPs, a change in SPR-dip during the measurement was observed as shown in Figure 5-6.

The widening of the SPR-dip to this extent is not present in non-amplified SPR interaction assays^{2,3} and can be fully explained by the presence of light-absorbing components (the GNPs) in the evanescent field.

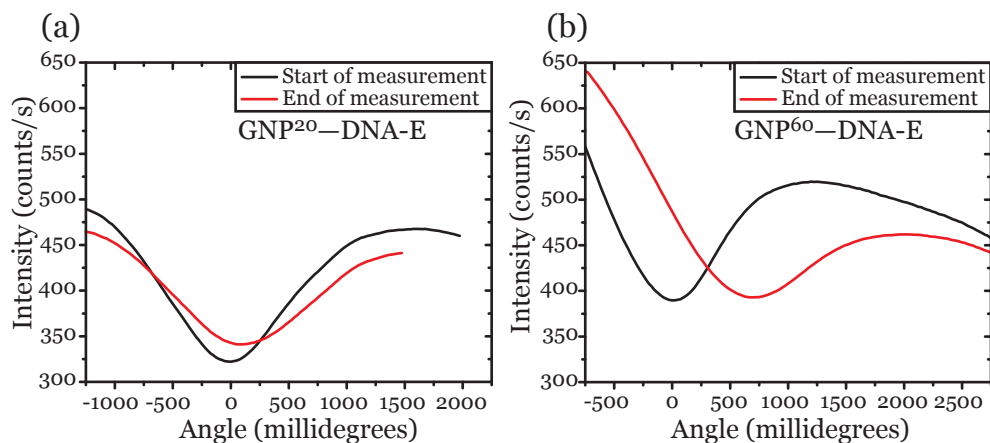


Figure 5-6: Comparison of the SPR-dip position and shape at the start and end of the measurement after (a) GNP²⁰-DNA-E amplification and (b) GNP⁶⁰-DNA-E amplification.

5.4.3 Comparison of measured data with simulations

A complete comparison between experiment and simulation comprises three aspects. **LOD:** To compare the prediction in Table 5-2 with the experimental data we use the simulated coverage found for $\Delta\phi = 10$ mdg. In experiments for the GNP²⁰ and GNP⁶⁰ we then find $\Gamma_{20} = 3 \times 10^{-5}$ and $\Gamma_{60} = 4 \times 10^{-6}$, respectively, which is in reasonable agreement with expectations. In reality, the experimental LOD is better in view of the experimental angular resolution that in modern instruments is better than 10 mdg.

Differential sensitivity: Assuming for the GNP²⁰ experiments a differential sensitivity as quoted in Table 5-2, we found an affinity constant close to that found by Corn *et al.*¹⁶ We interpret this as support for the validity of the GNP²⁰ simulation. For the GNP⁶⁰ experiments we find a differential sensitivity that is tenfold better than that found for the GNP²⁰ experiments, whereas the simulation predicts an improvement that is more than three orders of magnitude. However, we should realize that the fundament of the simulation (equation 5-1) describes a situation where there is an atomic mixture of components.¹⁷ It is clear that this is not the case, particularly for the higher coverages of GNP⁶⁰.

Dynamic range: Unfortunately, due to the limited angular span of the SPR instrument we were not able to make a comparison.

5.5 Conclusion

In this study we have discussed the application of an imaging SPR apparatus for sensitive detection of specific low molecular weight DNA target strands using functionalised gold nanoparticles as label for signal amplification. The large



amplification effects stem both from the large GNP's dielectric constant as compared to that of the surroundings, and from the relatively large aqueous volume that a GNP displaces upon binding to a receptor.

The simulation showed only a limited validity. An improvement might be to construct a model of the macroscopic dielectric constant based on Maxwell-Garnett theory where the GNP and the environment are considered as separate entities, each with their own dielectric identity.

Particularly the use of GNPs⁶⁰ results in sub-pM sensitivity, with an estimated LOD of $\Gamma = 10^{-6}$, in our experiments corresponding to 100 fM. However, for these particles response time is rather slow. It might be worthwhile to investigate whether gold coated magnetic beads improve the time response while maintaining sensitivity.

We also found that for the higher concentrations depletion of analyte is a sizeable effect. To avoid this, while maintaining the benefit of being able to analyze microliter quantities of analyte, receptor patch sizes should be decreased. In view of the SPR coherence length for the used wavelength ($\sim 100 \mu\text{m}$), patch sizes can easily be reduced while keeping SPR sensitivity.

5.6 Bibliography

- (1) Homola J., Yee S.S., Gauglitz G. Surface plasmon resonance sensors: review. *Sensors & Actuators: B Chemical* **1999**; *54*: 3-15.
- (2) Nelson B.P., Grimsrud T.E., Liles M.R., Goodman R.M., Corn R.M. Surface plasmon resonance imaging measurements of DNA and RNA hybridization adsorption onto DNA microarrays. *Analytical Chemistry* **2001**; *73*: 1-7.
- (3) He L., Musick M.D., Nicewarner S.R., Salinas F.G., Benkovic S.J., Natan M.J., Keating C.D. Colloidal Au-enhanced surface plasmon resonance for ultrasensitive detection of DNA hybridization. *Journal of the American Chemical Society* **2000**; *122*: 9071-7.
- (4) Berger C.E.H., Beumer T.A.M., Kooyman R.P.H., Greve J. Surface plasmon resonance multisensing. *Analytical Chemistry* **1998**; *70*: 703-6.
- (5) Schasfoort R., Tudos A. *Handbook of Surface Plasmon Resonance*. Royal Society of Chemistry: Cambridge, **2008**. p. 403.
- (6) Johnson P.B., Christy R.W. Optical constants of the noble metals. *Physical Review B* **1972**; *6*: 4370-9.
- (7) Wolf L.K., Gao Y., Georgiadis R.M. Sequence-dependent DNA immobilization: specific versus nonspecific contributions. *Langmuir* **2004**; *20*: 3357-61.
- (8) Sambles J.R., Bradbery G.W., Yang F. Optical excitation of surface plasmons: An introduction. *Contemporary Physics* **1991**; *32*: 173-83.
- (9) Peterson A.W., Heaton R.J., Georgiadis R.M. The effect of surface probe density on DNA hybridization. *Nucleic Acids Research* **2001**; *29*: 5163-8.
- (10) Peelen D., Smith L.M. Immobilization of amine-modified oligonucleotides on aldehyde-terminated alkanethiol monolayers on gold. *Langmuir* **2005**; *21*: 266-71.
- (11) Sauthier M.L., Carroll R.L., Gorman C.B., Franzen S. Nanoparticle layers assembled through DNA hybridization: Characterization and optimization. *Langmuir* **2002**; *18*: 1825-30.



- (12) Beusink J.B., Lokate A.M.C., Besselink G.A.J., Pruijn G.J.M., Schasfoort R.B.M. Angle-scanning SPR imaging for detection of biomolecular interactions on microarrays. *Biosensors & Bioelectronics* **2008**; *23*: 839-44.
- (13) Kretschmann E. Decay of non radiative surface plasmons into light on rough silver films. Comparison of experimental and theoretical results. *Optics Communications* **1972**; *6*: 185-7.
- (14) Liu G.L., Rodriguez V.B., Lee L.P. Time-resolved optical sensing of oligonucleotide hybridization via Au colloidal nanoparticles. *Journal of Nanoscience & Nanotechnology* **2005**; *5*: 1933-7.
- (15) Storhoff J.J., Elghanian R., Mucic R.C., Mirkin C.A., Letsinger R.L. One-pot colorimetric differentiation of polynucleotides with single base imperfections using gold nanoparticle probes. *Journal of the American Chemical Society* **1998**; *120*: 1959-64.
- (16) Wark A.W., Lee H.J., Corn R.M. Long-range surface plasmon resonance imaging for bioaffinity sensors. *Analytical Chemistry* **2005**; *77*: 3904-7.
- (17) Aspnes D.E. Optical properties of thin films. *Thin Solid Films* **1982**; *89*: 249-62.



Appendix A

In this appendix we discuss a model that describes the GNP-amplified SPR experiments outlined in Chapter 5. In particular we describe the situation where GNPs are added.

In the following we will GNPs denote by ‘analytes’, and the molecules of interest by ‘targets’.

For a simple surface reaction without mass transport limitation and without depletion we can write:

$$\frac{d[AB]}{dt} = k_{on} [A][B] - k_{off} [AB] \quad \text{Equation A-1}$$

where [A] is the analyte concentration, in this case functionalized GNPs, [B] is the immobilised receptor density, here the captured targets DNA-M, and [AB] is the concentration of the product. In Chapter 5 the angular change $\Delta\phi$ is proportional to [AB]. However, generally there is a difference between the analyte concentration close to the surface [A] and the bulk concentration of the analyte $[A_0]$. For this effect we can write:

$$\frac{d[A_0]}{dt} = -k_{tr} [A_0] + k_{tr} [A] \quad \text{Equation A-2}$$

where k_{tr} is related to the diffusion coefficient. Under conditions where GNPs are

added in a flow we can conclude: $\frac{d[A_0]}{dt} = 0 \Leftrightarrow [A_0] = [A]$

By combining equations A-1 and A-2 we get:

$$\frac{d[AB]}{dt} = k'_{on} [A_0][B] - k_{off} [AB] \quad \text{Equation A-3}$$

where k'_{on} is a combination of k_{on} and k_{tr} , of which we do not know the details. In the assay of Chapter 5 $[A_0]$ is the concentration of the GNPs which is constant during the entire assay and the same for all target interactions. As already mentioned, the receptor B is in fact the ‘immobilised’ or captured target concentration, and with a constant $[A_0]$ k'_{on} is the same for every [B]. Solving eq. A-3 results in:

$$[AB] = \frac{k'_{on} [A_0][B]}{k'_{on} [A_0] + k_{off}} \left(1 - e^{-(k'_{on} + k_{off})t} \right) \quad \text{Equation A-4}$$



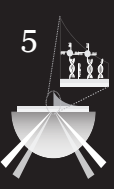
which we can convert for the proportional SPR rate of angular change:

$$\frac{\Delta\varphi}{\Delta t} \propto \frac{d[AB]}{dt} = k'_{on} [A_0][B] e^{-(k'_{on} + k'_{off})t}$$

Equation A-5

For short time periods: $\frac{\Delta\varphi}{\Delta t} \propto k'_{on} [A_0][B]$

Thus we expect that $\Delta\varphi$ is linear both in time and in [B].

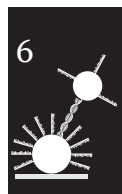




Chapter 6

Femtomolar DNA detection by parallel colorimetric darkfield microscopy of functionalised gold nanoparticles

We introduce a sensing platform for specific detection of DNA based on the formation of gold nanoparticle dimers on a surface. The specific coupling of a second gold nanoparticle to a surface bound nanoparticle by DNA hybridisation results in a red shift of the nanoparticle plasmon peak. This shift can be detected as a colour change in the darkfield image of the gold nanoparticles. Parallel detection of hundreds of gold nanoparticles with a calibrated true colour camera allowed us to detect specific binding of target DNA. This enabled a limit of detection below 1.0×10^{-14} M without the need for a spectrometer or a scanning stage.



6.1 Introduction

The interest in sensitive detection of specific DNA sequences has grown tremendously in the last decade. Examples are pandemic surveillances (as was shown during the 2009 swine flu outbreak)¹ and single nucleotide polymorphism detection for genetic diagnostic analysis of cancer and other diseases.^{2,3} The global use of DNA based molecular diagnostics becomes increasingly important. For all these needs it is essential that detection is sensitive, specific, rapid and preferably low-cost.

The most common methods for sensitive detection of specific DNA sequences require the use of optical reporters, mostly based on fluorescence.^{4,5} However, fluorescent detection suffers from two major disadvantages: the low stability of the reporter (photobleaching) and the low signal of a single reporter which makes it difficult to detect single recognition events. In addition, a dedicated complex apparatus is required for sensitive detection.

Currently the most popular sensitive detection method of DNA is based on real-time analysis of specific amplification using the polymerase chain reaction (PCR). The amplification of DNA is a time consuming and expensive approach.⁶ Therefore, there is currently a substantial research thrust into PCR-less detection schemes.⁷

Recent developments in optical detection methods based on surface plasmon resonance (SPR) or local surface plasmon resonance (LSPR) of gold nanoparticles provide an alternative approach. Oligodeoxynucleotide (DNA) functionalised gold nanoparticles (GNPs) which aggregate upon analyte binding are widely studied.⁸⁻¹¹ Aggregation of GNPs results in a change of colour of the colloidal solution as a result of plasmon coupling which can be monitored using a simple spectrophotometer.

In SPR the response can be amplified by using functionalised GNPs as mass label. This approach enables very sensitive detection for low molecular weight analytes¹²⁻¹⁴ but it still requires a dedicated apparatus. In LSPR the non-bleachable scattering of DNA-functionalised GNPs can be detected in a standard microscope under darkfield conditions with the naked eye or with a simple detector, e.g., a CCD-camera.^{15,16} LSPR based analyte detection relies on the measurement of spectral changes of individual^{17,18} or an ensemble¹⁹ of GNPs upon analyte binding. This change can be measured by a spectrophotometer or colour CCD-camera.

Previously, the group of Van Duyne²⁰ demonstrated that the presence of small numbers of molecules bound to immobilised silver nanoparticles could be detected via the change of their scattering spectrum. However, the ability to detect that small number of molecules is not sufficient to detect low concentrations; an additional condition is that the method should be capable of detecting very low coverage fractions of available binding sites. It then turns out that the measurement of only



Femtomolar DNA detection by colourimetric DF microscopy of GNPs

the spectral change of a GNP upon analyte binding does not provide sufficient sensitivity.²¹

In the present study, we use DNA functionalised GNPs for specific target DNA detection in the femtomolar range. The detection is based on the use of a darkfield (DF) microscope to monitor the individual scattering colour changes of hundreds of GNPs over a time period. The application of GNP sandwich detection by simultaneously monitoring the colour change of many individual GNPs as a result of analyte binding is depicted in Figure 6-1. First, GNPs are randomly immobilised on a 3-aminopropyltriethoxysilane (APTES) coated glass slide (step 1). Subsequently, thiolated DNA strands are immobilised onto the GNP surface. In a washing step unbound DNA strands are removed, leaving functionalised GNPs on the surface (step 2). Next, the analytes are introduced which specifically hybridise with the DNA on the immobilised GNPs (step 3). After a second washing step a second DNA functionalised ‘developer’ GNP is introduced and allowed to bind to the second part of the analyte (step 4). The resulting close proximity of two GNPs induces an appreciable change of scattered light peak wavelength. This approach should allow us to detect single analyte capture events. In this study we carried out proof-of-concept experiments where we detect analyte concentrations down to the femtomolar range. This is done by analyzing the changing scattering colour of hundreds of GNPs in parallel, after carrying out the above mentioned steps 3–4.

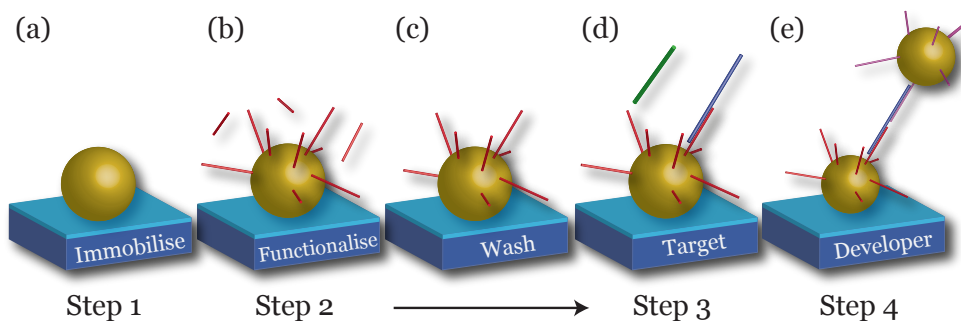
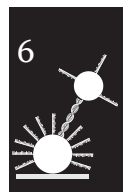


Figure 6-1: Schematic illustration of the strategy for the sensitive detection of a DNA analyte. (a) 80 nm GNP immobilised on APTES surface as step 1, followed by (b) DNA functionalisation in step 2; (c) unbound receptors are washed away followed by (d) the hybridisation of the analyte in step 3. (e) Finally, a developer GNP particle is added to form a twin GNP sandwich for single binding event detection in step 4.



6.2 Experimental

6.2.1 Materials and reagents

Citrate capped gold nanoparticles (80 nm average size with < 8% CV and 40 nm average size with < 7% CV) were purchased from British Biocell International (Cardiff, UK). Thiolated oligonucleotides (DNA) were purchased from Biolegio (Nijmegen, The Netherlands). Dithiothreitol (DTT), 3-aminopropyltriethoxysilane (APTES), sodium dodecyl sulphate (SDS), salts and reagents were purchased from Sigma-Aldrich (St. Louis, MO, USA). Illustra NAP-5 mini spin columns containing a Sephadex G-25 DNA grade matrix were purchased from G.E. Healthcare UK limited (Buckinghamshire, UK). All aqueous solutions were made with purified water (MilliQ) (> 18.2 M Ω ·cm) from a Millipore Academic purifier (Billerica, MA, USA). Aqueous solutions were degassed prior to use.

6.2.2 Choice of GNP set

The scattering peak wavelength of two GNPs shifts due to the close proximity.²²⁻²⁴ This can be formed in a sandwich assay by hybridisation of the target strand. The plasmon peak (λ_{\max}) shift depends on the size of both GNPs and the distance between them. The receptor GNPs must have a relatively large size in order to host a large number of DNA receptor molecules per GNP.²⁵ However, GNPs of sizes larger than 50 nm are less stable in solution, especially at increased ionic strength of the buffer.²⁶ Therefore we developed an assay where a sandwich was constructed from a large immobilised 80 nm receptor GNP (GNP⁸⁰) and a smaller 40 nm ‘developer’ GNP (GNP⁴⁰). The GNP⁴⁰ is chosen to give a strong response, while ensuring a stable, not aggregating particle in suspension. Additionally, if the large GNP is immobilised on the surface first, it eases imaging since the scattering cross section increases significantly with the increase of the size of the nanoparticles. Additionally, the GNP⁸⁰ have a larger surface area which can accommodate a high number of DNA receptors and therefore would lead to signal generation at a lower coverage fraction of the available binding sites.

Discrete dipole approximation simulations (DDA) of the scatter process were performed using the DDSCAT software package (v 7.1)^{27,28} to estimate the plasmon peak shift that we can expect from a GNP⁸⁰ to GNP⁴⁰ sandwich for a various interparticle distances (See Chapter 4). In addition, DDA was used to calculate light scattering spectra for both bare and DNA covered GNPs. 15-mer and 25-mer DNA strands were modelled as shells around the GNP with respective thicknesses of 5.1



nm and 8.5 nm, with refractive index of $n = 1.5$.²⁹ Individual GNP⁴⁰ and GNP⁸⁰ are able to host up to ~430 and ~1,400 single stranded DNA molecules, respectively.²⁵

6.2.3 Preparation of APTES coated glass slides

BK7 microscope slides (76 mm x 26 mm x 1 mm) from Menzel (Braunschweig, Germany) were placed in a glass holder. The slides were sonicated in MilliQ water for 15 minutes followed by a 15 minute cleaning step in piranha solution (H_2O_2 (35%) : H_2SO_4 (>96%), 1 : 3) at 95 °C (Caution! Piranha solution is highly corrosive) and a second 15 minute sonication step in MilliQ water. A 5% APTES solution was made using 99.9% ethanol; directly after mixing the solution the glass holder with slides was transferred from the MilliQ water to the APTES solution and incubated for 15 minutes. Subsequently, slides were sonicated in fresh MilliQ water three times for five minutes. After the washing steps silanisation was finalised by a two hour baking step at 120 °C.

6.2.4 GNP immobilisation

GNPs⁸⁰ were randomly immobilised by incubating a freshly coated APTES slide with a 4.0×10^{-13} M GNP solution for ten minutes. This resulted in such GNP coverage that individual particles had sufficient interparticle distance to be individually visible in the DF microscope. After incubation the slide was washed with MilliQ water and dried with nitrogen gas. For further use a 24-well microarray sticker (EMSDiasum; Hatfield, PA, USA) was applied on the GNP coated glass slide. The sticker created 10 μ l wells.

6.2.5 Functionalisation of DNA to GNPs

Table 6-1 contains the sequences of the oligonucleotides that were used in the experiments. Prior to functionalisation the protecting disulfide groups on the oligonucleotides were reduced using a DTT solution. A volume of 100 μ M DNA was mixed with an equal volume of 340 mM phosphate buffer at pH 8.0. Subsequently, DTT was added to a final concentration of 0.1 M. Samples were incubated on a orbital shaker for two hours at room temperature followed by a purification step using a MilliQ water rinsed NAP-5 centrifuge column. The DNA samples were diluted to 5 μ M with MilliQ and heated to 96 °C for five minutes to ensure single strand conformation. The last step prior to functionalisation was rapid cooling to 4 °C.

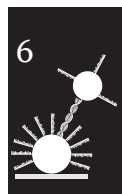


Table 6-1: Oligonucleotide sequences

Name	Linker (site)	Sequence 5' to 3'
DNA-D	Thiol (5')	GGA TTA CAT TAG ATT AGT TCT TTT T
DNA-E	Thiol (3')	GGG ATT AGG ATT AGG
DNA-M	None	GAA CTA ATC TAA TGT AAT CCG GTT CCT AAT CCT AAT CCC
DNA-Mx	None	GCA GCA GCA GCA GCA GCA GCA GCA GCA GCA GCA GCA GCA

For flow-cell measurements GNP⁸⁰ were randomly immobilised on a freshly prepared APTES coated microscope slide. Subsequently, the slide was mounted in a flow-cell for the incubations and measurements. GNPs were functionalised by incubation of the flow-cell with 5 μM DNA-D in running buffer (RB) consisting of 10 mM phosphate buffer (pH 7.4), 300 mM NaCl and 0.1% SDS, for two hours at room temperature followed by removal of unbound DNA strands by washing with running buffer.

For measurements of the concentration range using the 24-well microarray sticker, DNA-D was conjugated to immobilised GNP⁸⁰ by incubating 10 μl of the above described solution for two hours at room temperature. This was followed by a 5 \times washing step with 15 μl RB.

Developer GNPs were constructed by conjugation of DNA-E to GNP⁴⁰ in bulk by pre-incubating a 9 ml solution consisting of 0.5 μM DNA-E, 11 mM phosphate buffer (pH 7.4), 555 mM NaCl, 0.1% SDS at room temperature. After 15 minutes, 1 ml of stock GNP⁴⁰ solution (1.3×10^{-10} M) was added and incubated in a rotator at room temperature for 48 hours. After incubation the samples were washed by centrifugation for an hour at 3,900 $\times g$ and replacing the supernatant by 10 ml washing solution (0.01% SDS in MilliQ water). This step was repeated twice. In the last step the samples were resuspended in 1 ml washing solution and transferred to 1.5 ml Eppendorf tubes. Subsequently, three more washing steps were done at 8,000 $\times g$ for ten minutes replacing the supernatant with 1 ml washing solution. To resuspend the pellet from the bottom, the samples were sonicated for ten seconds while shaken. The colloidal suspensions of GNP⁴⁰-DNA-E were stored at 4 $^{\circ}\text{C}$ until further use. Both for the GNP⁸⁰ and the GNP⁴⁰ the success of conjugation was checked by recording extinction spectra.



6.2.6 Assay procedure

Imaging was performed in reflection mode on an Olympus GX71 microscope using a 20× darkfield (DF) objective with a 2× magnifier lens. Pictures were acquired using a Zeiss Axiocam HRc (Jena, Germany) spatial scanning colour camera. Spectra of individual GNPs were acquired using an Ocean Optics QE65000 fibre spectrometer (Dunedin, FL, USA). For real-time assays a continuous auto-focus feedback loop was used to reduce objective focus fluctuations due to, e.g., temperature changes.

Prior to fibre spectrometer measurement a white reference was taken to calibrate for the spectrum of the light source. This was done by placing a mirror in the sample plane. Additionally, a dark reference was taken to compensate for background scattering of the APTES surface. To this end the spectrum was measured of a GNP free area of the sample slide. To measure a GNP spectrum the scattering GNP of interest was aligned with the fibre using a laser guiding system. Subsequently the scattered light of the individual GNP was acquired for 30 seconds.

Prior to image analysis the stack of acquired images was aligned using the DipImage toolbox (version 2.2, University of Delft, the Netherlands) for MatLab. The scattering colour of the GNPs, which is directly related to λ_{\max} , was expressed as the ratio between the intensities of the red and green channel of the camera which we denoted as the r/g ratio. Previously we demonstrated that by measuring changes in r/g ratio we could detect changes of λ_{\max} as small as 1 nm.³⁰ A custom-made MatLab script was used to analyze the r/g ratio for each individual GNP in all images throughout the measurement. By comparing the images before and after incubation we counted the GNPs which changed colour upon developer GNP binding, out of the total number of GNPs in the image. The obtained ratio of changed versus the total number of GNPs was used to express the level of binding. It is important to note that we did not attempt to distinguish single binding events from multiple ones. An immobilised GNP⁸⁰ is able to host multiple GNPs⁴⁰ but this event is not likely at low target concentrations.

6.2.7 Flow through assay measurement

The flow-cell with immobilised and functionalised GNPs⁸⁰ was incubated with 1.0×10^{-9} M specific (DNA-M) or non-specific (DNA-Mx) target DNA diluted in RB at room temperature for one hour. Subsequently, the flow-cell was washed with RB and mounted to the microscope stage. Throughout the measurement images were acquired every minute. First, a baseline measurement was performed by incubating RB at a flow rate of 1 μ l/min followed by incubation with the developer particle GNP⁴⁰-DNA-E at a concentration of 1.0×10^{-10} M in RB. The measurement was finished by a washing step with RB to remove unbound developer particles.



6.2.8 Limit of detection measurement

Each well was incubated with 10 μl specific (DNA-M) or non-specific (DNA-Mx) target DNA diluted in RB. The concentration of the target particles ranged from 1.0×10^{-6} to 3.0×10^{-15} M. Each concentration was incubated for two hours in a humidity chamber at room temperature followed by five times washing with RB. A 24-well slide was mounted onto the microscope table and for each well an image was acquired under darkfield conditions. Subsequently, each well was incubated with 1.0×10^{-10} M GNP⁴⁰-DNA-E in RB for two hours at room temperature. After incubation each well was washed 5 \times with RB and the second image was acquired in this buffer.

6.3 Results and Discussion

6.3.1 The GNP sandwich response

From scatter simulations we see that a sandwich of 80 nm versus 40 nm would result in a large plasmon peak shift, as shown in Figure 6-2. In this particular case, using a 39 nucleotide long target, upon binding a sandwich is formed with an estimated GNP⁸⁰-GNP⁴⁰ edge-to-edge distance of 15 nm.^{31,32} This corresponds to a maximum λ_{max} -shift in the order of 15 nm, or $\Delta r/g \approx 0.4$.^{21,27} However, the magnitude of this shift depends also on the particles' size and on the direction of the pair axis relative to the polarisation direction of the light. Taking this into account, and under unpolarised light conditions it is expected that the shift of a single binding event can vary from at most 30 nm wavelength shift for a 5 nm gap to at least 5 nm wavelength shift for a 30 nm gap for the GNP⁸⁰-GNP⁴⁰ pair as shown in Figure 6-2.²¹

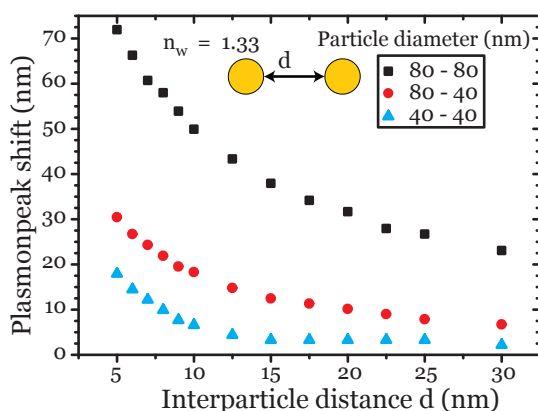


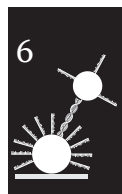
Figure 6-2: Calculated plasmon peak shift for various close proximity positions of two GNPs, embedded in water, under unpolarised light conditions for three different size pairs (black squares are used for the peak shift of two 80 nm particles, red spheres for the peak shift of an 80 nm particle in the proximity of a 40 nm particle, and blue triangles for two 40 nm particles).

Additionally, the surface coverage of individual GNPs was estimated. For the GNP⁴⁰ the maximum plasmon peak shift for a shell of 5.1 nm (DNA-E) is a λ_{max} shift of 6.1 nm. From these numbers we can estimate a coverage of ~ 70 conjugated strands per nm λ_{max} shift for the 15-mer DNA-E. For the GNP⁸⁰ the maximum plasmon peak shift for a shell of 8.5 nm (DNA-D) is a λ_{max} shift of 12.5 nm. This corresponds to a coverage of ~ 112 strands per nm shift for the 25-mer DNA-D. By analysing the peak shift as a result of DNA functionalisation we calculate the coverage percentage based on the maximum shift possible for the specific shell thickness (see Chapter 4).

6.3.2 Quality of functionalisation and GNP surface coverage

The binding of DNA strands to the surface of the GNPs resulted in a change of local refractive index. This change, expressed as a shift of the plasmon peak, was measured for immobilised single GNPs⁸⁰ using the micro spectrophotometer and a conventional spectrophotometer for in-bulk functionalised GNPs⁴⁰. From the shape of the spectral curve the shift of the peak as well as the presence of aggregates could be determined. In aqueous solution GNPs⁴⁰ have their plasmon peak at $\lambda \sim 527$ nm which shifts into the red upon binding of DNA-E. Aggregates can be seen as a second peak in the spectral curve, usually in the region $\lambda = 600$ to 700 nm. Samples were discarded when the absorbance of the second peak (aggregates) was $> 5\%$ of the absorbance of the primary peak (conjugated GNPs⁴⁰-DNA-E).

The functionalisation of immobilised GNPs was monitored for a number of individual particles by measuring the scattering spectra before and after functionalisation. The shift is a direct indication for the number of receptors functionalised to the surface of the GNP.^{33,34} For the GNPs⁴⁰-DNA-E the plasmon peak shifted from $\lambda \sim 527$ nm to $\lambda \sim 530$ nm; this shift of ~ 3 nm corresponds to approximately 200 receptor strands on the GNP surface. For the GNPs⁸⁰ a T5-spacer was incorporated at the thiol side of DNA-D; this was done to promote the hybridisation with the 39-mer target strand DNA-M and to reduce steric hindrance. Single particle spectral measurements indicate a scattering plasmon peak shift of ~ 6 nm which corresponds to ~ 700 DNA-D receptor strands per GNP as shown in Figure 6-3.



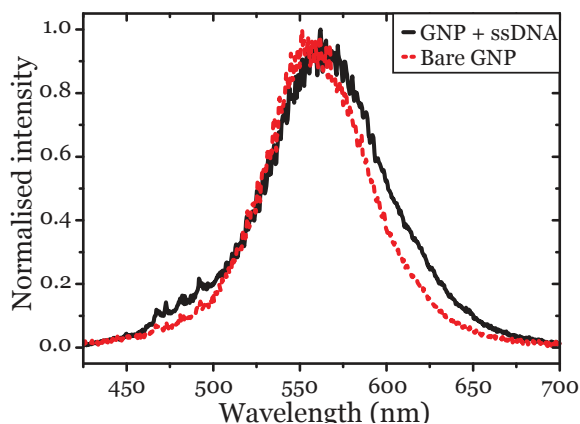


Figure 6-3: Scattering spectra of an individual immobilised GNP⁸⁰ before and after functionalisation. The scattering peak shifted from 558 to 564 nm.

6.3.3 Flow assay analysis

The immobilisation of GNPs⁸⁰ on the APTES surface was checked by DF microscopy. Figure 6-4 shows a part from a typical darkfield image of GNPs⁸⁰ on the glass/APTES substrate. Because of the polydispersity of the sample, a small portion of particles with different sizes and shapes were present. These could be seen as different colours in the DF image. The microscope slide was checked to have approximately 1,000 individual GNPs homogeneously spread over the surface with at least 95% of the GNPs scattering green. Particles which appeared red before the addition of the GNP⁴⁰-DNA-E were ignored in the analysis. We subsequently monitored the functionalisation of DNA-D to individual GNPs⁸⁰; we estimated the presence of approximately 700 receptors per GNP⁸⁰ from the ~ 6 nm shift observed in the peak wavelength of the scattering spectrum. The number of receptors per GNP⁴⁰-DNA-E was estimated at ~ 200 . While in theory a higher receptor density on the particle could increase the sensitivity (since we would get a binding even at a lower coverage fraction), the hybridisation becomes more difficult due to crowding if the DNA density is too high. Therefore we used only 300 mM of NaCl in the conjugation step, which gives about half of the maximum density possible for the DNA on the particles.³⁵



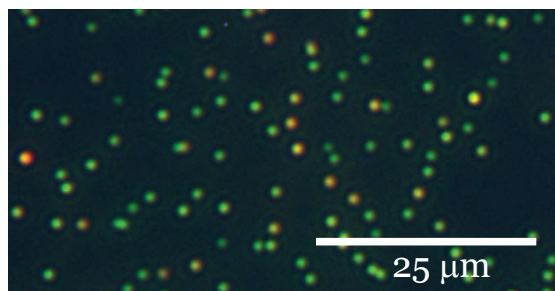


Figure 6-4: $63 \times 33 \mu\text{m}$ part from a darkfield image with a typical sensing area of $165 \times 220 \mu\text{m}$ (which contains on average around 1,000 individual GNPs).

In Figure 6-5 we show the response of several individual GNPs upon incubating with the developer GNP. The magnitude of the change depends on the number of bound GNPs⁴⁰ and on the distance between the first and second GNP.²¹ Upon binding, a stepwise change of $\Delta r/g$ up to 0.4 was observed for the specific target. No response was observed for the non-specific target incubation. The observation that for different nanoparticles a stepwise change in r/g takes place at different time points is strong evidence for the occurrence of a binding event. It is also seen that $\Delta r/g$ varies somewhat over the various binding events. We note that $\Delta r/g$ depends not only on the mutual distance of both GNPs but also on the orientation of the GNP⁴⁰ in the confined area around the GNP⁸⁰. The GNP⁴⁰ can be hybridised right on top of the GNP⁸⁰ but also on the side or any position in between. Furthermore, the variation in the size of the used GNPs influences the λ_{max} shift.

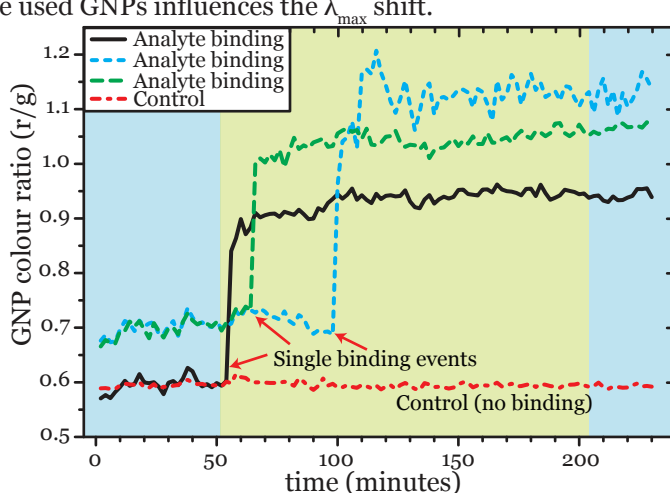


Figure 6-5: Individual GNP darkfield responses during incubation with the GNP⁴⁰. At $t = 0$ running buffer was incubated, at $t = 50$ min GNP⁴⁰–DNA-E was incubated, followed by a washing step with running buffer at $t = 205$ min. In the control a non-complementary analyte was incubated.

Additionally, the binding was checked using SEM. Figure 6-6 shows representative results from SEM imaging of the GNP⁸⁰ and GNP⁴⁰ hybridisation pairs. The variation in size of both GNP⁸⁰ and GNP⁴⁰ is visible; however, the scattering peak position of a dimer is always shifted in to the red compared to the single GNP⁸⁰. Since we look at each individual single GNP⁸⁰ before it possibly changes to a dimer upon binding of a GNP⁴⁰, the size variation does not influence our analysis strategy significantly. Due to the capillary force during drying, the interparticle gap appears only 2 to 5 nm under SEM conditions.



Figure 6-6: Scanning electron microscope images of GNP⁸⁰ and GNP⁴⁰ hybridisation pairs. The images were acquired using a Philips XL30 eSEM in environmental mode at 15 KV at 10,000× after sample drying under a flow of nitrogen gas.

6.3.4 Limit of detection measurement

In the following experiments we evaluated the sensitivity of the detection method by incubating immobilised and functionalised GNPs⁸⁰ with various target strand concentrations; results are shown in Figure 6-7. The response curve to specific target hybridisation shows saturation at high concentrations followed by a steep descent and low response at low concentrations. GNPs that changed $\Delta r/g > 0.1$ (corresponding to $\Delta\lambda_{\max} > 4$ nm) were recorded as positive. The response was expressed as the binding ratio of the number of particles with $\Delta r/g > 0.1$ versus the total number of particles in the image. A significant decrease of colour changed particles can be detected at concentrations below 1.0×10^{-13} M. Our results suggest that the limit for detection for this target DNA strand is lower than 1.0×10^{-14} M. When no target DNA was added we obtained a low response suggesting that without an analyte, GNPs⁴⁰ can hardly bind to the GNPs⁸⁰. When particles were incubated with a non-specific target strand the response varied. This indicates that the GNPs⁴⁰ can bind to a non-specific strand, albeit to a significantly lower extent.

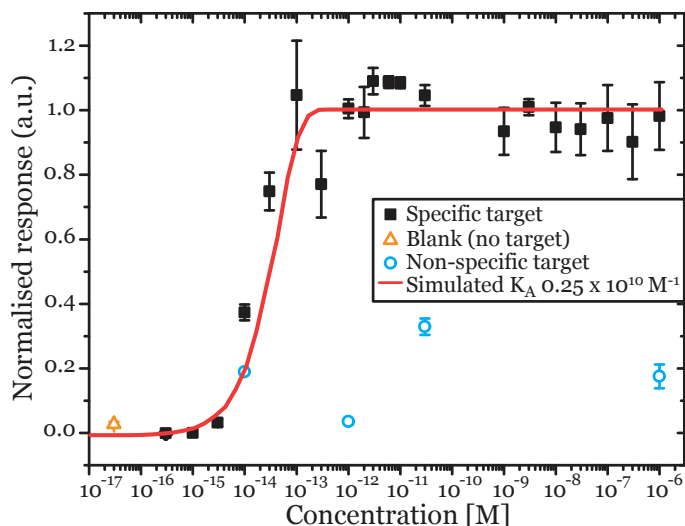
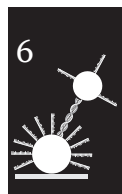


Figure 6-7: Dose-response relation based upon counting the fraction of GNPs that changed colour after incubation with the analyte. The blank sample is located at 3.0×10^{-17} M for illustrative purposes. The response was normalised in order to compare the data with a Monte Carlo simulated binding model. Error bars were constructed from triplicate measurements.

In order to estimate the affinity constant K_D , a Monte Carlo simulation of the binding process was set up, based on a simple Langmuir adsorption model (See Chapter 4). From the comparison of simulated and experimental data, as shown in Figure 6-7, we conclude that K_A lies near 0.25×10^{-10} M. This is also close to the value that we found from a conventional GNP amplified SPR experiment on the same DNA system (See Chapter 5). In order to visualise the target-DNA covered GNPs⁸⁰, we require the addition of a second set of GNPs⁴⁰ that bind to the bound target. The fraction bound of this second set is again subject to a binding equilibrium; with a concentration of $\sim 10^{-10}$ M of GNPs⁴⁰, ~ 660 receptors per GNP⁸⁰ and the found K_A of $\sim 0.25 \times 10^{-10}$ M we can safely assume that in this second equilibrium all bound targets are occupied with a GNP⁴⁰. This implies that the vertical axis of Figure 6-7 corresponds to the fraction of bound GNPs, as determined from the simulation.

6.3.5 Comparison with other detection methods based on gold nanoparticles

In Table 6-2 we compare various DNA detection approaches from literature with our two GNP close proximity approach. Conventional imaging SPR is label free but it cannot detect very low concentration of DNA due to the low molecular weight of the target.³⁶ Using GNPs as a label, the limit of detection (LOD) in SPR can be improved



by three to six orders of magnitude.^{12,37} While the use of a PNA receptor in the work of D'Agata¹² resulted in a lower detection limit than the one we show in this paper, we believe this is a product of the higher affinity of PNA–DNA interactions compared to DNA–DNA interactions, and not a result of higher instrument sensitivity. The bio-barcoding assay does show a very high sensitivity; however, it is much more complex and time consuming than the approach we propose, mostly due to the double amplification step it uses.³⁸

Table 6-2: Comparison of various DNA sensing schemes based on GNPs.

Method	Type	LOD	Dynamic range (M)	Reference
Imaging SPR	DNA receptor DNA target	10 nM	NA	36
GNP amplified imaging SPR	DNA receptor DNA target GNP–DNA	10 pM	10^{-8} to 10^{-14}	37
GNP amplified imaging SPR	PNA receptor DNA target GNP–DNA	1 fM	NA	12
Bio barcode	GNP–DNA receptor DNA target Silver staining	7 aM	10^{-15} to 10^{-17}	38
Two GNP proximity	GNP–DNA receptor DNA target GNP–DNA	~10 pM	10^{-11} to 10^{-13}	17
Two GNP proximity Parallel detection	GNP–DNA receptor DNA target GNP–DNA	10 fM	10^{-12} to 10^{-15}	This study

6.4 Conclusion

In this study we have shown the use of a simple darkfield reflection microscope in combination with a CCD-colour camera to detect the light scattering changes of hundreds of GNPs in parallel as a result of a two GNP sandwich formation. Because only a single developer GNP is needed to cause a detectable change in the colour of the receptor GNP, the parallel monitoring of the receptor GNPs resulted in the detection of target DNA strands at the femtomolar range.

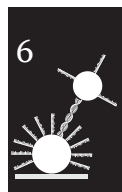
By capturing multiple images at different times in a flow through assay we show that it is possible to monitor the binding of the developer GNP onto the previously hybridised small target DNA strand without the need of spectroscopic detection.

A binding model based on Monte Carlo simulations was developed to assess the binding constant from the binding curve.

We believe the detection limit and dynamic range could be further improved by using a larger number of receptor gold nanoparticles in the field of view reducing the non-specific binding. We envision that this approach could lead to a rapid and ultra sensitive detection method which could replace the real-time PCR approach in a number of applications.

6.5 Bibliography

- (1) Trifonov V., Khiabani H., Rabadan R. Geographic dependence, surveillance, and origins of the 2009 influenza A (H1N1) virus. *The New England Journal of Medicine* **2009**; *361*: 115-9.
- (2) Ibrahim M.S., Lofts R.S., Jahrling P.B., Henchal E.A., Weedn V.W., Northrup M.A., Belgrader P. Real-time microchip PCR for detecting single-base differences in viral and human DNA. *Analytical Chemistry* **1998**; *70*: 2013-7.
- (3) Perkel J. SNP genotyping: six technologies that keyed a revolution. *Nature Methods* **2008**; *5*: 447-53.
- (4) Ginzinger D. Gene quantification using real-time quantitative PCR: An emerging technology hits the mainstream. *Experimental Hematology* **2002**; *30*: 503-12.
- (5) Sassolas A., Leca-Bouvier B.D., Blum L.J. DNA biosensors and microarrays. *Chemical Reviews* **2008**; *108*: 109-39.
- (6) Sohni Y., Kanjilal S., Kapur V. Performance evaluation of five commercial real-time PCR reagent systems using TaqMan assays for *B. anthracis* detection. *Clinical Biochemistry* **2008**; *41*: 640-4.
- (7) Nam J.M., Stoeva S.I., Mirkin C.A. Bio-bar-code-based DNA detection with PCR-like sensitivity. *Journal of the American Chemical Society* **2004**; *126*: 5932-3.
- (8) Chen S.H., Lin K.I., Tang C.Y., Peng S.L., Chuang Y.C., Lin Y.R., Wang J.P., Lin C.S. Optical detection of human papillomavirus type 16 and type 18 by sequence sandwich hybridization with oligonucleotide-functionalized Au nanoparticles. *IEEE Transactions on Nanobioscience* **2009**; *8*: 120-31.
- (9) Jung C., Chung J.W., Kim U.O., Kim M.H., Park H.G. Real-time colorimetric detection of target DNA using isothermal target and signaling probe amplification and gold nanoparticle cross-linking assay. *Biosensors & Bioelectronics* **2011**; *26*: 1953-8.
- (10) Jyoti A., Pandey P., Singh S.P., Jain S.K., Shanker R. Colorimetric detection of nucleic acid signature of Shiga toxin producing *Escherichia coli* using gold nanoparticles. *Journal of Nanoscience & Nanotechnology* **2010**; *10*: 4154-8.
- (11) Thaxton C.S., Georganopoulou D.G., Mirkin C.A. Gold nanoparticle probes for the detection of nucleic acid targets. *Clinica Chimica Acta* **2006**; *363*: 120-6.
- (12) D'Agata R., Corradini R., Ferretti C., Zanolli L., Gatti M., Marchelli R., Spoto G. Ultrasensitive detection of non-amplified genomic DNA by nanoparticle-enhanced surface plasmon resonance imaging. *Biosensors & Bioelectronics* **2010**; *25*: 2095-100.

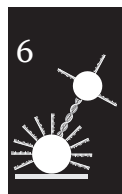


- (13) Liu H., Yamaguchi A., Hayashida M., Matsuo S., Misawa H. Construction of DNA-Au nanoparticles multilayer and its application to detection of DNA hybridization. *Japanese Journal of Applied Physics* **2004**; *43*: 2767-70.
- (14) Yang X., Wang Q., Wang K., Tan W., Li H. Enhanced surface plasmon resonance with the modified catalytic growth of Au nanoparticles. *Biosensors & Bioelectronics* **2007**; *22*: 1106-10.
- (15) Schultz S., Smith D.R., Mock J.J., Schultz D.A. Single-target molecule detection with nonbleaching multicolor optical immunolabels. *Proceedings of the National Academy of Sciences of the United States of America* **2000**; *97*: 996-1001.
- (16) Stuart D.A., Haes A.J., Yonzon C.R., Hicks E.M., Van Duyne R.P. Biological applications of localised surface plasmonic phenomena. *IEE Proceedings Nanobiotechnology* **2005**; *152*: 13-32.
- (17) Chen J.I.L., Chen Y., Ginger D.S. Plasmonic nanoparticle dimers for optical sensing of DNA in complex media. *Journal of the American Chemical Society* **2010**; *132*: 9600-1.
- (18) McFarland A.D., van Duyne R.P. Single silver nanoparticles as real-time optical sensors with zeptomole sensitivity. *Nano Letters* **2003**; *3*: 1057-62.
- (19) Elghanian R., Storhoff J.J., Mucic R.C., Letsinger R.L., Mirkin C.A. Selective colorimetric detection of polynucleotides based on the distance-dependent optical properties of gold nanoparticles. *Science* **1997**; *277*: 1078-81.
- (20) Willets K., van Duyne R.P. Localized surface plasmon resonance spectroscopy and sensing. *Annual Review of Physical Chemistry* **2007**; *58*: 267-97.
- (21) Ungureanu F., Wasserberg D., Yang N., Verdood R., Kooyman R.P.H. Immunosensing by colorimetric darkfield microscopy of individual gold nanoparticle-conjugates. *Sensors & Actuators: B Chemical* **2010**; *150*: 529-36.
- (22) Brown L.V., Sobhani H., Lassiter J.B., Nordlander P., Halas N.J. Heterodimers: plasmonic properties of mismatched nanoparticle pairs. *ACS Nano* **2010**; *4*: 819-32.
- (23) Reinhard B.M., Siu M., Agarwal H., Alivisatos A.P., Liphardt J. Calibration of dynamic molecular rulers based on plasmon coupling between gold nanoparticles. *Nano Letters* **2005**; *5*: 2246-52.
- (24) Sönnichsen C., Reinhard B.M., Liphardt J., Alivisatos A.P. A molecular ruler based on plasmon coupling of single gold and silver nanoparticles. *Nature Biotechnology* **2005**; *23*: 741-5.
- (25) Hill H.D., Millstone J.E., Banholzer M.J., Mirkin C.A. The role radius of curvature plays in thiolated oligonucleotide loading on gold nanoparticles. *ACS Nano* **2009**; *3*: 418-24.
- (26) Reynolds R.A., Mirkin C.A., Letsinger R.L. Homogeneous, nanoparticle-based quantitative colorimetric detection of oligonucleotides. *Journal of the American Chemical Society* **2000**; *122*: 3795-6.
- (27) Draine B.T., Flatau P.J. Discrete-dipole approximation for scattering calculations. *Journal of the Optical Society of America A* **1994**; *11*: 1491.
- (28) Draine B.T., Flatau P.J. Discrete-dipole approximation for periodic targets: theory and tests. *Journal of the Optical Society of America A* **2008**; *25*: 2693-703.
- (29) Samoc A., Miniewicz A., Samoc M., Grote J.G. Refractive-index anisotropy and optical dispersion in films of deoxyribonucleic acid. *Journal of Applied Polymer Science* **2007**; *105*: 236-45.
- (30) Ungureanu F., Halamek J., Verdood R., Kooyman R.P.H. The use of a colour camera for quantitative detection of protein-binding nanoparticles. *Proceedings of SPIE* **2009**; *7192*: 71920O.



Femtomolar DNA detection by colourimetric DF microscopy of GNPs

- (31) Park S.J., Lazarides A.A., Storhoff J.J., Pesce L., Mirkin C.A. The structural characterization of oligonucleotide-modified gold nanoparticle networks formed by DNA hybridization. *The Journal of Physical Chemistry B* **2004**; *108*: 12375-80.
- (32) Sebba D.S., Lazarides A.A. Robust detection of plasmon coupling in core-satellite nanoassemblies linked by DNA. *The Journal of Physical Chemistry C* **2008**; *108*: 12375-80.
- (33) Liu G.L., Rodriguez V.B., Lee L.P. Time-resolved optical sensing of oligonucleotide hybridization via Au colloidal nanoparticles. *Journal of Nanoscience & Nanotechnology* **2005**; *5*: 1933-7.
- (34) Storhoff J.J., Elghanian R., Mucic R.C., Mirkin C.A., Letsinger R.L. One-pot colorimetric differentiation of polynucleotides with single base imperfections using gold nanoparticle probes. *Journal of the American Chemical Society* **1998**; *120*: 1959-64.
- (35) Hurst S.J., Lytton-Jean A.K.R., Mirkin C.A. Maximizing DNA loading on a range of gold nanoparticle sizes. *Analytical Chemistry* **2006**; *78*: 8313-8.
- (36) Nelson B.P., Grimsrud T.E., Liles M.R., Goodman R.M., Corn R.M. Surface plasmon resonance imaging measurements of DNA and RNA hybridization adsorption onto DNA microarrays. *Analytical Chemistry* **2001**; *73*: 1-7.
- (37) He L., Musick M.D., Nicewarner S.R., Salinas F.G., Benkovic S.J., Natan M.J., Keating C.D. Colloidal Au-enhanced surface plasmon resonance for ultrasensitive detection of DNA hybridization. *Journal of the American Chemical Society* **2000**; *122*: 9071-7.
- (38) Thaxton C.S., Hill H.D., Georganopoulou D.G., Stoeva S.I., Mirkin C.A. A bio-barcode assay based upon dithiothreitol-induced oligonucleotide release. *Analytical Chemistry* **2005**; *77*: 8174-8.





Chapter 7

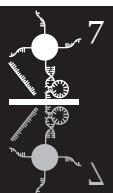
Alternative gold nanoparticle detection strategies

This chapter describes some preliminary experiments on two methods which are promising alternatives to the sandwich gold nanoparticle assay. Each method utilises the scattering of gold in a unique way. The main objective of both methods is to identify each single scattering nanoparticle as a single analyte receptor. After analyte binding the receptor particle would change colour as shown in Chapter 6. This would enable a quick determination of the ratio between occupied and free receptors allowing a rapid analysis of the analyte concentration.



7.1 The *KIT*-assay

Together with the Royal Tropical Institute (Koninklijk instituut voor de tropen (KIT), Amsterdam) an assay was investigated for the detection of *Staphylococcus aureus*. The assay originally developed by KIT is of the flow-through type and uses fluorescent strands.¹ It is intended for rapid assessment of ribosomal RNA (rRNA) from bacterial colonies or other sample material, e.g., milk or body fluids. The assay was developed to compete with quantitative PCR (q-PCR). Although q-PCR is widely accepted, it requires a complex apparatus compared to a less sophisticated fluorescent imager. Fluorescent imagers are generally used for imaging electrophoresis DNA gels and are present in most biochemical laboratories. At the end of the assay an image is acquired and the concentration can be calculated from the fluorescent intensity using a calibrated intensity curve. However, fluorescent intensity depends not only on the number of fluorescent reporters but also on the intensity of the excitation lamps. Conventional fluorescent imagers use standard fluorescent gas-discharge lamps where the intensity of the emitted light is dependent on many factors, such as lamp temperature and power-on hours. In this study we propose to replace the fluorescent strands with oligonucleotide (DNA) functionalised gold nanoparticles (GNPs). Instead of measuring the fluorescent intensity we look at the scattering colour change of hundreds of individual reporter GNPs under darkfield conditions. With this approach no internal calibration curve is required since the scattering colour change depends on the reporter and developer GNPs and not on the intensity of the excitation source. The assay adapted for GNPs is depicted in Figure 7-1. First, DNA receptor strands are randomly immobilised on a glass slide (step 1). Subsequently, DNA functionalised 60 nm reporter GNPs are hybridised to the receptor strands. In a washing step, unbound GNPs are removed (step 2). Next, the target strands are introduced which specifically hybridise with the DNA receptor strands immobilised on the surface (step 3). After a second washing step a second DNA functionalised ‘developer’ GNP is introduced and allowed to bind to the free part of the target (step 4). The resulting close proximity of two GNPs induces an appreciable change of the scattered light peak wavelength, as described in Chapter 6. This approach should allow us to detect single analyte capture events. In this study proof-of-concept experiments were performed to analyse the change in scattering colour of hundreds of GNPs in parallel, after carrying out the aforementioned steps. In principle, each reporter GNP visible in the field of view after step 2 is hybridised to an active receptor strand; the number of visible GNPs is thus equal to the number of active receptors present on the surface. After analyte and developer GNP incubation the binding ratio can be determined by counting the reporter GNPs



that have undergone a colour change. With a known affinity constant the analyte concentration can then be calculated using the Langmuir isotherm (see Chapter 4).^{2,3} A measurement can be performed using a conventional darkfield microscope set-up with a colour CCD-camera, as described in Chapter 6.

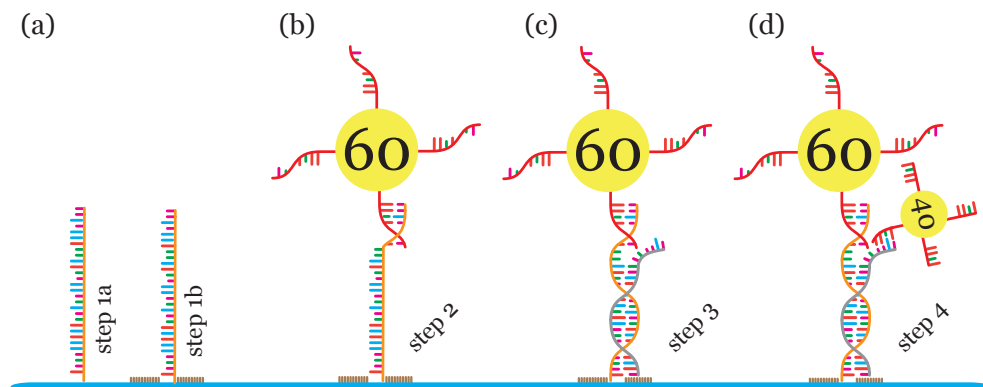


Figure 7-1: Scheme of the modified KIT-assay: (a) receptor strands are immobilised on the surface and the surface is filled to reduce non-specific binding, (b) a 60 nm reporter GNP hybridises with the receptor strand and is seen under darkfield conditions as an active receptor. (c) The target strand hybridises, (d) a 40 nm developer GNP hybridises with the target strand. The close proximity between the two GNPs results in a shift of the plasmon peak of the 60 nm GNP.

With 1000 reporter GNPs/active receptors on the surface and single molecule sensitivity the theoretical binding ratio between the number of covered receptors and the total number of available receptors (Γ_{\min}) can be as low as 0.001. If we consider an affinity constant of $0.25 \times 10^{10} \text{ M}^{-1}$ for a DNA target hybridising over 18 nucleotides⁴ this method can have a theoretical detection limit of $4.0 \times 10^{-13} \text{ M}$.

7.1.2 Experiments

7.1.2.1 Materials and reagents

Citrate-capped gold nanoparticles (60 nm average size with < 6% CV and 40 nm average size with < 7% CV) were purchased from British Biocell International (Cardiff, UK). Thiolated oligonucleotides (DNA) were purchased from Biolegio (Nijmegen, The Netherlands). Short thiol-PEG was purchased from Polypure (Oslo, Norway). Dithiothreitol (DTT), 3-aminopropyltriethoxysilane (APTES), sodium dodecyl sulphate (SDS), Zonyl-FNS100 (FNS), PEG-NHS-ester disulfide (NHS-PEG-NHS), N-Succinimidyl 3-maleimidopropionate (NHS-Maleimide), salts and reagents were purchased from Sigma-Aldrich (St. Louis, MO, USA). Illustra NAP-5



mini spin columns containing Sephadex G-25 DNA grade matrix were purchased from G.E. Healthcare UK limited (Buckinghamshire, UK). All aqueous solutions were made with purified water (MilliQ) ($> 18.2 \text{ M}\Omega\cdot\text{cm}$) from a Millipore Academic purifier (Billerica, MA, USA). Aqueous solutions were degassed prior to use.

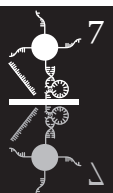
7.1.2.2 Choice of GNP set

As shown in Figure 7-1, the two GNPs are in close proximity to each other; this results in a wavelength shift of the light scattering peak.⁵⁻⁷ The shift of the plasmon peak (λ_{max}) depends on the distance between and the size of both GNPs. In order to detect the first GNP under darkfield conditions the size of 60 nm (GNP⁶⁰) was preferred. This results in a reasonable exposure time of one second for the colour camera; however, GNPs with a size larger than 50 nm are less stable in solution especially at an increased ionic strength of the buffer.⁸ In addition, the DNA coverage on the GNPs must be low in order to reduce steric hindrance since only one strand would be sufficient to hybridise with the receptor strand. However, a low DNA coverage reduces the stability of the particles. To increase stability, FSN⁹ was used as a strong surfactant. Moreover, the uncovered area on the GNP surface after DNA functionalisation was filled with short thiol-PEG molecules¹⁰ to reduce GNP aggregation during incubation in the working buffer (WB) (10 mM PB pH 7.4, 300 mM NaCl and 0.1% FSN).

A 40 nm gold nanoparticle (GNP⁴⁰) was selected as a developer to give a strong response in close proximity with the GNP⁶⁰ while ensuring stable, non-aggregating particles in solution.

7.1.2.3 Preparation of receptor surface

For single step immobilisation of the DNA receptor strands we used gold coated BK7 glass slides. This surface allows direct thiol coupling of thiol functionalised DNA or other thiol based linkers, e.g., 6-mercapto-hexanol (MH). Prior to use the gold slides were rinsed with MilliQ water and cleaned in piranha solution (1 H_2O_2 (35%) : 3 H_2SO_4 (>96%)) at 95 °C for two minutes followed by MilliQ washing and drying with nitrogen gas. Subsequently, a 24-well microarray sticker (EMSDiasum, Hatfield, PA, USA) was applied on the slides. The sticker created 10 μl wells for direct immobilisation of samples. The various incubation methods studied are summarised in Table 7-1. In this study we have selected sequences of two *Staphylococcus aureus* genes, viz. 23S (23s rRNA gene) and TufA (translational elongation factor gene), to be used as target strands. The 23S target strand was used as positive sample and the TufA strand as the negative control. In step 1a the 23S receptor strands were first treated with DTT to reduce thiol dimers⁴ and subsequently incubated on the gold



surface at a 1 μM concentration for two hours in WB followed by a washing step with WB. In step 1b the remaining areas on the surface were filled to reduce non-specific surface binding. This was done by incubating surface with MH or BSA for two hours in WB, followed by washing. Additionally, a number of samples were co-immobilised with MH or BSA, as this was expected to reduce steric hindrance on the surface.

Table 7-1: Sample composition and the respective surface treatment

Type	Receptor strand	Target strand	Step 1a Strand immobilisation	Step 1b surface blocking
+	Thiol 23S	23S	5 μM thiol-DNA	None
-	Thiol 23S	TufA	5 μM thiol-DNA	None
+	Thiol 23S & MH	23S	5 μM thiol-DNA & 1 μM MH	1 μM MH
-	Thiol 23S & MH	TufA	5 μM thiol-DNA & 1 μM MH	1 μM MH
o	MH	-	1 μM MH	1 μM MH
+	Thiol 23S & BSA	23S	5 μM thiol-DNA & 1% w/v BSA	1% w/v BSA
-	Thiol 23S & BSA	TufA	5 μM thiol-DNA & 1% w/v BSA	1% w/v BSA
o	BSA	-	1% w/v BSA	1% w/v BSA

Note: +: positive sample, -: negative sample and o: control sample. All samples were diluted in WB. In step 1a in some samples the DNA was co-immobilised with a blocking agent.

7.1.2.4 Functionalisation of DNA to GNPs

Table 7-2 shows the sequences of the oligonucleotides that were used in the experiments. Prior to functionalisation to the GNPs the protecting disulfide groups on the thiol-DNA were cleaved using a DTT solution.^{11,12} A volume of 20 μM DNA was mixed with an equal volume of 340 mM phosphate buffer at pH 8.0. Subsequently, DTT was added to a final concentration of 0.1 M. Samples were incubated on a orbital shaker for two hours at room temperature followed by a purification step using a MilliQ water rinsed NAP-5 centrifuge column. The samples were diluted to 5 μM with MilliQ and heated to 96 $^{\circ}\text{C}$ for five minutes to ensure single strand conformation. The last step prior to functionalisation was fast cooling to 4 $^{\circ}\text{C}$.

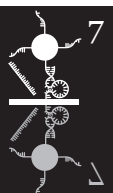


Table 7-2: Oligonucleotide sequences for the KIT assay.

Name	Linker (site)	Coupled to	Sequence 5' to 3'
23S-Receptor strand	5' thiol or amine	Surface	TTT TTT TTT TTT ACC TTC TTT GAT TCA TCT TTC CAG ATG ATT CGT CTA ATT CGT CCT TTG TAA CTC CGT ACG GGA TGC ATG TCT TGT GGT
23S-Reporter GNP	5' thiol	GNP ⁶⁰	TTT TTA CCA CAA GAC ATG CAT CCC GTA TAG
23S-Developer GNP	3' thiol	GNP ⁴⁰	AGT GTC CTA CAA CCC CAA CAA GCA AGC TTT TTT
23S-Target	-	-	TGC TTG TTG GGG TTG TAG GAC ACT CTA TAC GGA GTT ACA AAG GAC GAC ATT AGA CGA ATC ATC TGG AAA GAT GAA TCA AAG AAG GTA A
TufA-Target	-	-	CAA ACT CGT GAA CAC ATT CTT TTA TCA CGT AAC GTT GGT GTA CCA GCA TTA GTA GTA TTC TTA AAC AAA GTT GAC ATG GT

The ability of the DNA strands to hybridise as designed was assessed by a hybridisation assay in working buffer. Specific and non-specific combinations were mixed with a 1 μM end concentration per strand. The solutions were heated to 96 $^{\circ}\text{C}$ for five minutes and gently cooled to room temperature. The matrix migration speed of 10 μl of the hybridised DNA complexes was tested in a 5% agarose gel at 100 volts for one hour. Using a reference sample the length of the hybridised DNA strands could be determined.

Reporter-GNP⁶⁰ and developer-GNP⁴⁰ were constructed by conjugation with various DNA strands as indicated in Table 7-2. Bulk conjugation was performed by pre-incubating a 9 ml solution consisting of 0.1 μM DNA, 11 mM phosphate buffer (pH 7.4), 111 mM NaCl, 0.1% FSN at room temperature. After 15 minutes, 1 ml of stock GNPs⁶⁰ or GNPs⁴⁰ solution (1.3×10^{-10} M) was added and incubated on a rotator at room temperature for 48 hours. After the conjugation step 1 μM short thiol-PEG was incubated with the functionalized GNPs for one hour to fill the remaining area on the GNP surface. Samples were washed twice with 10 ml washing solution (0.01% SDS in MilliQ water) by centrifugation for one hour at $3,900 \times g$. In the last step the samples were resuspended in 1 ml washing solution and transferred to 1.5 ml



Eppendorf tubes. Subsequently, three more washing steps were done at $8,000\times g$ for ten minutes with 1 ml washing solution. To resuspend the pellet from the bottom, the samples were sonicated for 10 seconds while shaken. The colloidal suspensions of functionalised GNPs were stored at $4\text{ }^{\circ}\text{C}$ until further use. For both the reporter-GNP⁶⁰ and the developer-GNP⁴⁰ extinction spectra were recorded to check the success of conjugation. After conjugation spectra were red-shifted over 3 nm, indicating the presence of at least 200 DNA strands on the GNP surface. Additionally the ability to hybridise the functionalised GNPs with the DNA strands in a colloidal suspension was tested. The 23S-receptor strand was mixed with the reporter-GNP⁶⁰, the specific 23S-target strand and the developer-GNP⁴⁰. The suspension was heated to $96\text{ }^{\circ}\text{C}$ for five minutes and gently cooled to room temperature. Alternatively, the 23S-target strand was replaced by the non-specific TufA-target strand or was incubated without any target strand.

7.1.2.5 Assay procedure

Imaging was performed in reflection mode on an Olympus GX71 microscope using a $20\times$ darkfield (DF) objective with a $2\times$ magnifier lens. Pictures with a field of view of $165\times 220\text{ }\mu\text{m}$ were acquired using a Zeiss Axiocam HRc (Jena, Germany) spatial scanned colour camera.

Prior to image analysis the stack of acquired images was aligned using the DipImage toolbox (version 2.2, University of Delft, the Netherlands) for MatLab. The scattering colour of the GNPs, which is directly related to λ_{max} , is expressed as the ratio between the intensities of the red and green channel of the camera which we denote as the r/g ratio. Previously, we demonstrated that changes in λ_{max} as small as 1 nm could be detected by measuring changes in r/g ratio.¹³ A custom-made MatLab script was used to analyze the change in r/g ratio ($\Delta r/g$) of each individual GNP for all images throughout the measurement.

A stack of images consisted of three images: (1) reporter-GNP, (2) target and (3) developer-GNP. Each image was acquired after the washing step. The stack was analyzed for the colour change of individual GNPs. This enabled us to compare the scattering colour of the same GNP during the experiment.

Each well was incubated with $10\text{ }\mu\text{l}$ of $1.0\times 10^{-10}\text{ M}$ reporter-GNP⁶⁰ in WB for 15 minutes. Subsequently, each well was incubated with $1.0\times 10^{-9}\text{ M}$ specific 23S-target or non-specific TufA-target DNA for two hours in a humidity chamber at room temperature. The last incubation step consisted of hybridisation with the developer-GNP⁴⁰ target binder at a concentration of $1.0\times 10^{-10}\text{ M}$ in WB for 15 minutes. Each incubation step was completed by five washing steps followed by image acquisition in WB.



7.1.3 Results and discussion

7.1.3.1 The GNP sandwich response

From close proximity GNP scatter simulations we see that a sandwich of 60 and 40 nm GNPs would result in a large plasmon peak shift as shown in Figure 7-2. For the particular case considered here, the GNPs are in close proximity because of the Y-shape of the DNA arm. The GNP⁶⁰–GNP⁴⁰ edge-to-edge distance is based on the coverage of the DNA around both GNPs. The actual distance between GNP⁶⁰ and GNP⁴⁰ depends on many factors, e.g., GNP surface coverage by DNA, ionic strength of the buffer, temperature, etc. We estimate a distance between 15 and 30 nm, which is expected to generate the maximum λ_{\max} shift of 10 to 4 nm or $\Delta r/g \approx 0.27$ to 0.1, respectively.^{14,15} Moreover, the magnitude of the λ_{\max} shift depends also on the particles' sizes, and on the direction of the pair axis relative to the polarisation direction of the light. The distance estimations were based on illustrations to scale, in which the DNA persistence length was taken into account. The closest distance is determined by the DNA shell around each particle. Taking all this into account, it is expected that under unpolarised light conditions the wavelength shift associated with a single binding event can vary from at most 27 nm for a 5 nm gap to at least 4 nm for a 30 nm gap for the GNP⁶⁰–GNP⁴⁰ pair as shown in Figure 7-2.¹⁵

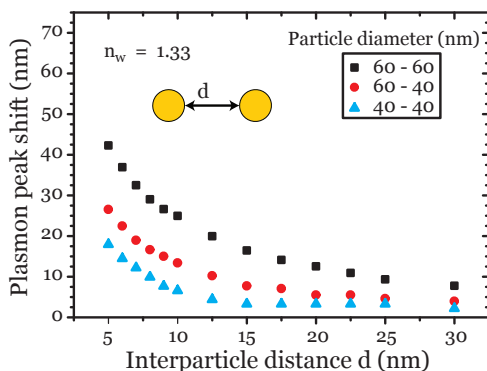


Figure 7-2: Calculated plasmon peak shift for various close proximity positions of two GNPs, embedded in water, under unpolarised light conditions, for three different size pairs.

7.1.3.2 Assay performed in solution

Prior to the darkfield assays the synthetically manufactured DNA strands were tested in various hybridisation assays. In the first assay the strands were mixed and hybridised followed by agarose gel electrophoresis. From the calibrated migration distance in the matrix we concluded that the strands were able to hybridise as

intended. Additionally, the aggregation of the colloidal suspension as the result of specific hybridisation was successful. Eppendorf tubes with the receptor strand, reporter-GNP⁶⁰, 23S-target strand and developer-GNP⁴⁰ slowly lost their intense red colour. Tubes without or with the TufA-target strand did not show this effect. We can conclude that the functionalised reporter and developer GNPs are both active and that the hybridisation of the 23S-target strand is specific.

7.1.3.3 Darkfield assay

In the following experiments we evaluated the specificity of the detection method by incubating functionalised reporter-GNP⁶⁰ with receptor strands immobilised on the surface. As already mentioned, each individual reporter-GNP⁶⁰ visualised by the darkfield microscope represents an individual active receptor on the surface. The number of reporter-GNPs⁶⁰ in the field of view was counted allowing us to compare the surface modification methods. In order to reduce false positives and false negatives the GNPs were selected on the following criteria: start r/g: 0.4 – 1.2, roundness: 75 – 100% and size: 10 – 80 pixels, during the measurement (see Chapter 6 for more details). The total number of reporter-GNPs⁶⁰ per measurement which passed the criteria is shown in Figure 7-3.

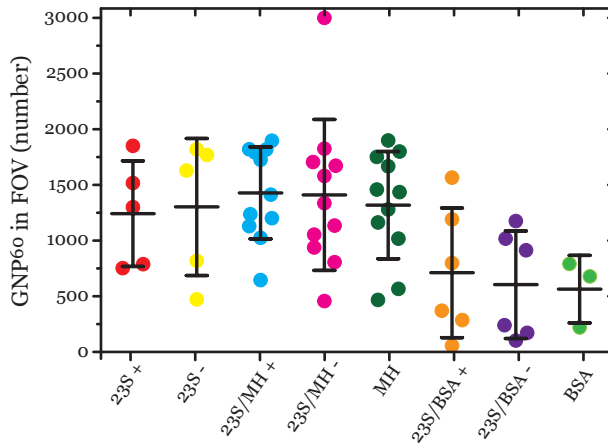


Figure 7-3: Total amount of GNPs⁶⁰ in the field of view (FOV) per measurement. Each data point represents a well and for each condition the mean with standard deviation is shown.

The number of reporter-GNPs⁶⁰ in the FOV varies per surface incubation method. The samples which have a surface coating of the receptor strand with or without MH show on average the same particle density in the FOV. The samples which have a surface coating with the receptor strand and BSA show a lower particle density, indicating that BSA does reduce the surface binding. This corresponds to the results



observed in the SPR blocking experiments described in Chapter 3.2. However, the results also hint at the possibility that conjugated GNPs preferably adsorb at the blocking agent.

Incubation with specific 23S and non-specific TufA target strands did not show any colour changes as was expected. Subsequently, addition of the developer-GNP⁴⁰ particle should result in a GNP⁶⁰–GNP⁴⁰ pairs on receptor strands hybridised with the target strand and reporter-GNP⁶⁰. Reporter-GNPs⁶⁰ with $\Delta\lambda_{\max} > 4$ nm) were recorded as positive. The response was expressed as the binding ratio of the number of particles with $\Delta r/g > 0.1$ versus the total number of particles in the image. The binding ratios of the various receptor strand immobilisation strategies, as indicated in Table 7-1, are shown in Figure 7-4.

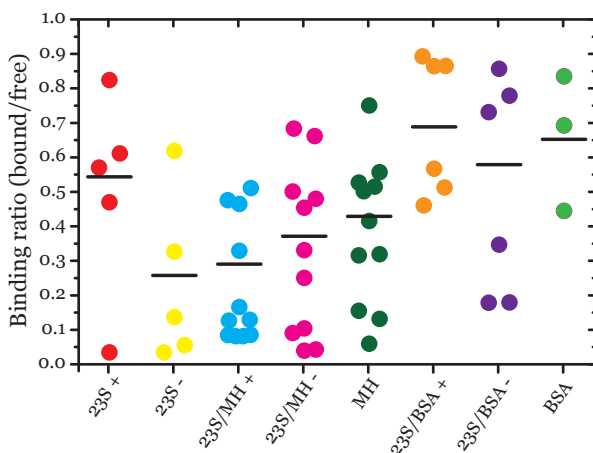


Figure 7-4: Results showing the binding ratio of the GNPs using various incubation methods. Each data point represents a well and the black line represents the average of the data.

The best results were obtained when the receptor strands were immobilised without any subsequent surface modification. However, these data are only from five consecutive measurements and outliers are not reliable. All other incubation methods did not show any consistent responses. Moreover, in the control experiments there was a high variability in the percentage of GNPs⁶⁰ with colour change, even when no receptor strands were present. The wide range of responses could be due to random non-specific binding of both reporter-GNPs⁶⁰ and developer-GNPs⁴⁰. Since we studied the $\Delta r/g > 0.1$ compared to the total number of reporter-GNPs⁶⁰ the non-specific binding of the developer-GNPs⁴⁰ to the surface is not recorded.

7.1.3.4 Electron microscopy

After darkfield imaging the slide was analysed using electron microscopy. The 50 nm gold layer allowed direct SEM analysis without modifications to obtain a conducting surface. Of four areas (23S target, TufA target, MH-no strand and 23S target + BSA surface blocking) random images were made and analysed for GNP⁶⁰–GNP⁴⁰ pairs only. A selection of cropped areas of these images is shown in Figure 7-5.

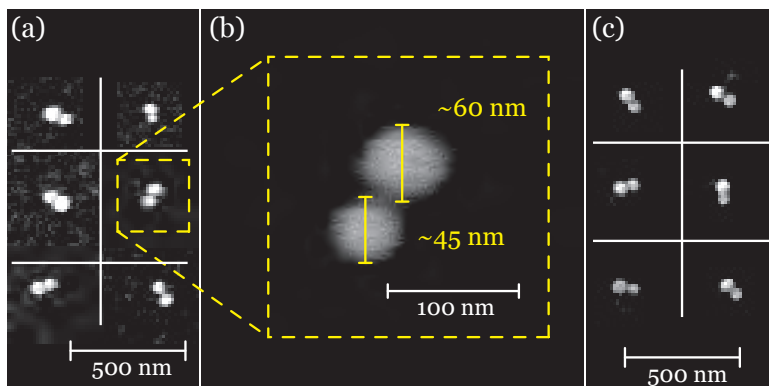


Figure 7-5: Scanning electron microscope images of gold nanoparticles. (a) Six images of GNP⁶⁰–GNP⁴⁰ pairs at 10,000× magnification of the positive sample (23S target). (b) Enlargement of one pair at 80,000× magnification, showing a ~45 nm and ~60 nm particle. (c) Six GNP pairs in the positive sample using BSA as surface blocking agent.

The samples and their respective SEM results are summarised in Table 7-3. On all surfaces GNP⁶⁰–GNP⁴⁰ pairs were found; these were, however, expected only in the positive samples but not in the negative and receptor strand free samples (control). It remains unknown if these pairs are the result of direct hybridisation of developer-GNP⁴⁰ with the reporter-GNP⁶⁰ due to the presence of the high ionic strength buffer. However, without the presence of a blocking agent the difference between the positive and negative sample is approximately five times, which is in line with the darkfield results.



Table 7-3: Summary of SEM results.

Sample	Surface preparation			Frequency of GNP pairs
	Step 1a	Step 1b	Step 3	
Positive	23S-receptor strand	-	23S-target	1: 17 μm^2
Positive-blocked	23S-receptor strand	BSA	23S-target	1: 30 μm^2
Negative	23S-receptor strand	-	TufA-target	1: 87 μm^2
Control	MH	MH	-	1: 109 μm^2

Note: All samples were incubated with reporter-GNP⁶⁰ in step 2 and subsequently with reporter-GNP⁴⁰ in step 4, as illustrated in Figure 7-1. The quoted pair frequency is obtained by taking the average of the number of found pairs over the area of three independent wells.

7.1.4 Conclusions and recommendations

The surface modifications and surface blocking to reduce non-specific binding of the reporter-GNP⁶⁰ have a high impact on this assay. In the absence of surface blocking with MH or BSA the darkfield experiments showed a significant difference between negative and positive samples. However, when a blocking agent was used, the results were surprising. In all samples containing a blocking agent the response was similar regardless if the positive or negative target strand was used.

At the target strand concentration of 1 nM it was expected that most of the available receptor sites would be occupied. Four out of five measurements of the positive sample (incubated with the 23S-target strand) yielded positive results (i.e., > 50% particles with colour change). Similarly, four out of five measurements of the negative sample (with the non-specific TufA target strand) had negative results, i.e., < 30% change. This is in line with earlier observations in Chapter 6: for this high concentration of target DNA, a non-specific sample can result in up to 30% background binding. It could be a contribution of non-specific partial binding of the TufA target strand with the receptor strand and the developer-GNP⁴⁰.

The samples which used MH or BSA as blocking agent have very widespread binding responses (Figure 7-3). The control measurements also show a large amount of binding of GNP⁶⁰ to the surface indicating that neither BSA nor MH reduces non-specific binding of DNA functionalised GNPs directly to the surface. We can conclude from these results that BSA or MH cannot be used for this type of assay. On the other hand, we can point out that in absence of any blocking agent the response was according to the hypothesis.

The SEM data are in general agreement with the darkfield data: on average the positive sample had a four times higher binding rate as compared to the negative sample. Moreover, the control sample showed an even lower amount of binding. This is expected and agrees with the darkfield data from the samples which were not co-immobilised. Therefore, we can conclude that the binding in this assay is due to specific hybridisation, only when no blocking agents are used.

Apparently, this type of assay works without the presence of surface blocking agents. However, with the right surface blocking agent which reduces non-specific binding to a lower level ($< 30\%$) the presence of false-positives can most likely significantly be reduced. The commonly used blocking agents studied here show an adverse blocking effect. Chapter 3 showed that polyethylene glycol (PEG) reduced non-specific binding. A good strategy would be to coat the surface with a short PEG linker on which the receptor strand could be immobilised.

We have shown that the adaptation of a specific DNA hybridisation assay can be used with gold nanoparticle reporters, thereby eliminating a number of drawbacks of the use of fluorescent reporters. A typical measurement would include 1000 GNPs per FOV where one GNP is representing a receptor with single molecule sensitivity. In this system the theoretical limit of binding ratio Γ_{\min} , as the ratio between number of covered receptors and total number of receptors available, could reach 0.001. As described in this Chapter, this assay works for two highly different DNA target strands. With further optimisation, such as more stringent hybridisation conditions, we envision that even target strands with a higher sequence similarity can be distinguished.

7.2 Detection based on the distance of GNP from planar gold

A single GNP system with a close proximity to a planar gold layer can be used as an alternative to the two GNP proximity assay described in Chapter 6 and its related single receptor KIT-assay of section 7.1. In principle this method allows label-free detection of DNA hybridisation using a standard darkfield microscope, because, in comparison to the KIT-assay, this assay does not utilize a developer-GNP and thereby eliminates one incubation step.

In 2008 Mock *et al.*¹⁶ observed that a blue shift of the maximum of the scattering spectra (λ_{\max}) of gold nanoparticles (GNPs) occurs when the distance between the GNP and a planar gold film is increased. It was studied by increasing the distance between the GNP and the gold surface with polyelectrolyte layers. For every 1 nm increase in the distance the λ_{\max} decreased ~ 6 nm. This was measured using darkfield



illumination and air as the measuring medium. Employing this approach, it was possible to measure the distance up to 25 nm using 60 nm GNPs; with larger GNPs the distance could be increased even further. We propose that we can utilise this effect for the detection of DNA hybridisation as shown in Figure 7-6.

The flexibility of a polymer like DNA is described by the persistence length. The persistence length of a single stranded DNA (ssDNA) is approximately two bases, implying that DNA as a polymer can bend every two bases.¹⁷ When hybridised with the complementary strand the persistence length will increase to approximately 50 base pairs for double stranded DNA (dsDNA). The dsDNA strand will therefore remain stretched and stiff over 50 base pairs,¹⁸ corresponding to ~17 nm. Taking in account the GNP-gold layer distance effect described by Mock *et al.* and the persistence length difference of ssDNA and dsDNA, we envisage this as a new 'label'-free detection strategy. It is label-free in the sense that no extra labelled strand is required after hybridisation with the target strand.

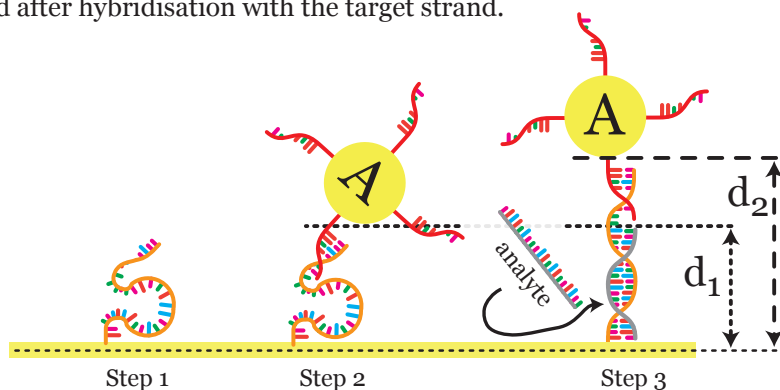


Figure 7-6: Proposed detection strategy. In step 1 a single stranded DNA (receptor strand) is immobilised on the surface followed by step 2 where a GNP hybridises with the surface strand. The short persistence length of single stranded DNA allows the GNP to be close to the planar gold surface (d_1). When the target strand (analyte) is hybridised to the surface strand in step 3, the DNA becomes stiffer due to double strand conformation increasing the persistence length (d_2). The GNP has now increased its distance from the surface. This increase in distance from the planar gold surface should result in a blue shift of the scattering plasmon peak maximum.

We assume that ssDNA is not completely stretched; this is due to the short persistence length as compared to dsDNA.¹⁸ In addition, the persistence length depends on the ionic strength of the buffer.¹⁷ Once the GNP is attached to the ssDNA (step 2) the particle will have a limited movement over the surface. The Brownian motion allows multiple positions of the GNP and therefore, according to Mock *et al.*, the scattering colour of the GNP obtained by the CCD-camera will continuously change. From the moment the target DNA strand is hybridised with the receptor strand (step 3), it

will have the double strand conformation and the persistence length will increase from a few nanometers to tens of nanometers,^{17,18} indicating that the hybridised strands have become stiffer and stretched. This translates to an appreciable blue shift; however, if the distance of GNP from surface is more than 25 nm, a normal λ_{\max} will be observed. This detection strategy is similar to that of Ginger and co-workers¹⁹ except that we propose it on a planar gold surface rather than on an immobilised GNP. With a similar distribution of reporter GNPs/receptor strands as in the KIT-assay the sensitivity of the assay, once fully optimised, should be comparable.

7.2.2 Experiments

7.2.2.1 Materials and reagents

Polymethylmethacrylate 15 kDa (PMMA) and anisole were purchased from Sigma-Aldrich (St. Louis, MO, USA). All other materials were used as described in Section 7.1.2.1.

7.2.2.2 Spin-coating of PMMA layer and height calibration

Two surface types were used for immobilisation, commercially obtained IBIS-SPR (Enschede, Netherlands) sensor slides and self-made SPR sensor slides. Both slides had dimensions of $20 \times 20 \times 1$ mm and were made from BK7 glass coated with a 50 nm gold layer. Prior to use the slides were rinsed with MilliQ water and cleaned with piranha solution (as in section 7.1.2.3) followed by rinsing with copious amounts of MilliQ water.

The calibration of the distance between GNPs and gold layer was performed with an Olympus GX71 darkfield microscope using sensor slides with known layer heights of spin-coated PMMA. Three spin-coat methods were used, and each method resulted in a PMMA layer with different thickness for spacing 80 nm GNPs from the planar gold layer. In the first approach 2% PMMA in anisole was spun at 6,000 rpm for one minute, resulting in a layer of medium thickness. If opting for a thicker PMMA layer, 2% PMMA in anisole was spun at 1,000 rpm for one minute; it was called the thick layer. To achieve the thinnest layer (denoted as thin layer), 0.1% PMMA in anisole was spun at 6,000 rpm. Each layer was analysed by measuring the SPR angle change as described in the next section. PMMA was dried by a baking step at 120 °C for five minutes. Some slides with PMMA were stripped using glacial acetic acid²⁰ to compare the thickness of the PMMA-coated layer with the plain gold layer. A second baking step at 120 °C for one hour was used to harden the PMMA layer.

Imaging SPR (iSPR) analysis of the PMMA layer thickness was performed on an IBIS-iSPR instrument. After spin-coating with PMMA the sensor slide was mounted



onto the prism using refractive index matching oil. The prism holder with the sensor slide was mounted in the SPR apparatus and the cuvet was filled with MilliQ water ($n = 1.33$). Regions of interest (ROI) were selected with a size of 100 by 100 pixels, corresponding to $600 \times 600 \mu\text{m}$. The angle offset was set to 0 millidegrees (mdg) for the bare gold layer. The thickness of the PMMA was calculated using a refractive index of $n = 1.4838^{21}$ which corresponds to 80 mdg shift per 1 nm PMMA at a wavelength of 840 nm.²² During the measurement the angle of incidence was increased by 1 mdg steps for each ROI simultaneously. The SPR-dip position varied depending on the thickness of the PMMA layer. The thickness of the layer could be calculated by comparing the uncoated and PMMA coated surface. In addition, atomic force microscopy (AFM) was used to analyse the surface topography.

7.2.2.3 GNP⁸⁰ – gold layer proximity spaced by PMMA

APTES was coated on top of the PMMA layer²³ to enable immobilisation of GNPs. The procedure described in Chapter 3 was slightly modified. In brief: APTES was diluted to 5% v/v in MilliQ water instead of ethanol²⁴ and PMMA coated sensors were not cleaned with piranha before APTES coating since piranha would damage the PMMA layer.

GNPs⁸⁰ were immobilised on the APTES coated PMMA layer as described in Chapter 3 to study the effect of the distance between the gold layer of the sensor and the GNP. The sensor slides coated with PMMA and GNP⁸⁰ were mounted on a standard microscope slide ($76 \times 26 \times 1 \text{ mm}$, BK7) with the PMMA/GNP/gold layer facing the microscope slide. Two Parafilm spacers created a volume between the sensor layer and the glass as illustrated in Figure 7-7. This volume was filled with MilliQ water and spectra of GNPs at various distances to the gold sensor surface were measured according to the methods described later.

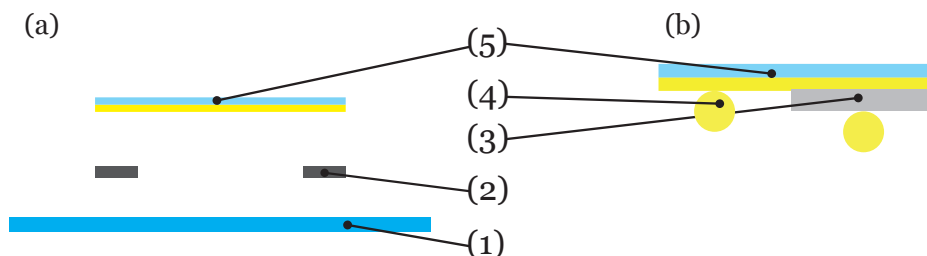


Figure 7-7: Sensor positioning illustration. (a) On top of a clean microscope slide (1) two Parafilm spacers (2) are placed on which the sensor surface (5) rests. (b) The close-up of the sensor surface shows the assay procedure on which PMMA (3) acts as a spacer for the GNP (4) on the gold layer of the sensor.

7.2.2.4 GNP⁸⁰ – gold layer proximity spaced by DNA

A 4-well microarray sticker (EMSDiasum; Hatfield, PA, USA) was applied on the sensor surface. The sticker created 10 μl wells which eased further incubation steps. Two methods were utilised for the immobilisation of DNA receptor strands on the sensor surface. In the first method the cleaned gold layer was incubated with 5 μM MHA in 10% ethanol overnight followed by rinsing with 10% ethanol. The MHA monolayer was activated with 50 mM EDC in 500 mM NHS/MES buffer at pH 5.3 for one hour at room temperature (RT), followed by a washing step with MES buffer. Immediately, the activated surface was incubated with 5 μM amine functionalised 23S-receptor strand (Table 7-2) in phosphate buffer pH 8.0 (PB-8) (10 mM PB, pH 8.0, with 300 mM NaCl) for one hour at RT followed by washing with PB-8. Subsequently, 5 μM solution of ethanolamine in PB-8 was used to inactivate unreacted receptors for 30 minutes. In an alternative approach, thiol-modified DNA molecules were directly immobilised on the sensor surface. Prior to immobilisation the gold layer was cleaned using the previously described piranha cleaning method. The thiol functionalised 23S-receptor strand was immobilised at various concentrations of 1 μM , 100 nM and 10 nM in phosphate buffer pH 7.4 (PB-7) (10 mM PB, pH 7.4, with 100 mM NaCl) for two hours at RT followed by several washing steps with PB-7. To reduce non-specific surface binding of GNPs in a later stage, the surface was blocked with 1 mM MH in 1% ethanol for one hour at RT. Subsequently, the surface was washed with MilliQ water.

In the following steps, GNPs⁸⁰ were functionalised with DNA to form a reporter-GNP⁸⁰ which is able to hybridise with the immobilised receptor strand on the sensor surface. Each well was incubated with 10 μl 1.0×10^{-10} M reporter-GNP⁸⁰ in working buffer (WB) (10 mM PB pH 7.4, 300 mM NaCl and 0.1% FSN) for one hour in a humidity chamber at RT. Subsequently, each well was incubated with 10 μl specific (23S-target) or non-specific (TufA-target) DNA at a concentration of 1 nM for two hours in a humidity chamber at RT. Each incubation cycle was finished by five washing steps and followed by image acquisition and spectral analysis in WB. Additionally, bulk hybridisation experiments with and without functionalised GNPs were conducted as described in section 7.1.4.

7.2.2.5 Imaging and image analysis

Imaging of GNPs on PMMA/gold and DNA/gold surfaces was performed in reflection mode on an Olympus GX71 microscope using a 20 \times darkfield (DF) objective with a 2 \times magnifier lens. Pictures were acquired using a Zeiss AxioCam HRC spatial scanned colour camera. Prior to image analysis the stack of acquired images was aligned



using the DipImage toolbox for MatLab. Additionally, an Ocean Optics QE65000 fiber spectrometer was used to measure the scattering spectra of individual particles.

7.2.3 Results and discussion

7.2.3.1 PMMA spin-coating analysis

In the following experiments we evaluated the thickness of the three PMMA layers; the results are shown in Figure 7-8.

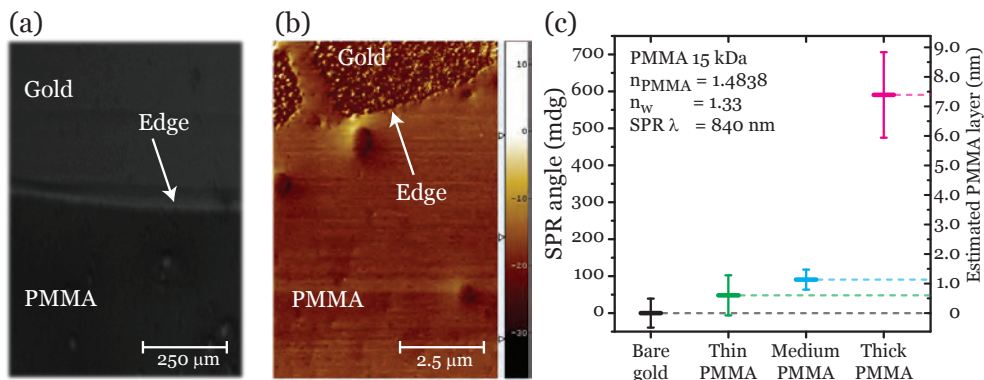


Figure 7-8: (a) Image from IBIS-iSPR apparatus; the thick PMMA layer appears darker at this angle of incident light. (b) AFM image of thick PMMA coated sensor; this indicates that the stripping of PMMA with glacial acetic acid was not very successful since small dots are still present in the stripped area. (c) PMMA layer height was calculated from the SPR angle shift for three various preparation methods (thin = 0.1% PMMA at 6,000 rpm, medium = 2% PMMA at 6,000 rpm and thick = 2% PMMA at 1000 rpm, all for one minute).

The thickness of the spin-coated PMMA layer can be measured using iSPR. However, the iSPR measurement is an ensemble measurement over the selected ROI. Thus iSPR measurements give an average thickness and do not provide information on the smoothness of the layer. The iSPR was able to clearly distinguish the ‘thick’ (~7.4 nm) PMMA layer as shown in Figure 7-8a, whereas AFM (Figure 7-8b) revealed the degree of smoothness. The spin-coated PMMA has a smooth surface structure and the layer thickness varies between 1 and 7 nm depending on the preparation method (Figure 7-8c). The removal of PMMA with glacial acetic acid caused surface imperfections (residuals). These residuals were not visible in iSPR but were visible in the AFM image. This could explain the variance in the ‘bare gold’ results from the iSPR. We estimate that the layer thicknesses of the spin-coated PMMA are < 1 nm for the thin layer preparation method, ~1.1 nm for the medium layer preparation method and ~7.4 nm for the thick layer preparation method. For the thick PMMA

layer the AFM height corresponded to that found in SPR; however for the medium and thin PMMA layers AFM measured a thicker layer. For both surfaces the AFM measured an average surface height of 1 nm fluctuating ± 1 nm over a distance of 2.5 μm , indicating that the surface is not smooth. This could be caused by the length of the PMMA base molecule (15 kDa). The use of a shorter molecule could result in a more homogeneous layer. On the other hand, the surface homogeneity observed here is satisfactory for our needs.

7.2.3.2 GNP⁸⁰ – gold layer proximity

To study the response of GNP⁸⁰ – gold layer proximity system in our darkfield measuring setup, the various spin-coated PMMA layers were covered with 80 nm GNPs. The scattering spectra of individual GNPs were analysed under darkfield conditions and the results are shown in Figure 7-9.

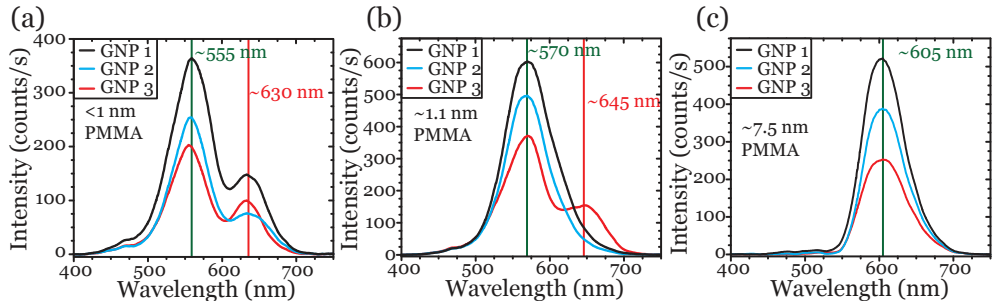


Figure 7-9: Spectra of three random 80 nm GNPs at various distances from a gold surface: (a) distance < 1 nm; (b) distance ~ 1.1 nm; (c) distance ~ 7.5 nm. The spacer layer was composed of spin-coated PMMA with an estimated refractive index of 1.4838; the measurement was performed in MilliQ water ($n = 1.33$).

GNPs at a distance very close to the gold layer exhibit a double peak (Figure 7-9a), whereas at larger distances in most cases a single peak appears, red-shifted relative to the main peak in Figure 7-9a.

At this stage, where the experimental data are somewhat scarce, it is difficult to provide a firmly based interpretation of the data displayed in Figure 7-9. In their DF experiments on a similar GNP-gold layer system Mock *et al.* also observed the occurrence of two peaks at very small GNP-layer distances, at approximately the same wavelength as we have found. They did not provide an interpretation of this finding. Furthermore, upon increasing the distance they found a blue shift, at distances > 3 nm.

If we adopt the following tentative interpretation, then our experimental data are mostly in line with those of Mock and co-workers.

It is known that upon increasing the distance between two GNPs a red shift of the GNP



spectrum occurs for the polarization direction of the incoming light perpendicular to the line that joins the centres of the two particles; if the polarization is parallel to this line a blue shift is found.^{25,26} The system of interest here can indeed be considered as a two particle assembly: the GNP close to the gold layer induces a virtual mirror GNP at the other side of the gold layer interface.

DF excitation results in predominantly s-polarized light (polarization parallel to the interface) at the interface, that causes a red shift when the distance GNP–gold layer increases. We assign the main peaks in Figure 7-9 to the scatter spectrum of GNPs excited with s-polarized light, and the secondary peak in Figure 7-9a to the scatter spectrum excited with p-polarized light. Thus, the scatter spectra in Figure 7-9b,c are mainly due to excitation with s-polarized light. Furthermore, we suspect that only in Figure 7-9a we detect a scatter spectrum due to p-polarized light (at $\lambda_{\text{max}} = 630 \text{ nm}$); at such a close distance to the surface, the s-excited GNP spectrum will be relatively weak because in that geometry the dipoles associated with the ‘real’ and the ‘mirror’ GNP mutually almost cancel. On the other hand, the strong p-scatter spectrum of the GNP-pair will be excited by light with a rather small p-component.

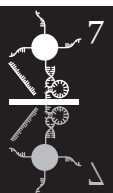
We are aware of the fact that this does not explain the occurrence of the second peak in Figure 7-9b for one GNP. But one should realize that our AFM data show that in a number of cases the PMMA layer has a non-uniform thickness. For this reason we consider this finding is due to the fact that the third GNP in Figure 7-9b is closer to the gold layer.

Finally, it is clear that more experimental data are needed to provide a firmer basis for our interpretation.

7.2.3.3 GNP – gold layer proximity spaced by DNA

The reporter-GNPs were tethered to the receptor strand DNA strands for sensing purposes. The receptor strand on the surface had a length of 91 nucleotides; this corresponds to ~31 nm length when fully stretched. This distance is expected to be sufficiently far away from the gold surface to result in an appreciable wavelength shift of the GNP scatter spectrum.

Functionalised GNPs⁸⁰ were hybridised to the surface strands, and the spectra were analysed in WB ($n = 1.34$) under darkfield conditions, as shown in Figure 7-10.



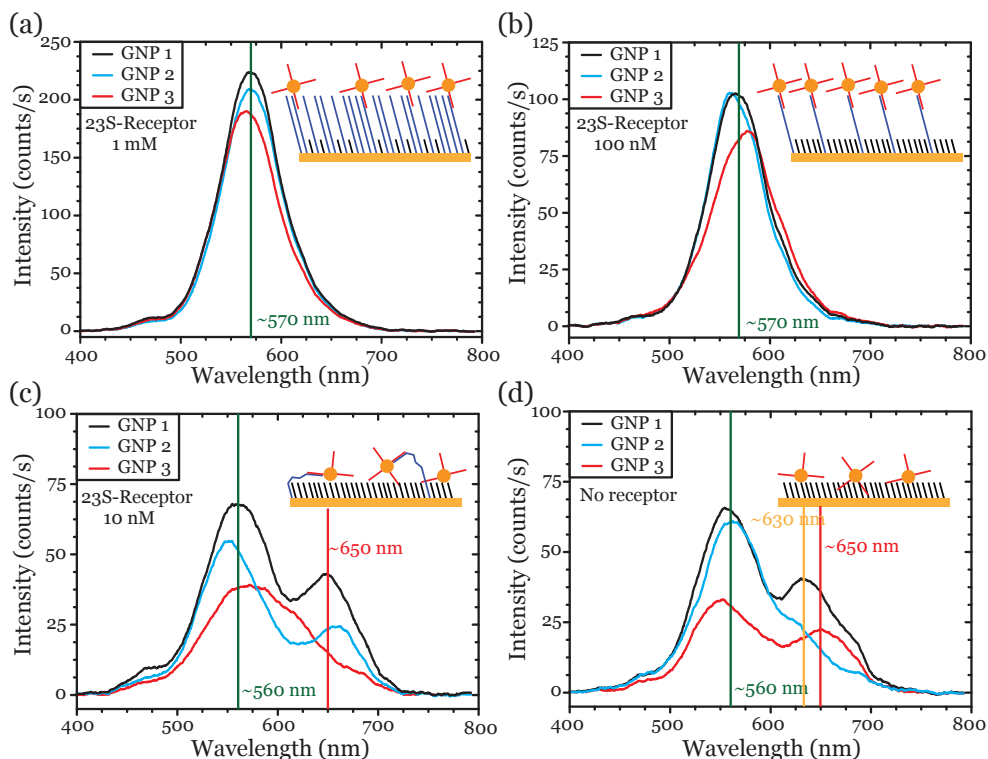


Figure 7-10: GNP⁸⁰ spectra of four different surface preparations. (a) High concentration (1 μ M) of the receptor strand results in a single peak scattering maximum with the peak at \sim 570 nm. (b) At a tenfold lower receptor strand concentration (100 nM) the scattering peak maximum is also around 570 nm. (c) At very low (10 nM) receptor strand concentration the spectra consists of two peaks with the first peak around 560 nm and the second around 650 nm. (d) When only mercaptohexanol is present on the surface the spectra consists of two peaks, similar to the 10 nM sample in panel (c). The insets illustrate the surface layout on top of the gold surface. Yellow reporter-GNPs are tethered by the receptor strand (blue) via hybridised DNA strands (red); additionally, the surface is filled with mercaptohexanol (black).

If the gold surface is functionalised with a high density of 23S-receptor strands, the hybridised reporter-GNP⁸⁰ shows a somewhat red-shifted spectrum compared to a glass surface. We think that the reporter-GNPs⁸⁰ have an increased distance from the gold surface due to the high surface density, as illustrated in Figure 7-10a. When the receptor strand density is decreased by 10-fold (Figure 7-10b), the scattering spectra of reporter-GNPs⁸⁰ do not change significantly. Apparently, the GNP distance to the gold surface remains the same as compared to that in Figure 7-10a. When the receptor strand density is decreased another 10-fold, the hybridised reporter-GNPs⁸⁰ show a completely different response as compared to the two previous concentrations



of the receptor strands (Figure 7-10c). This might mean that the flexible ssDNA 23S-receptor strand bends and allows the hybridised reporter-GNPs⁸⁰ to lie on the mercaptohexanol blocking layer. This layer spaces the reporter-GNPs⁸⁰ within 1 nm from the planar gold surface allowing interaction between both gold surfaces resulting in two scattering plasmon peaks because of the presence of both p- and s-polarized light. The flexibility of the 23S-receptor strands can explain the various spectra seen in Figure 7-10c because the distance to the surface can vary for each GNP. When no receptor strand is present, the reporter-GNPs⁸⁰ still can bind to the surface non-specifically; this results in similar GNP spectra as with the lowest tested density of receptor strands shown in Figure 7-10d. Unfortunately, we were not able to distinguish between reporter-GNP⁸⁰ that were hybridised with the receptor strand and reporter-GNP⁸⁰ that were non-specifically bound to the surface.

Furthermore, the following step, incubation with the 23S-target DNA, did not yield the expected results. To prove the concept described in the introduction, it was expected that the 23S receptor strand would stretch upon incubation with the 23S-target DNA due to its double strand conformation increasing the persistence length,¹⁸ and resulting in a blue shift of the GNP spectrum. We did not observe this effect for the monitored GNPs: the spectrum did not change for any of the monitored GNPs.

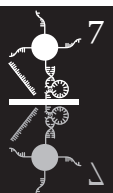
The main problem remains the non-specific surface binding of the reporter-GNPs⁸⁰ to the surface. Therefore it is hard to distinguish between the actual hybridised reporter-GNPs⁸⁰ and the non-specifically attached GNPs.

7.2.4 Conclusions and recommendations

Spin-coating of PMMA to act as a spacer layer is a simple and good solution to calibrate the GNP distance response from the gold surface. Using a SPR instrument the height of the layer could be successfully estimated. However, in contrast to the AFM, the SPR was not able to show the surface smoothness or irregularities. Moreover, AFM measurements indicated that the stripping of PMMA with glacial acetic acid requires improvements.

We also could analyze the spectra of GNP light scattering when spaced at different distances from the planar gold surface. The measurements were performed at three different distances from the surface, although the distance should be increased for an optimal calibration curve. In addition, the refractive index of PMMA ($n = 1.4838$) comes close to that of DNA ($n = \sim 1.50$); this allows a good estimation of the distance to the surface for DNA spaced GNPs.

To establish a firmer based interpretation of the observed phenomena it is necessary to collect more experimental data, with better thickness definitions, and more



uniform surfaces. Also optical excitation in a total internal reflection setup would be helpful, since this modality allows for a better manipulation of polarization directions.

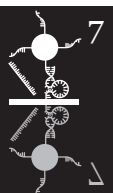
The DNA tethered GNPs showed differences in scattering spectra at varying receptor strand surface density. Unfortunately, the non-specific binding of GNPs to surface was too high to distinguish the background signal from the signal caused by low concentration of receptor strands. Non-specific binding should be solved first in order to make this assay work. Additionally, the DNA system can be improved. In the current experiments the receptor strand was able to fold randomly which was allowed by the short ssDNA persistence length. The implementation of a hairpin loop in the receptor strand would allow the unbound receptor strands to have a more rigid but shorter (folded) structure. This could result in a more clear difference between target-bound and free receptor strands.

7.3 Bibliography

- (1) Anthony R.M., Schuitema A.R.J., Oskam L., Klatser P.R. Direct detection of *Staphylococcus aureus* mRNA using a flow through microarray. *Journal of Microbiological Methods* **2005**; *60*: 47-54.
- (2) Langmuir I. The constitution and fundamental properties of solids and liquids. Part 1. Solids. *Journal of the American Chemical Society* **1916**; *38*: 2221-95.
- (3) Langmuir I. The constitution and fundamental properties of solids and liquids. II Liquids. *Journal of the American Chemical Society* **1917**; *39*: 1848-906.
- (4) Verdood R., Gill R., Ungureanu F., Molenaar R., Kooyman R.P.H. Femtomolar DNA detection by parallel colorimetric darkfield microscopy of functionalized gold nanoparticles. *Biosensors & Bioelectronics* **2011**; *27*: 77-81.
- (5) Brown L.V., Sobhani H., Lassiter J.B., Nordlander P., Halas N.J. Heterodimers: plasmonic properties of mismatched nanoparticle pairs. *ACS Nano* **2010**; *4*: 819-32.
- (6) Reinhard B.M., Siu M., Agarwal H., Alivisatos A.P., Liphardt J. Calibration of dynamic molecular rulers based on plasmon coupling between gold nanoparticles. *Nano Letters* **2005**; *5*: 2246-52.
- (7) Sönnichsen C., Reinhard B.M., Liphardt J., Alivisatos A.P. A molecular ruler based on plasmon coupling of single gold and silver nanoparticles. *Nature Biotechnology* **2005**; *23*: 741-5.
- (8) Reynolds R.A., Mirkin C.A., Letsinger R.L. Homogeneous, nanoparticle-based quantitative colorimetric detection of oligonucleotides. *Journal of the American Chemical Society* **2000**; *122*: 3795-6.
- (9) Zu Y., Gao Z. Facile and controllable loading of single-stranded DNA on gold nanoparticles. *Analytical Chemistry* **2009**; *81*: 8523-8.
- (10) Xiao L., Wei L., He Y., Yeung E.S. Single molecule biosensing using color coded plasmon resonant metal nanoparticles. *Analytical Chemistry* **2010**; *82*: 6308-14.
- (11) Hurst S.J., Lytton-Jean A.K.R., Mirkin C.A. Maximizing DNA loading on a range of gold nanoparticle sizes. *Analytical Chemistry* **2006**; *78*: 8313-8.
- (12) Hill H.D., Millstone J.E., Banholzer M.J., Mirkin C.A. The role radius of curvature plays in thiolated oligonucleotide loading on gold nanoparticles. *ACS Nano* **2009**; *3*:



- 418-24.
- (13) Ungureanu F., Halamek J., Verdoold R., Kooyman R.P.H. The use of a colour camera for quantitative detection of protein-binding nanoparticles. *Proceedings of SPIE* **2009**; 7192: 719200.
 - (14) Draine B.T., Flatau P.J. Discrete-dipole approximation for scattering calculations. *Journal of the Optical Society of America A* **1994**; 11: 1491.
 - (15) Ungureanu F., Wasserberg D., Yang N., Verdoold R., Kooyman R.P.H. Immunosensing by colorimetric darkfield microscopy of individual gold nanoparticle-conjugates. *Sensors & Actuators: B Chemical* **2010**; 150: 529-36.
 - (16) Mock J.J., Hill R.T., Degiron A., Zauscher S., Chilkoti A., Smith D.R. Distance-dependent plasmon resonant coupling between a gold nanoparticle and gold film. *Nano Letters* **2008**; 8: 2245-52.
 - (17) Murphy M.C., Rasnik I., Cheng W., Lohman T.M., Ha T. Probing single-stranded DNA conformational flexibility using fluorescence spectroscopy. *Biophysical Journal* **2004**; 86: 2530-7.
 - (18) Brinkers S., Dietrich H.R.C., de Groote F.H., Young I.T., Rieger B. The persistence length of double stranded DNA determined using dark field tethered particle motion. *The Journal of Chemical Physics* **2009**; 130: 215105.
 - (19) Chen J.I.L., Chen Y., Ginger D.S. Plasmonic nanoparticle dimers for optical sensing of DNA in complex media. *Journal of the American Chemical Society* **2010**; 132: 9600-1.
 - (20) Kamanyi A.E., Grill W., Ngwa W., Luo W. Advances in phase-sensitive acoustic microscopy studies of polymer blend films: annealing effects and micro-elastic characterization of PS/PMMA blends. *Journal of Microscopy* **2010**; 238: 134-44.
 - (21) Mairal T., Frese I., Llaudet E., Redondo C.B., Katakis I., von Germar F., Drese K., O'Sullivan C.K. Microfluorimeter with disposable polymer chip for detection of coeliac disease toxic gliadin. *Lab on a Chip* **2009**; 9: 3535-42.
 - (22) Schasfoort R., Tudos A. *Handbook of Surface Plasmon Resonance*. Royal Society of Chemistry: Cambridge, **2008**. p. 403.
 - (23) Vlachopoulou M.E., Tserepi A., Pavli P., Argitis P., Sanopoulou M., Misiakos K. A low temperature surface modification assisted method for bonding plastic substrates. *Journal of Micromechanics & Microengineering* **2009**; 19: 015007.
 - (24) Sarveswaran K., Hu W., Huber P.W., Bernstein G.H., Lieberman M. Deposition of DNA rafts on cationic SAMs on silicon [100]. *Langmuir* **2006**; 22: 11279-83.
 - (25) Ungureanu F. Sensing with colours. University of Twente, **2012**.
 - (26) Crow M.J., Seekell K., Wax A. Polarization mapping of nanoparticle plasmonic coupling. *Optics Letters* **2011**; 36: 757-9.



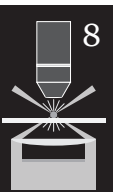




Chapter 8

Concluding remarks and recommendations for future work

This chapter summarises the overall results obtained in this research project on the development of optical based gold nanoparticle DNA sensing methods. We conclude this chapter with some recommendations to improve the limit of detection and increase the dynamic range of the gold nanoparticle sensor. An optimal method should be not only sensitive but also have a wide dynamic range.



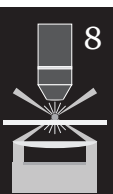
8.1 Conclusion

The main goal of this project was to design and develop a gold nanoparticle based optical biosensor for the specific detection of DNA hybridisation events. The sensor system is developed for biological samples, e.g., medical samples for disease diagnostics, bacterial food contaminants or other biological threats using simple optical components. The major effort in this project includes the functionalisation of gold nanoparticles with receptor molecules while ensuring that the receptors remain biologically active. In Chapter 1 and Chapter 2, respectively, the aim of the project and the theoretical background have been described.

Chapter 3: We studied various surface modifications methods. Each method was developed with the method of detection in mind. For optical microscopy transparent and semi-transparent surfaces were modified while for surface plasmon resonance only semi-transparent gold coated glass could be used. The procedure of silanisation of glass was optimised for the immobilisation of gold nanoparticles with the lowest possible background interference. In addition, two methods for the functionalisation of gold nanoparticles using thiol modified DNA strands were developed, *viz.* (1) gold nanoparticles are functionalised in a colloidal suspension and (2) particles immobilised on a surface are functionalised. The biological activity of the functionalised GNPs was demonstrated by subsequent hybridisation and melting cycles of complementary functionalised particles. Both immobilisation and functionalisation procedures were combined and merged into a simple-to-construct flow-cell that enables analysis of the hybridisation process in real-time.

Chapter 4: We modelled the plasmon peak shift for various sized GNPs as a response to the binding of DNA strands. This enabled us to estimate the loading of strands on the surface of particles either in colloidal solution or immobilised on a surface. In addition, we modelled the effect of close proximity of two GNPs by varying particle sizes and interparticle distances. With this knowledge we developed threshold values for darkfield analysis. Moreover, we employed a Monte Carlo simulation to estimate the affinity constant of the GNP–DNA hybridisation assay.

Chapter 5: Conventional surface plasmon resonance (SPR) is less suitable for the detection of low molecular weight targets (< 10 kDa). To overcome this problem, various signal amplification strategies have been developed by other groups, such as fluorescent or mass labels. We have used GNPs as both mass and plasmon interaction labels. We have compared the response by amplifying the SPR signal with 20 and

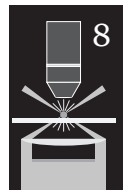


60 nm GNPs. As expected, the larger particles are able to substantially amplify the signal, thus making it possible to detect the presence of small target strands in the picomolar range.

Chapter 6: We developed a GNP based biosensor capable of detecting specific hybridisation of a target DNA molecule using a conventional optical darkfield microscope. By combining the lessons from Chapters 3 and 4, we were able to successfully immobilise GNPs on a glass surface, functionalise them with DNA receptor strands and specifically hybridise a target strand. We could monitor the final step in the reaction, the developer GNP hybridisation, either as a function of time or as an endpoint measurement. An advantage of the real-time measurement is the conversion to an easily interpretable sensorgram, in which the single binding events over the incubation period are shown. An advantage of the endpoint measurements is the possibility to analyse a large number of samples in a short time period.

Chapter 7: The opportunities to use gold nanoparticles for bioassays are nearly endless. Here we have done a preliminary investigation into two additional DNA sensing strategies. In the first method a conventional DNA detection assay is converted from fluorescence to GNPs. The advantage here is the ability to measure single binding events out of a known number of receptors and the use of a conventional darkfield microscope for detection. We have shown that the assay is specific for DNA target strands with low sequence similarity. Moreover, the assay was successfully performed without any surface blocking agent. With optimisation of the various hybridisation steps this assay could be adapted easily for the specific detection of other DNA target strands from *Staphylococcus aureus* or other sequence specific bacterial DNA strands.

The second assay is based on a new detection approach. Instead of utilizing the plasmon interaction between two gold nanoparticles we use a single GNP within close proximity of a planar gold surface as used in conventional SPR. Essentially, the single GNP ‘sees’ a mirror image of itself, since the gold layer acts a mirror, and we have now to do with a (virtual) two GNP system, that obeys similar rules as those for the close proximity assay. In this approach the distance between the GNP and the surface was varied by the height difference of single and double stranded DNA. Double stranded DNA is more rigid compared to single stranded DNA, hence a larger distance from the surface results. We studied this approach and conclude that a thorough investigation on the physics is required before this method can be utilised in a sensor system. In view of the fact that this method is essentially label-free, such an investigation would be very worthwhile also within the context of sensor research.



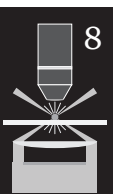
8.2 Improving the close proximity GNP assay

As shown in Chapter 6, the GNP assay based on the close proximity of two GNPs is capable of detecting low concentrations of target strands. However, various modifications to the assay are conceivable in order to further improve the detection limit. A few of these are described here. Modifications can be aimed at decreasing non-specific interactions, increasing the number of receptors, or improving affinity. A successful implementation of any of these modifications results in a decrease of the minimal detectable ratio between the number of covered receptors and total receptors available (Γ_{\min}) as described in Chapter 4. In order to compete with DNA amplifying methods, such as PCR and biobarcoding^{1,2} we aim to reach attomolar sensitivity.

8.2.1 Reducing non-specific binding

Throughout the experiments described in this thesis non-specific binding has been observed. In this type of assays there are essentially two categories of non-specific binding: the first is the adsorption of GNPs to the surface, and the second is the binding of non-specific target strands to the immobilised receptors. For a detection method with single molecule sensitivity it is essential that the individual bound target is truly specific. In protein assays GNP adsorption is usually reduced using well-known proteins, i.e., BSA^{3,4} or dissolved skimmed milk powder.^{5,6} These proteins or protein cocktails fill in the empty places on the surface. However, in DNA assays the surface cannot be randomly blocked with large proteins (> 50 kDa) as they will hinder the specific binding of the target strands onto the small receptors (between 10 and 20 kDa). As an alternative small molecules can be used.³ Depending on the surface a wide variety of molecules are available, each with different reactive end groups. It is important to choose a molecule which possesses a neutral charge or a charge similar to that of the developer GNP in the same buffer conditions, so that these GNPs have no tendency to bind to the surface. As shown in Chapter 3, large polyethylene glycol (PEG) molecules succeeded very well in preventing GNPs from binding to the surface.⁷ However, the long PEG molecule can hinder the hybridisation of the target molecule with the receptor DNA strands. An advantage of PEG is the wide variety of lengths that is available, ranging from 300 Da to > 15 kDa.

To reduce the non-specific hybridisation of random DNA to the receptor strands, more stringent assay conditions can be chosen by adjusting the incubation and buffer conditions. In DNA hybridisation the specific target strand has the highest affinity with the receptor, and thus the highest melting temperature (T_m). By increasing the incubation temperature close to the T_m of the target strand, the specificity can



be improved. This phenomenon is the basis of the PCR detection/amplification method.^{8,9} Additionally, the binding strength can be reduced by introducing chemical compounds, e.g., formamide.^{10,11} This lowers the T_m of the correct target–receptor interaction to approximately 20 °C above ambient. For any non-specific strand T_m becomes lower than the ambient temperature, therefore in an optimised assay non-specific hybridisation does not occur at all. However, optimizing an assay using this approach can be challenging.

As indicated here, surface chemistry is and will remain a major part of biosensors and their assays. For this type of biosensing assay the path towards perfection is still long and probably exceedingly hard. Every successful commercial biosensor on the market was preceded with a long study mainly directed to optimise the specificity of the assay. With the progress in optics and imaging, detecting even single binding events becomes relatively easy these days; however, it becomes progressively harder to optimise the chemistry.

8.2.2 Increasing the number of receptors

There are various methods to increase the number of monitored receptors. By far the simplest method is to capture more images of the same measurement, thus increasing the GNP count and number of receptors. At least a 40× magnification is required for 80 nm GNPs, therefore using a lower magnification is not suggested. The set-up we used has a motorised XYZ-stage, allowing accurate movements in any of these directions and consistent automated focus. The current field of view (FOV) measures 225 μm by 165 μm, which is a small fraction of the total area of the 50 mm by 4 mm flow-cell used in Chapters 3 and 6. The original FOV contains about 10^3 80 nm GNPs. We can increase the analysis area to 1 mm² by capturing multiple images. The images need a 20% overlap to ensure good image stitching during analysis. Approximately 42 images are necessary to capture 1 mm², presenting approximately 27,000 GNPs, each functionalised with 700 active receptors. Since we are able to detect the binding of one individual target strand out of the total number of available receptors, we improve the Γ_{\min} from 1.4×10^{-6} (1,000 GNPs, each with 700 receptors) to 5.3×10^{-8} (27,000 GNPs, each with 700 receptors).

Another, somewhat more complex, possibility is to increase the number of GNPs by a perfect arrangement on the surface. This can be achieved by using nano-imprint lithography.¹² To ensure that GNPs can be discerned as individual particles under dark-field conditions, the distance between two adjacent GNPs should be at least 2.25 μm (thus, a circle with a radius of 1.125 μm) in our microscope system as discussed in Chapter 6 (40× magnification, Zeiss axiocam HRc). In the late 18th century Joseph Louis Lagrange described that circles could be packed with the highest density if they



were packed according to a hexagonal arrangement, i.e., a honeycomb. The optimal distance of $2.25 \mu\text{m}$ between GNPs in such an arrangement will result in a surface area of $\sim 13 \mu\text{m}^2$ per GNP. In the FOV of our microscope this increases the total number of particles to $\sim 3,000$ and improves the Γ_{\min} to 5.1×10^{-7} . When combined with the multi-image method, the total number of particles increases to $\sim 76,000$ with a Γ_{\min} to 1.9×10^{-8} .

An additional strategy to raise the number of available receptors is to increase the size of the GNPs. A 100 nm GNP is able to host approximately 1,100 receptors (1/2 of max to reduce steric hindrance).¹³ This is 400 receptors more compared to an 80 nm GNP resulting in a base Γ_{\min} of 9.1×10^{-7} (for 1,000 GNPs). Increasing the receptor GNP size further to 150 nm doubles the amount of receptors which can be safely immobilised to $\sim 2,500$ receptors per particle and can likewise enhance the Γ_{\min} to 3.9×10^{-7} . The various sized GNPs with their receptor numbers are summarised in Table 8-1. We stress that the quoted Γ_{\min} are theoretical numbers, for a situation where non-specific interactions are absent.

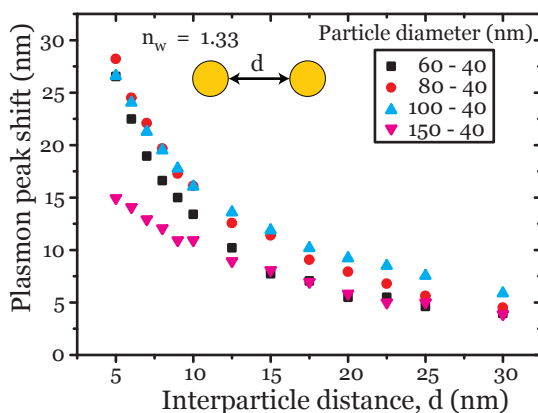


Figure 8-1: Comparison of the close proximity response of various sized GNP sets. The threshold for a single molecule detection should be $\Delta\lambda > 5 \text{ nm}$.

In addition, a large receptor GNP will respond differently to the binding of the 40 nm developer GNP as shown by a DDSCAT simulation depicted in Figure 8-1. The plasmon peak shift of a larger receptor GNP paired with a 40 nm developer GNP does not differ very much compared to the $\text{GNP}^{80}\text{-GNP}^{40}$ pair. At the most interesting range of the inter-particle distances between 15 and 30 nm the $\text{GNP}^{100}\text{-GNP}^{40}$ pair even shows a larger λ_{\max} change than $\text{GNP}^{80}\text{-GNP}^{40}$ or $\text{GNP}^{60}\text{-GNP}^{40}$ pairs. Even the $\text{GNP}^{150}\text{-GNP}^{40}$ pair has a minimal λ_{\max} shift of 5 nm, and is, therefore, a suitable pair.

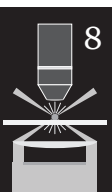


Table 8-1: Summary of various sized GNPs with their single molecule sensitivity and response to the binding of a single 40 nm developer GNP.

GNP (nm)	Receptors (#)	Γ_{\min}^a	λ_{shift}^b (nm)	λ_{\max}^c (nm)
60	445	2.3×10^{-6}	7.7	519.5
80	700	1.4×10^{-6}	11.4	525.9
100	1100	9.1×10^{-7}	11.9	536.8
150	2500	4.0×10^{-7}	8.1	583.8

- Minimum of the fraction of receptors that have to be covered with a target and developer GNP in order to be detected, assuming that this method has single molecule sensitivity.
- The scattering plasmon peak shift of receptor GNP upon binding of a 40 nm developer GNP at an interparticle distance of 15 nm.
- The scattering plasmon peak of the particle before binding of a 40 nm developer GNP.

8.2.3 Increasing sensitivity by improving affinity constant

Besides increasing the amount of receptor molecules, a receptor molecule with a higher affinity constant can be used. As an example, polyamide nucleic acid (PNA) can be used for an optimal DNA or RNA target hybridisation.¹⁴ The sugar backbone of the DNA in this synthetic molecule is replaced by an amide backbone (peptide backbone). This also makes PNA strands neutrally charged in contrast to the negatively charged DNA strands. Compared to the DNA–DNA interaction the PNA–DNA interaction is stronger at low NaCl concentrations;¹⁵ therefore an increase in affinity constant can be expected from such a system. Park and co-workers studied the effect of NaCl ionic strength on the binding properties between PNA and DNA complexes.¹⁶ At a high ionic strength of 127 mM NaCl, an affinity constant of $8.0 \times 10^8 \text{ M}^{-1}$ was obtained for a 15-mer PNA–DNA pair. At a low ionic strength of 20 mM NaCl, it increased to $8.5 \times 10^8 \text{ M}^{-1}$. Since it is difficult to compare affinity constant values for different DNA or PNA sequences it is best to compare the melting temperature. A higher melting temperature indicates a higher affinity constant. In Chapter 3 we studied the T_m of our 18-mer DNA–DNA strands. From these results we estimated the T_m at 20 mM and 127 mM NaCl to be $\sim 39^\circ\text{C}$ and $\sim 53^\circ\text{C}$, respectively. These values are much lower compared to the PNA–DNA complex which at 20 mM has a T_m of $\sim 77^\circ\text{C}$ and at 127 mM a T_m of $\sim 75^\circ\text{C}$.¹⁶ This indicates that the PNA strands hybridise better than DNA in a low ionic strength environment. It is conceivable that the neutrally charged PNA strands will also improve the stability of the functionalised particles. The use of PNA



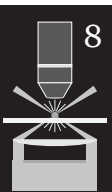
can improve the sensitivity of the assay tenfold; moreover, the advantage of low ionic strength can increase the sensitivity even a 100 times compared to DNA-DNA.¹⁷

Recently, locked nucleic acid (LNA) was developed. The ribose bridge in LNA is strengthened (locked) by a methylene bridge forcing the LNA monomers to have the North-conformation. The N-conformation 'locks' the 3' ribose, increasing the energy necessary to break the bond. The locked LNA conformation already has a single helix shape allowing quicker and better hybridisation with the short target DNA or RNA; this increases the melting temperature of the polymer.¹⁸⁻²¹ An additional advantage of LNA is the large difference in melting temperature between hybridisation with a perfect complementary strand and a single mismatched strand (single nucleotide polymorphism (SNP)).^{22,23} The ability to discriminate SNPs opens a wide field of interesting application sectors, e.g., forensic screening or mutation screening.²⁴⁻²⁶ Until now no affinity comparison studies with LNA-DNA has been performed. Studies focussed on T_m show a large increase in the T_m similar to that of the PNA-DNA system.^{20,27-29} Therefore we could expect a similar increase in sensitivity while working at low temperatures with low ionic strength buffers.

8.2.4 Improving the dynamic range

The dynamic range of a biosensor points out at which lowest concentration of the analyte a signal is observed (limit of detection) and at which concentration the signal is saturated ($\Gamma_{\min} / \Gamma_{\max}$). This means that if the sample concentration is outside this range it will either saturate the sensor or not be detected at all. Therefore multiple dilution steps could be required before a measurement is carried out. A solution to this problem is to either increase the dynamic range or make a system that can measure multiple sample concentrations simultaneously. On the other hand, for medical diagnostics it is preferred to obtain results rapidly without making a dilution range, reducing the costs of an analysis.

In order to increase the dynamic range of the GNP sensor, various sized GNPs can be combined on a single surface, each with a different amount of receptors presented on the surface. It would be more convenient to use the same GNP size with different amounts of receptors but this is hard to achieve in a single flow-cell. A typical sensing area would contain sectors with different sized GNPs as shown in Figure 8-2. Each sector would be analysed separately and, subsequently, the results would be compared with those of the other sectors. An advantage of this approach is that each sector gives results which should be closely matched with the other sectors, thus increasing the reliability. A disadvantage of the system is the close relation in size between each sector. The dynamic range increases with GNPs ranging from 60 nm to 150 nm. The smallest dynamic range is obtained from a uniform 60 nm sensor



(445 receptors/GNP, 2,800 GNPs), ranging from Γ_{\min} of 8.0×10^{-7} to Γ_{\max} of 3.5×10^{-4} . By using two GNP sizes, each having 1,400 GNPs in the FOV, the dynamic range marginally increases, ranging from a Γ_{\min} of 2.4×10^{-7} to a Γ_{\max} of 3.5×10^{-4} , as shown in Figure 8-2. However, the response of a single sized developer GNP (such as 40 nm GNP) might be limited at GNPs larger than 150 nm.

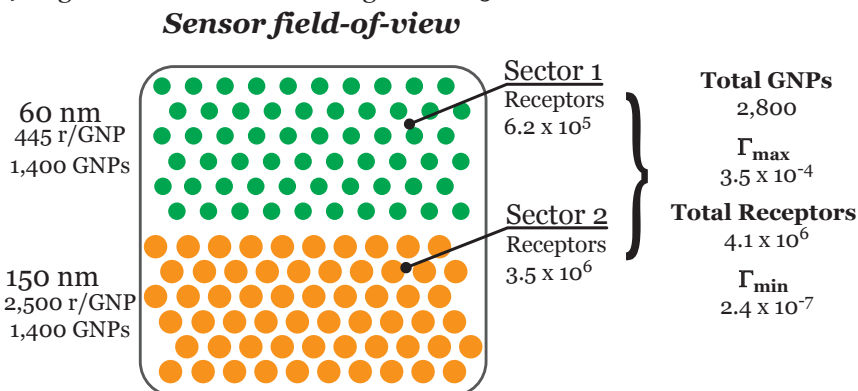


Figure 8-2: A sensor with various sized GNPs. Layout of field-of-view with GNPs separated by size in two sectors, each sector has a different range in sensitivity since each GNP size can host different numbers of receptors per nanoparticle, as indicated next to the scheme.

8.2.5 Dedicated apparatus

In the experiments of this thesis we tried to modify and optimise a standard microscope setup. As an alternative, we could think of constructing a dedicated instrument for GNP based sensing. An advantage of this approach would be an apparatus constructed from a low number of standard available components ensuring a relatively cheap system, as illustrated in Figure 8-3a.

When constructing a dedicated apparatus all components have to be optimised for maximum sensitivity. This means that we have to image as many GNPs as possible which can be achieved by using a large standard 10 Megapixel CCD array with a size of 30×20 mm. When we use a grid of 5×5 pixels to image a single GNP and leave an equal dark space between each GNP, we are able to image 3×10^5 GNPs on a single CCD sensor. With a $5 \times$ magnification this results in a sensor chip surface with a size of 6×4 mm. For a DNA sensor chip using 80 nm GNPs we estimate 700 receptor molecules per GNP resulting in total number of receptors of 2.1×10^8 . With single molecule sensitivity we can theoretically obtain a Γ_{\min} of 4.8×10^{-9} . With an affinity constant of $K = 2.0 \times 10^7 \text{ M}^{-1}$ (¹⁷) this would result in a minimum detectable concentration of $\sim 9.6 \times 10^{-16} \text{ M}$. This could be further improved towards attomolar sensitivity by using larger GNPs, high affinity receptor strands and fully optimised incubation procedures.



The sensor chip can be easily imaged onto the CCD array using a standard microscope objective. If we choose a focal distance of 10 mm this results in dimensions of the complete optical assembly in the order of 10 cm. Additionally, this focal distance should leave plenty of room for liquid handling of the sample buffers on the sensor chip.

A simple method for illumination is to use a hemispherical prism with a focussed light spot in a total internal reflection configuration. As lightsource a xenon arc would be most suitable, although cheaper incandescent lamps or even high-power LEDs can be used. Alternatively, the available sunlight can be used via a set of mirrors and lenses, as commonly used in simple microscopes. Before coupling the light into the prism, a polariser can be used to choose between s-, p- and unpolarised light. The light polarisation can be exploited to obtain information on the orientation of the GNP pair axis relative to the substrate, whereas analysis of the scattered polarization allows to distinguish a single scattering GNP from a GNP pair (cf. Figure 8-3b)^{30,31} Additionally, two dedicated bandpass filters could be used to differentiate a GNP pair from a single GNP. By capturing images with both green and red filters before the assay and after the interaction is completed, it is possible to see which GNPs have changed from green to red, i.e., have bound an analyte and developer GNP. This eliminates the use of a colour CCD, e.g., Bayer array, of which the used filters might not optimally match the changing colour properties of GNPs.

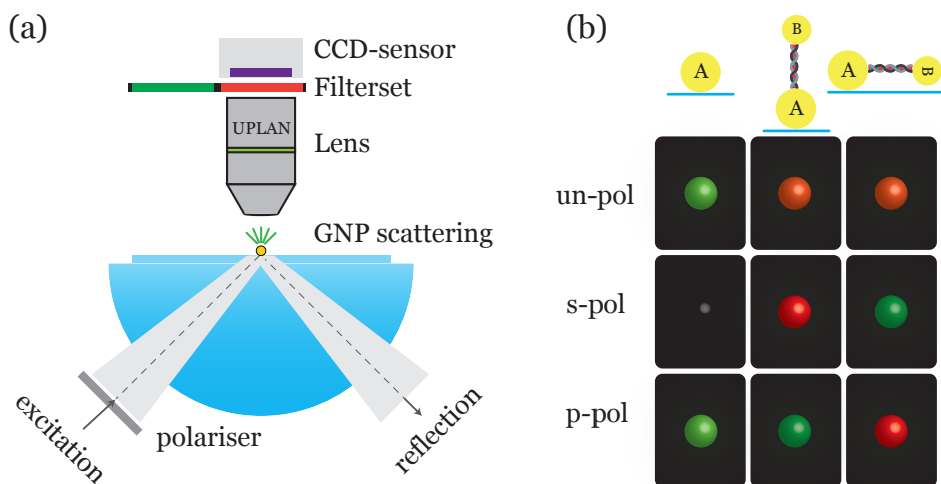


Figure 8-3: (a) Components of a dedicated apparatus with optional filter set or polariser. (b) The effect of polarised light on a single GNP and GNP-pairs with two different orientations.

8.3 Conclusion

There is room for improvement. However, this chapter has argued that the GNP–GNP assay can become more sensitive by analysing more GNPs and thus counting more receptors. Additionally, the sensitivity can be further improved by increasing the size of the GNP and thus increasing the number of receptors per GNP. Therefore, in order to enhance the limit of detection (LOD) to sub-femtomolar concentrations it is suggested to use a larger reporter GNP compared to counting more GNPs. For instance, a receptor GNP of 150 nm can still give a detectable λ_{\max} shift of > 5 nm when combined with a 40 nm developer GNP.

Presently the GNP assay suffers mostly from non-specific binding. The basic assay is functional, which is proven in Chapters 6 and 7. Non-specific interactions have to be eliminated to reach true single molecule sensitivity. Unfortunately, that would be practically impossible. However, reducing the unwanted interactions to the minimum is very important when analysing complex media, such as milk, full blood, or sputum. Using short PEG molecules, better designed receptor strands and optimising the assay towards more stringent hybridisation conditions can improve the reliability of this assay for targets at very low concentration, finally reaching the attomolar range.

The versatility of the assay is high. For early detection of viruses the sensor can be modified to contain the highest possible amount of receptors, thus focussing on very low concentrations. When a less sensitive, but improved dynamic range is preferred, a sensor with multiple sized GNPs can be used. A wide dynamic range is appealing since it allows the analysis of a wide variance of sample concentrations. Each size would have a unique response to the target concentration. Additionally, analyzing multiple sectors with various GNP sizes in parallel will automatically result in replicate measurements. However, it is a practical challenge to fabricate a sensor containing various sized GNPs organised in a single sensing area. On the other hand, different sized and randomly spread GNPs can be separated in an image using the size specific light scattering maxima.

With an apparatus specifically developed for DNA sensing, designed to have the highest achievable receptor density it should be possible to reach sensitivity in the attomolar range. An additional advantage is the low number of components necessary to construct such a device.

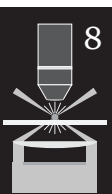
A GNP based biosensor for DNA or RNA using simple and cheap components for analysis can become a breakthrough. The application field is almost endless. In medical diagnostics the system could be used for screening disease markers, e.g., Tuberculosis (*Mycobacterium tuberculosis*), Legionella (*Legionella pneumophila*)



and viral hepatitis. In the food processing industry such a sensor can be applied to detect the freshness of dairy products or other perishable foods often threatened by bacterial contaminants. Additionally, the sensor can be used to check for DNA or RNA based biological warfare agents such as Anthrax (*Bacillus anthracis*) and viruses.

8.4 Bibliography

- (1) Thaxton C.S., Hill H.D., Georganopoulou D.G., Stoeva S.I., Mirkin C.A. A bio-barcode assay based upon dithiothreitol-induced oligonucleotide release. *Analytical Chemistry* **2005**; *77*: 8174-8.
- (2) Goluch E.D., Nam J.M., Georganopoulou D.G., Chiesl T.N., Shaikh K.A., Ryu K.S., Barron A.E., Mirkin C.A., Liu C. A bio-barcode assay for on-chip attomolar-sensitivity protein detection. *Lab on a Chip* **2006**; *6*: 1293-9.
- (3) Taylor S. Impact of surface chemistry and blocking strategies on DNA microarrays. *Nucleic Acids Research* **2003**; *31*: 87e.
- (4) Festag G., Steinbrück A., Wolff A., Csaki A., Möller R., Fritzsche W. Optimization of gold nanoparticle-based DNA detection for microarrays. *Journal of Fluorescence* **2005**; *15*: 161-70.
- (5) Pollet J., Delpont F., Janssen K.P.F., Tran D.T., Wouters J., Verbiest T., Lammertyn J. Fast and accurate peanut allergen detection with nanobead enhanced optical fiber SPR biosensor. *Talanta* **2011**; *83*: 1436-41.
- (6) Wu W.Y., Bian Z.P., Wang W., Zhu J.J. PDMS gold nanoparticle composite film-based silver enhanced colorimetric detection of cardiac troponin I. *Sensors & Actuators: B Chemical* **2010**; *147*: 298-303.
- (7) Martins V.C., Cardoso F.A., Germano J., Cardoso S., Sousa L., Piedade M., Freitas P.P., Fonseca L.P. Femtomolar limit of detection with a magnetoresistive biochip. *Biosensors & Bioelectronics* **2009**; *24*: 2690-5.
- (8) Saiki R., Gelfand D., Stoffel S., Scharf S., Higuchi R., Horn G., Mullis K., Erlich H. Primer-directed enzymatic amplification of DNA with a thermostable DNA polymerase. *Science* **1988**; *239*: 487-91.
- (9) Mullis K. *Dancing Naked in the Mind Fields*. Pantheon Books: New York, **1998**.
- (10) Fuentes M., Mateo C., García L., Tercero J.C., Guisán J.M., Fernández-Lafuente R. Directed covalent immobilization of aminated DNA probes on aminated plates. *Biomacromolecules* **2004**; *5*: 883-8.
- (11) Elenis D.S., Ioannou P.C., Christopoulos T.K. A nanoparticle-based sensor for visual detection of multiple mutations. *Nanotechnology* **2011**; *22*: 155501.
- (12) Lucas B.D., Kim J.S., Chin C., Guo L.J. Nanoimprint lithography based approach for the fabrication of large-area, uniformly-oriented plasmonic arrays. *Advanced Materials* **2008**; *20*: 1129-34.
- (13) Hill H.D., Millstone J.E., Banholzer M.J., Mirkin C.A. The role radius of curvature plays in thiolated oligonucleotide loading on gold nanoparticles. *ACS Nano* **2009**; *3*: 418-24.
- (14) Nielsen P., Egholm M., Berg R., Buchardt O. Sequence-selective recognition of DNA by strand displacement with a thymine-substituted polyamide. *Science* **1991**; *254*: 1497-500.
- (15) Egholm M., Buchardt O., Christensen L., Behrens C., Freier S.M., Driver D.A., Berg R.H., Kim S.K., Norden B., Nielsen P.E. PNA hybridizes to complementary



- oligonucleotides obeying the Watson-Crick hydrogen-bonding rules. *Nature* **1993**; *365*: 566-8.
- (16) Park H., Germini A., Sforza S., Corradini R., Marchelli R., Knoll W. Effect of ionic strength on PNA-DNA hybridization on surfaces and in solution. *Biointerphases* **2007**; *2*: 80-8.
 - (17) Nelson B.P., Grimsrud T.E., Liles M.R., Goodman R.M., Corn R.M. Surface plasmon resonance imaging measurements of DNA and RNA hybridization adsorption onto DNA microarrays. *Analytical Chemistry* **2001**; *73*: 1-7.
 - (18) McTigue P.M., Peterson R.J., Kahn J.D. Sequence-dependent thermodynamic parameters for locked nucleic acid (LNA)-DNA duplex formation. *Biochemistry* **2004**; *43*: 5388-405.
 - (19) Kaur H., Arora A., Wengel J., Maiti S. Thermodynamic, counterion and hydration effects for the incorporation of locked nucleic acid (LNA) nucleotides in duplex. *Nucleic Acids Symposium Series (2004)* **2008**; *52*: 425-6.
 - (20) Vester B., Wengel J. LNA (locked nucleic acid): high-affinity targeting of complementary RNA and DNA. *Biochemistry* **2004**; *43*: 13233-41.
 - (21) Lee H.J., Wark A.W., Corn R.M. Enhanced bioaffinity sensing using surface plasmons, surface enzyme reactions, nanoparticles and diffraction gratings. *The Analyst* **2008**; *133*: 596-601.
 - (22) Demidov V.V., Frank-Kamenetskii M.D. Two sides of the coin: affinity and specificity of nucleic acid interactions. *Trends in Biochemical Sciences* **2004**; *29*: 62-71.
 - (23) Castoldi M., Schmidt S., Benes V., Noerholm M., Kulozik A.E., Hentze M.W., Muckenthaler M.U. A sensitive array for microRNA expression profiling (miChip) based on locked nucleic acids (LNA). *RNA (New York, NY)* **2006**; *12*: 913-20.
 - (24) Chua A., Yean C.Y., Ravichandran M., Lim B., Lalitha P. A rapid DNA biosensor for the molecular diagnosis of infectious disease. *Biosensors & Bioelectronics* **2011**.
 - (25) Mariotti E. Surface plasmon resonance biosensor for genetically modified organisms detection. *Analytica Chimica Acta* **2002**; *453*: 165-72.
 - (26) Kalogianni D.P., Litos I.K., Christopoulos T.K., Ioannou P.C. Dipstick-type biosensor for visual detection of DNA with oligonucleotide-decorated colored polystyrene microspheres as reporters. *Biosensors & Bioelectronics* **2009**; *24*: 1811-5.
 - (27) Sørensen M.D., Petersen M., Wengel J. Functionalized LNA (locked nucleic acid): high-affinity hybridization of oligonucleotides containing N-acylated and N-alkylated 2'-amino-LNA monomers. *Chemical Communications* **2003**; *2*: 2130-1.
 - (28) Christensen U., Jacobsen N., Rajwanshi V.K., Wengel J., Koch T. Stopped-flow kinetics of locked nucleic acid (LNA)-oligonucleotide duplex formation: studies of LNA-DNA and DNA-DNA interactions. *The Biochemical Journal* **2001**; *354*: 481-4.
 - (29) Singh S.K., Koshkin A.A., Wengel J., Nielsen P. LNA (locked nucleic acids): synthesis and high-affinity nucleic acid recognition. *Chemical Communications* **1998**: 455-6.
 - (30) Crow M.J., Seekell K., Wax A. Polarization mapping of nanoparticle plasmonic coupling. *Optics Letters* **2011**; *36*: 757-9.
 - (31) Aaron J., de la Rosa E., Travis K., Harrison N., Burt J., José-Yacamán M., Sokolov K. Polarization microscopy with stellated gold nanoparticles for robust monitoring of molecular assemblies and single biomolecules. *Optics Express* **2008**; *16*: 2153.





Summary

Dark field (DF) optical detection of gold nanoparticles (GNPs) is a single-molecule method which can be used for sensitive and specific detection of nucleic acid strands such as DNA and RNA. This thesis describes the development of a novel biosensor based on scattering GNPs, from a theoretical idea on paper to a working sensor system which is sensitive for specific DNA detection in the femtomolar range. Furthermore, the modification chemistry and theoretical simulations are described to provide insight into the reported sensing method and experimental setup. The light scattering and absorption properties of GNPs can be utilised for the detection of DNA. Binding of molecules to the GNP influences the local refractive index. The increase in refractive index can be measured as a proportional red-shift of the GNP extinction maximum; therefore GNPs are suitable for use as nanoparticle chemical sensors. Utilizing this approach it is possible to detect DNA in naturally occurring quantities. In total, five different DNA detection assays were investigated.

Chapter 2 provides an overview of DNA detection methods based on optical principles in the present and in the past. We continue with the first use of GNPs for sensing purposes, followed by more complex and increasingly more sensitive detection of specific DNA target strands. Recent developments in GNP synthesis allow the fabrication of high quality homogeneously sized particles. These particles can be used for DF detection of binding events using nothing more than a conventional microscope, colour camera and analysis software.

Chapter 3 describes a part of the long road towards the fabrication of a GNP based DNA biosensor. On this road many obstacles had to be passed by solving biochemical problems such as immobilisation of the DNA receptors to GNPs, immobilisation of GNPs on surface, surface modifications and assay condition optimisations to increase immobilisation yield. The chapter is finalised with the development of a flow-cell which is easy to fabricate and fits in a standard microscope.

After the biochemical background described in Chapter 3, in **Chapter 4** the physics background is described. The detection principle is based on surface plasmon resonance (SPR) which nowadays is a commonly used method for protein interaction analysis. For each individual GNP the effect of SPR can be monitored in a local area directly around the particle, as so-called local SPR (LSPR). The LSPR effect changes by modifying the refractive index in the local area and the response can be observed as a change in scattering colour. Scattering simulations were performed to estimate the binding of DNA strands to individual GNPs. Based on the change in scattering colour it is possible to estimate the number of receptor strands. Additionally, by using Monte Carlo simulations a model was developed to estimate the affinity constant for a DNA sandwich assay, in which a target strand is captured by two GNPs.

Conventional SPR is not sensitive enough to detect low molecular weight molecules such as short DNA strands. In **Chapter 5** we overcome this problem by amplifying the signal using two types of GNPs. First, the expected response was modelled for 20 and 60 nm GNPs and it was followed by comparing the simulations with experimental data. The 20 nm GNPs enabled monitoring the binding of a low molecular weight DNA target strand. The signal amplification with 20 nm GNPs resulted in a measurable 10 millidegree response, whereas in a non-amplified assay the angular change is not sufficient to be measured. For the much larger 60 nm GNP a ten fold increase in sensitivity was observed. With Chapter 5 we prove that low molecular weight molecules can be detected using GNP amplification in a commercial SPR apparatus.

The true colourimetric DNA assay is described in **Chapter 6**. First, GNPs were functionalised with DNA strands. Then, the yield of functionalisation was monitored allowing estimation of the number of molecules present on the GNP surface. Using the simulations from Chapter 4, we could estimate the total number of receptors in the sensing area. By combining the Monte Carlo simulations and the experimental data from a concentration dependent assay, we were able to calculate the affinity constant of the target DNA strand. Additionally, we present a real-time assay where we can directly observe single binding events.

In **Chapter 7** the development of two additional assays is described. The first assay is based on a conventional fluorescence based detection of DNA targets originating from *Staphylococcus aureus*. In this assay we studied the feasibility of replacement of the fluorescent probe with GNPs. In essence, this is possible. However, in view of the single molecule sensitivity of our method, some optimisation in terms of background binding reduction is required to make this method suitable for everyday use. The second assay is based on an alternative approach where a GNP is tethered above a planar gold layer using single stranded DNA (ssDNA). Due to the plasmon interactions of both the planar gold and the GNP, the scattering colour of the GNP is depending on the distance from the planar gold layer. Differences in ssDNA and double strand DNA enable us to use this method for DNA hybridisation detection. This means that the distance of the GNP to the surface and the subsequent change in scattering colour will change once the target strand hybridises. In this chapter we show preliminary experiments of this interesting phenomenon.

In **Chapter 8** the results of previous chapters are summarised. In addition to that, we describe a few methods and suggestions to improve the sensitivity of the conventional GNP assay which was described in Chapter 6. For improved sensitivity we first suggest some possibilities to reduce non-specific binding, then cover additional modifications which might increase the limit of detection: by increasing the total number of receptors in the sensing area and by increasing the sensing area. These suggestions are followed by some possibilities to improve limit of detection by using receptors with a higher affinity for the target strands. In addition, we describe an idea how we can construct a dedicated device from simple optical components. Surprisingly, the sensitivity of this device could be ten to thousand fold more sensitive than the standard microscope system.

Samenvatting

De optische detectie van gouden nanodeeltjes (GNPs) met behulp van donkerveld microscopie (DF) is een methode welke in staat is om de specifieke binding van één enkele streng van DNA of RNA gevoelig te meten. In dit proefschrift wordt de ontwikkeling van een nieuw type biosensor beschreven, gebaseerd op de lichtverstrooiing van de GNPs. In zeven hoofdstukken wordt de ontwikkeling van een idee op papier uitgewerkt tot een werkende biosensor. Deze biosensor is in staat specifieke stukjes DNA te detecteren met femtomolair gevoeligheid. Verder zijn chemische modificaties van diverse oppervlakten en theoretische simulaties beschreven, deze geven een verhelderend beeld van deze nieuwe, zeer gevoelige, detectie methode.

De absorptie- en verstrooiingseigenschappen van GNPs kunnen benut worden voor de detectie van DNA. Het binden van moleculen aan de GNPs zorgt voor een verandering van de lokale brekingsindex, direct rondom de GNP. Een toename van deze lokale brekingsindex door een toename van het aantal moleculen, zoals DNA, zorgt voor een proportionele verschuiving van het extinctie-spectrum-maximum naar een hogere golflengte. Deze eigenschap maakt het mogelijk om individuele GNPs te gebruiken als chemische sensor. Hierdoor kan DNA worden gedetecteerd in concentraties waarin het van nature voorkomt in cellen. Voor dit proefschrift zijn vijf verschillende methoden bestudeerd gebaseerd op GNPs.

Hoofdstuk 2 geeft een overzicht van klassieke en moderne optische methoden voor het detecteren van DNA strengen. Deze literatuurstudie volgt de ontwikkeling van het gebruik van GNPs, vanaf de aanvang in de jaren 70 tot de huidige gevoeligere methodes. Recente ontwikkelingen in de fabricage van stabiele GNP oplossingen met uniforme grootte hebben hier een belangrijke bijdrage aan geleverd. Met behulp van een donkerveld (DF) microscoop, uitgevoerd met kleuren camera en analyse software, kunnen deze GNPs gebruikt worden voor gevoelige detectie van DNA.

Hoofdstuk 3 beschrijft de ontwikkeling van de biochemische aspecten van de GNP–DNA biosensor. Dit onderzoek kende vele uitdagingen, zoals het immobiliseren van de DNA receptor-strengen op het oppervlak van de GNPs en het immobiliseren van de GNPs op het oppervlak. In diverse protocollen worden geoptimaliseerde methoden beschreven. Dit hoofdstuk sluit af met het ontwerpen van een eenvoudig te fabriceren vloeistof kamer. Deze kan worden geplaatst op een conventionele microscoop.

Hoofdstuk 4 beschrijft de fysische achtergrond van dit onderzoek. Hier staat de biochemische detectie op basis van oppervlak plasmon resonantie (SPR) centraal. SPR is een veelgebruikte methode waarmee interacties tussen eiwitten geanalyseerd kunnen worden. Ook voor individuele GNPs is het mogelijk het SPR effect te analyseren, dit in een lokaal gebied direct rondom het GNP. Dit effect noemen we lokaal SPR (LSPR) en is zeer gevoelig voor veranderingen van de brekingsindex in dit lokale gebied. Deze veranderingen kunnen worden waargenomen als een kleurverandering van de GNP. Aan de hand van simulaties hebben we de mate van kleurverandering bepaald voor het binden van DNA aan één enkele GNP. Met behulp van deze kleurveranderingen kunnen we de mate van bedekking van receptor-DNA aan een GNP bepalen. Daarnaast hebben we een model ontworpen op basis van Monte Carlo simulaties voor het bepalen van de affiniteitconstante van het analyte-DNA. In deze methode wordt een analyte gevangen door één receptor-DNA streng en een tweede versterker-DNA–GNP complex.

In **Hoofdstuk 5** laten we zien dat het mogelijk is het SPR signaal te versterken met behulp van GNPs. Conventionele SPR is niet gevoelig genoeg voor het detecteren van moleculen met een laag molecuul gewicht zoals korte analyte-DNA strengen. Met behulp van een model hebben we de response voor de 20- en 60 nm GNPs gesimuleerd. We hebben de gesimuleerde data en experimentele resultaten met elkaar vergeleken. Bij een meting zonder versterking was het niet mogelijk de kleine analyte-DNA strengen te detecteren, terwijl bij een versterking met behulp van de 20 nm GNPs een meetbaar signaal van 10 milligraden werd gemeten. Met behulp van de 60 nm GNPs was het mogelijk 10 maal gevoeliger te meten dan de 20 nm GNPs. In dit hoofdstuk laten we zien dat het mogelijk is om analytes met een laag molecuul gewicht in een commercieel SPR systeem te detecteren door middel van GNP versterking.

In **Hoofdstuk 6** wordt de detectie van analyte-DNA met behulp van GNP kleuranalyse is beschreven. Als eerste werden GNPs op het oppervlak geïmmobiliseerd, vervolgens werden receptor-DNA strengen gebonden aan deze GNPs. Aan de hand van kleurveranderingen was het mogelijk het aantal receptor-DNA strengen per GNP te bepalen, en zo het totale aantal receptor-DNA strengen in het hele sensorgebied vast te stellen. Door het combineren van de experimentele data met de Monte Carlo simulaties zijn we in staat de affiniteitconstante te bepalen voor de binding van het analyte-DNA. Verder laten we zien dat we in staat zijn de binding van één enkele DNA streng te volgen in de tijd.

In **Hoofdstuk 7** wordt de ontwikkeling van twee alternatieve methoden beschreven. In de eerste methode wordt conventionele fluorescentie analyse van *Staphylococcus aureus* DNA aangepast voor detectie op basis van GNP-verstrooiing. In essentie was dit mogelijk, echter voor het detecteren van één enkele binding is optimalisatie noodzakelijk. Hierbij is het reduceren van niet-specifiek achtergrond signaal essentieel.

De tweede methode is gebaseerd op de plasmon interacties tussen GNPs en een goud oppervlak. De kleurschittering van de GNP is afhankelijk van de afstand van de GNP tot de goud laag. De receptor-DNA–GNPs zijn met behulp van enkel strengs DNA aan het oppervlak verbonden. Door de lage stijfheid van de enkele DNA streng kunnen deze GNPs vrijelijk bewegen, gelimiteerd door de maximale lengte van het DNA. Hierdoor varieert de afstand van de GNP tot het oppervlak en ook de kleurschittering. De hybridisatie van analyte-DNA resulteert in dubbel strengs DNA met een hogere stijfheid. De GNPs behouden nu een constantere afstand tot het gouden oppervlak, waardoor ook de kleurschittering constant blijft. Bovendien is de tijdsgemiddelde afstand van de GNP tot het oppervlak groter. Hiermee laten we de potentie zien om met deze techniek een biosensor te maken.

In **hoofdstuk 8** wordt dit proefschrift samengevat. Aansluitend hierop beschrijven we een aantal suggesties om de GNP sensor uit hoofdstuk 6 verder te ontwikkelen.

Belangrijk is:

- Om de niet specifieke binding aan het oppervlak te reduceren;
- De detectielimiet verder verbeteren;
- Aantal receptor-DNA strengen in het detectiegebied verhogen;
- Het vergroten van het detectiegebied;
- Verhogen van de affiniteit, zodat de analyte met een hogere specificiteit bindt aan de receptor-DNA strengen.

Als bijkomend resultaat van het onderzoek hebben we vastgesteld dat een op zich zelf staand detectie systeem de gevoeligheid met een factor 10 tot 1000 maal kan verbeteren ten opzichte van de standaard microscoop, gebruikt in dit onderzoek.

Acknowledgements

The word ac•knowl•edg•ment is a noun created by combining the verb “to acknowledge” and the suffix “-ment” which first occurred in the late 16th century. Basically it is an expression of appreciation. Hereby I would like to thank you all for your help, support, ideas and criticism. It has been a good, a joyful time and a wonderful experience.

We never stop¹

UCUUAGUUAUAGAAUGGUGCUAACGAUACCCAUGCCAACA
AGUCCUUUUAGCGCGCACUCCUGACUCACGAGUUCAUUAGCCAU

Closing thoughts

Every time I looked down into the eyepieces of the microscope with a sample of gold nanoparticles it was like looking up at the night sky. Just see for yourself:

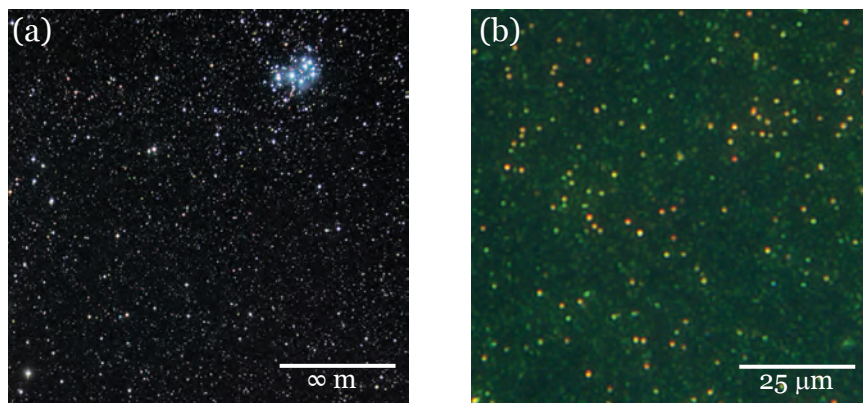


Figure: (a) Image of the night sky of constellation Messier object 45 (Pleiades). (b) Darkfield image of various (40 to 80 nm) sized gold nanoparticles.

¹ Includes 21 & 22

Curriculum Vitae

Remco Verdoold was born on the 18th of November 1982, in Rotterdam, the Netherlands. In 2005 he obtained his engineering degree, a Dutch equivalent of the Bachelor degree, at the Saxion University for professional education in Enschede, in the field of biomolecular technologies and analytical (bio)chemistry. Subsequently, in 2006 he obtained his Master of Science degree with distinction in food biotechnology at the University of Ulster in Coleraine, Northern Ireland, UK.

In October 2006 Remco Verdoold joined the Biochip Group which later merged into the Nanobiophysics Group at the University of Twente in Enschede, The Netherlands, as PhD candidate under the supervision of dr. Rob Kooyman and Prof. dr. Vinod Subramaniam. The main research aim was to develop strategies for sensitive and specific detection of DNA using gold nanoparticles as individual sensors or reporters. The results of this multidisciplinary research, involving surface modification, gold nanoparticle functionalisation and dark field microscopy, are described in this thesis. Currently Remco Verdoold has started working as a post-doctoral fellow at the Vrije Universiteit in Amsterdam in the (IDEAS)^{µm} group of dr. Davide Iannuzzi on the Align-and-Shine technology for the development of fiber-top sensors and systems.

(IDEAS)^{µm} = InterDisciplinary Engineering and Applied Sciences at the µm scale.

List of Publications

Journal articles (peer-reviewed)

J.B. Beussink, **R. Verdoold**, and R. Schasfoort, “High density protein micro arrays,” *BioForum Europe*, vol. 04, 2006, p. 60.

F. Ungureanu, J. Halamek, **R. Verdoold**, and R.P.H. Kooyman, “The use of a colour camera for quantitative detection of protein-binding nanoparticles,” *Proceedings of SPIE*, vol. 7192, 2009, p. 71920O. DOI: 10.1117/12.806522.

R. Verdoold, F. Ungureanu, D. Wasserberg, and R.P.H. Kooyman, “Gold nanoparticle assays: towards single molecule unamplified DNA detection,” *Proceedings of SPIE*, vol. 7312, 2009, p. 73120N. DOI: 10.1117/12.818120.

O. Sunnotel, **R. Verdoold**, P.S.M. Dunlop, W.J. Snelling, C.J. Lowery, J.S.G. Dooley, J.E. Moore, and J.A. Byrne, “Photocatalytic inactivation of *Cryptosporidium parvum* on nanostructured titanium dioxide films,” *Journal of Water and Health*, vol. 8, Mar. 2010, pp. 83-91. DOI: 10.2166/wh.2009.204.

F. Ungureanu, D. Wasserberg, N. Yang, **R. Verdoold**, and R.P.H. Kooyman, “Immunosensing by colorimetric darkfield microscopy of individual gold nanoparticle-conjugates,” *Sensors & Actuators B: Chemical*, vol. 150, Sep. 2010, pp. 529-536. DOI: 10.1016/j.snb.2010.08.044.

R. Verdoold, R. Gill, F. Ungureanu, R. Molenaar and R.P.H. Kooyman, “Femtomolar DNA detection by parallel colorimetric darkfield microscopy of functionalized gold nanoparticles”, *Biosensors & Bioelectronics*, vol. 27, 2011, pp 77-81. DOI: 10.1016/j.bios.2011.06.019.

Conference contributions (oral presentations)

R. Verdoold, F. Ungureanu, D. Wasserberg, R. Molenaar, J. Halamek, R.P.H. Kooyman, "Gold nanoparticle assays for single molecule DNA and protein detection", Micro and Nano conference 2008, Ede, the Netherlands, November 18th 2008.

F. Ungureanu, J. Halamek, **R. Verdoold**, and R.P.H. Kooyman, "The use of a colour camera for quantitative detection of protein-binding nanoparticles," SPIE conference, Photonix 2009, San Fransisco (CA), United States of America, April 14th 2009.

R. Verdoold, F. Ungureanu, D. Wasserberg and R.P.H. Kooyman, Gold nanoparticle assays for single molecule detection of unamplified DNA, SPIE conference, Security, Defense and Sensing 2009, Orlando (FL), United States of America, April 14th 2009.

R. Verdoold, F. Ungureanu, D. Wasserberg, R. Molenaar and R.P.H. Kooyman, "Gold nanoparticle assays: Towards single binding event detection", BioNano Europe conference, Münster, Germany, June 15th 2010.

Conference contributions (poster presentations)

R. Verdoold, F. Ungureanu, J. Halamek and R. Kooyman "Multiplex gold nanoparticle assays for single molecule DNA and protein detection", 3rd BMTI symposium, Enschede, The Netherlands, April 3rd 2007.

R. Verdoold, F. Ungureanu, J. Halamek and R. Kooyman "Multiplex gold nanoparticle assays for single molecule DNA and protein detection", Annual MESA+ symposium, Enschede, The Netherlands, September 11th 2007.

F. Ungureanu, **R. Verdoold**, J. Halamek and R.P.H. Kooyman, "Multiplex gold nanoparticle assays: The road towards single molecule DNA and protein detection", MicroNano Conference 2007, Wageningen, the Netherlands, November 15th and 16th 2007.

R. Verdoold, F. Ungureanu, J. Halamek and R.P.H. Kooyman, "Towards gold nanoparticle based sensing, how to detect proteins or DNA", EU Fluoromag meeting, Enschede, the Netherlands, March 17th 2008.

J. Halamek, **R. Verdoold**, F. Ungureanu and R.P.H. Kooyman, "Towards gold nanoparticle based immunosensing", EU Fluoromag meeting, Enschede, the Netherlands, March 17th 2008.

R. Verdoold, F. Ungureanu, J. Halamek and R.P.H. Kooyman, "Towards gold nanoparticles based sensing, how to detect proteins or DNA", 1st MESA+ & Münster University meeting, Enschede, the Netherlands, April 1st 2008.

R. Verdoold, F. Ungureanu, J. Halamek and R.P.H. Kooyman, "Towards gold nanoparticles based sensing, how to detect proteins or DNA", 1st Labelfree biosensing conference, Boekelo, the Netherlands, April 8th and 9th 2008.

R. Verdoold, F. Ungureanu, D. Wasserberg and R.P.H. Kooyman, “Gold nanoparticle assays: Towards single particle DNA and protein detection”, Annual MESA+ symposium, Enschede, the Netherlands, September 23rd 2008.

R. Verdoold, F. Ungureanu, D. Wasserberg and R.P.H. Kooyman, “Gold nanoparticle assays: Towards single particle DNA and protein detection”, FOM biophysical meeting, Veldhoven, the Netherlands, September 29th and 30th 2008.

R. Verdoold, D. Wasserberg, F. Ungureanu, J. Halamek and R.P.H. Kooyman “Gold nanoparticle assays: Towards single particle DNA and protein detection” MicroNano conference 2008, Ede, the Netherlands, November 17th till 19th 2008.

R. Verdoold, D. Wasserberg, F. Ungureanu, T. Brinkman, E. Tromp and Rob Kooyman, “Gold nanoparticle assays: towards sensitive detection of nonamplified DNA” 1st biosensing conference, Bristol, United Kingdom, November 10th till 13th 2009.

R. Verdoold, F. Ungureanu, D. Wasserberg, T. Brinkman, R. Molenaar and R.P.H. Kooyman “Functionalised gold nanoparticles - towards sensitive detection of biomolecules”, Annual MESA+ meeting 2009, Enschede, the Netherlands, September 21st 2009.

R. Verdoold, F. Ungureanu, D. Wasserberg, T. Brinkman, R. Molenaar and R.P.H. Kooyman “Functionalised gold nanoparticles - towards sensitive detection of biomolecules”, Micro Nano conference 2009, Delft, the Netherlands, November 5th and 6th 2009.

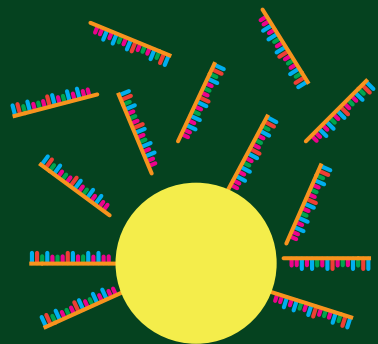
F. Ungureanu, **R. Verdoold**, D. Wasserberg, and R.P.H. Kooyman “Colorimetric darkfield microspectroscopy of gold nanoparticles as sensing platforms”, SPIE conference, Optics + Photonics, San Diego, USA, August 1-5 2010.

R. Verdoold, F. Ungureanu, D. Wasserberg, R. Molenaar and R.P.H. Kooyman, “Gold nanoparticle assays: Towards single binding event detection”, BioNano Europe conference, Münster, Germany, June 15th 2010.

R. Verdoold, F. Ungureanu, D. Wasserberg, R. Molenaar and R.P.H. Kooyman, “Gold nanoparticle assays: Towards single binding event detection”, Annual MESA+ meeting 2010, Enschede, the Netherlands, September 23rd 2010.

F. Ungureanu, **R. Verdoold**, R. Molenaar D. Wasserberg, and R.P.H. Kooyman, “Gold nanoparticle assays for sensitive detection of biological molecules using colorimetric DF microscopy,” Micro Nano conference 2010, Enschede, the Netherlands, November 17th and 18th 2010.

R. Verdoold, R. Gill, F. Ungureanu, R. Molenaar and R.P.H. Kooyman, “Gold nanoparticle assays: Towards sensitive detection of nonamplified DNA”, Annual meeting of Photonics 4 life 2011, Heraklion, Greece, May 28th and 29th 2011.



©

ISBN 978-90-365-3408-6



9 789036 534086 >